

## New atom movement mechanism for tracking path on disordering $\text{AuCuI}$ ( $A_8^{\text{Au}} A_4^{\text{Cu}}$ ) compound

You-qing XIE<sup>1,2,3</sup>, Hong-jian PENG<sup>4</sup>, Xin-bi LIU<sup>1,2,3</sup>, Xiao-bo LI<sup>5</sup>, Yao-zhuang NIE<sup>6</sup>

1. School of Materials Science and Engineering, Central South University, Changsha 410083, China;
2. Powder Metallurgy Research Institute, Central South University, Changsha 410083, China;
3. State Key Laboratory of Powder Metallurgy, Central South University, Changsha 410083, China;
4. School of Chemistry and Chemical Engineering, Central South University, Changsha 410083, China;
5. College of Materials Science and Engineering, Xiangtan University, Xiangtan 411105, China;
6. School of Physics and Electronics, Central South University, Changsha 410083, China

Received 13 July 2014; accepted 9 October 2014

**Abstract:** Taking experimental path on disordering  $\text{AuCuI}$  ( $A_8^{\text{Au}} A_4^{\text{Cu}}$ ) composed of  $A_8^{\text{Au}}$  and  $A_4^{\text{Cu}}$  stem alloy genes as an example, three discoveries and a method were presented. The ability of  $\text{AuCuI}$  ( $A_8^{\text{Au}} A_4^{\text{Cu}}$ ) to keep structure stabilization against changing temperature is attributed to the fact that the  $A_8^{\text{Au}}$  and  $A_4^{\text{Cu}}$  potential well depths greatly surpass their vibration energies, which leads to the subequilibrium of experimental path. A new atom movement mechanism of  $\text{AuCuI}$  ( $A_8^{\text{Au}} A_4^{\text{Cu}}$ ) to change structure for suiting variation in temperature is the resonance activating-synchro alternating of alloy genes, which leads to heterogeneous and successive subequilibrium transitions. There exists jumping order degree, which leads to the existence of jumping  $T_j$ -temperature and an unexpected so-called “retro-effect” about jumping temperature retrograde shift to lower temperatures upon the increasing heating rate. A set of subequilibrium holographic network path charts were obtained by the experimental mixed enthalpy path method.

**Key words:** intermetallics; alloy gene; order/disorder transformation; resonance activating-synchro alternating mechanism; thermodynamic properties; equilibrium and subequilibrium holographic network path charts

## 1 Introduction

Four philosophic propositions of system sciences were proposed, which are the systematic structure diversity, systematic properties diversity, systematic correlativity (or entirety) and systematic openness propositions [1], and the systematic metal materials science (SMMS) framework was established [2]. Now, we have proposed a systematic kinetics proposition: “A system has not only the ability to keep structure stabilization against a changing environment, but also a mechanism to change structure for suiting variation in environments”. It is a philosophic foundation for establishing kinetics of systems. Its scientific connotation can be deeply understood via studying kinetic behaviors on disordering  $\text{AuCuI}$  ( $A_8^{\text{Au}} A_4^{\text{Cu}}$ ), which has been considered a classic paragon with complete

order-disorder transition path studied by different experimental techniques and various theories for about a century. However, four foundational questions have been remained without clear-cut answers: 1) Why does the  $\text{AuCuI}$  ( $A_8^{\text{Au}} A_4^{\text{Cu}}$ ) compound keep its order degree unchanging until so much higher  $T_{\text{onset}}$ -temperature (about 600 K)? 2) What mechanism controls kinetic behaviors on disordering  $\text{AuCuI}$  ( $A_8^{\text{Au}} A_4^{\text{Cu}}$ )? 3) How to explain the forming process of the statistic periodic antiphase (SPAP)  $\text{AuCuII}$  [3,4]? 4) How to explain the retro-effect about the jumping  $T_j$ -temperature appearing an unexpected retrograde shift to lower temperatures upon the increasing heating rate [5–7]. These questions are concerned with stable and metastable (or equilibrium and subequilibrium) order-disorder transition paths, as well as atom movement mechanism for studying diffusion, phase transformations and ageing reactions in solids. However, up to now, researchers have got used to

**Foundation item:** Project (51071181) supported by the National Natural Science Foundation of China; Project (2013FJ4043) supported by the Natural Science Foundation of Hunan Province, China

**Corresponding author:** You-qing XIE; Tel: +86-731-88879287; E-mail: [xieyouq8088@163.com](mailto:xieyouq8088@163.com)  
DOI: 10.1016/S1003-6326(14)63464-6

recognizing the experimental phenomena observed during very slow variation in temperature to be thermodynamic equilibrium, such as the middle jumping  $T_j$ -temperature is erroneously considered the terminal  $T_c$ -critical temperature of order-disorder equilibrium transition [8], and then to treat experimental phenomena by equilibrium thinking mode, lacking an essential definition of thermodynamic equilibrium order-disorder transition.

Due to the discoveries of alloy gene (AG) sequences and their informational transmission mode and establishments of the alloy gene arranging (AGA)-Gibbs free energy partition function, holographic alloy positioning (HAP) system and equilibrium holographic network phase (EHNP) diagrams of AuCu-type sublattice system [1], our knowledge of relations of order degree ( $\sigma$ ), state ( $q$ ) and temperature ( $T$ ) for a given component alloy has been changed from single causality to systematic correlativity. In this work, a new atom movement mechanism was discovered, equilibrium and subequilibrium holographic network path (EHNP and SHNP) charts on disordering AuCuI ( $A_8^{Au} A_4^{Cu}$ ) were established and the four questions mentioned above were explained.

## 2 EHNP charts of thermodynamic properties

The essential on disordering AuCuI ( $A_8^{Au} A_4^{Cu}$ ) is that the  $A_8^{Au}$  and  $A_4^{Cu}$  stem alloy genes are split into the  $A_i^{Au}$  and  $A_i^{Cu}$  sequences in the disordered state. The essential definition of equilibrium order-disorder transition is defined as that “the AG-Gibbs energy levels ( $G_i^{Au}(T)$ ,  $G_i^{Cu}(T)$ ) and AG-concentrations ( $x_i^{Au}(T)$ ,  $x_i^{Cu}(T)$ ) occupied at the  $G_i^{Au}(T)$ - and  $G_i^{Cu}(T)$ -energy levels can respond immediately and change synchronously with each small variation in temperature and proceed along the minimal Gibbs energy path”. It gives an equilibrium thermodynamic standard for studying subequilibrium transition and is useful in understanding the development and preservation of subequilibrium structures and their attendant properties, although it can not be reached in practice. The systematic correlativity between different properties and between various properties and structures for a given component alloy in equilibrium path may be described by a set of the EHNP  $q-T-\sigma$  charts. An EHNP chart consists of curves linked by the network ( $q$ ,  $T$ ,  $\sigma$ )-points, where the  $q$ -state denotes the AG-concentrations ( $x_i^{Au}$ ,  $x_i^{Cu}$ ), mixed Gibbs energy  $\Delta G^m$ , mixed characteristic Gibbs energy  $\Delta G^{*m}$ , (i.e., chemical potential), mixed enthalpy  $\Delta H^m$ , mixed potential energy  $\Delta E^m$ , mixed volume  $\Delta V^m$ , configurational entropy  $S^c$ , configurational entropy energy  $TS^c$ , generalized vibration free energy  $X^v$ , generalized vibration energy  $U^v$ , generalized vibration

entropy  $S^v$ , generalized vibration entropy energy  $TS^v$ , heat capacity  $c_p$ , thermal expansion coefficient  $\alpha$  and activities ( $\alpha_{Au}$ ,  $\alpha_{Cu}$ ). Now, the minimum mixed Gibbs energy  $\Delta G_{min}^m - T$  path and corresponding  $\sigma_e - T$  path have been obtained by the iso-order degree (or isothermal) Gibbs energy equilibrium path method (Fig. 1). Then, a set of EHNP charts of thermodynamic properties have been calculated by the AGA-Gibbs free energy partition function (Fig. A.1, Figs. A.3–A.13, Fig. A.18 in Appendix A). The common behaviors of equilibrium transitions are as follows: 1) The order→disorder transition upon heating and disorder→order transition upon cooling proceed along the same minimal mixed Gibbs energy  $\Delta G_{min}^m - T$  path, without a so-called hysteresis phenomenon; 2) The  $\Delta G_{min}^m - T$  path is continuous and has no jumping phenomenon. These are the equilibrium transition criteria. The EHNP charts provide standards for establishing experimental SHNP charts on disordering AuCuI ( $A_8^{Au} A_4^{Cu}$ ).

## 3 SHNP charts of thermodynamic properties

The essential definition of subequilibrium order→disorder transition is that the AG-Gibbs energy levels can respond immediately with each small variation in temperature, but the AG-concentrations (probabilities) occupied at the AG-Gibbs energy levels can not change synchronously, even by extremely heating rate, that leads to its higher Gibbs energy path than equilibrium path. This transition needs a special atom movement mechanism together with superheated driving Gibbs energy. It is often the case that the structures and properties of subequilibrium state alloys are more desirable than those associated with equilibrium state alloys. We have obtained the experimental mixed enthalpy  $\Delta H_s^m - T$  path on disordering AuCuI ( $A_8^{Au} A_4^{Cu}$ ), based on the assessment of experimental data [3,9]. The subequilibrium order degree  $\sigma_s - T$  path has been obtained by the experimental  $\Delta H_s^m - T$  path method based on the iso-order degree mixed enthalpy  $\Delta H_\sigma^m - T$  equilibrium path chart (Figs. 1(b)–(d) and Fig. A.2 in Appendix A). Namely, the experimental  $\Delta H_s^m - T$  path is translated into the subequilibrium  $\sigma_s - T$  path, through the  $\Delta H_\sigma^m - T$  equilibrium path chart. Then, a set of the SHNP charts of thermodynamic properties are calculated by the AGA-Gibbs free energy partition function and shown in Figs. A.3 to A.18 in Appendix A. These charts are calculated by the temperature step  $\Delta T=1$  K and order degree step  $\Delta\sigma=0.00001$ . The common behaviors of the SHNP charts are as follows: 1) The order degree keeps unchanged in a broad temperature range from 0 K to 593 K by slow heating rate (Fig. 1(d)); 2) There exists complex variation in order degree, during the temperature

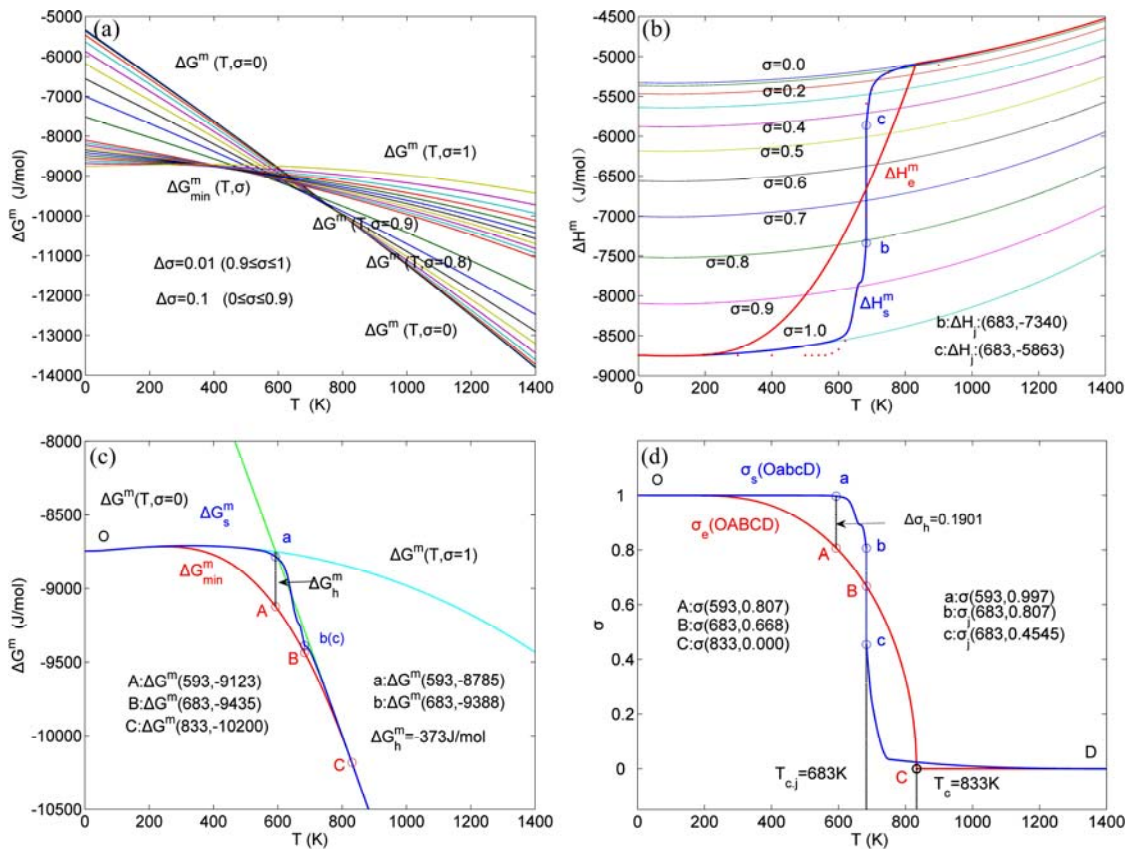


**Fig. 1** EHNP and SHNP charts on disordering  $\text{AuCuI}(A_8^{\text{Au}}A_4^{\text{Cu}})$ : (a) Minimal mixed Gibbs energy  $\Delta G_{\min}^m - T$  path obtained by iso-order degree Gibbs energy equilibrium path method; (b) Experimental mixed enthalpy  $\Delta H_s^m - T$  path method based on network chart of the iso-order degree mixed enthalpies equilibrium paths, attaching equilibrium  $\Delta H_e^m - T$  path; (c)  $\Delta G_{\min}^m$  ( $OABC$ ) and  $\Delta G_s^m$  ( $Oabc$ ) paths of equilibrium and subequilibrium order→disorder transitions, where  $\Delta G_h^m$  denotes superheated driving Gibbs energy; (d)  $\sigma_e$  ( $OABCD$ ) and  $\sigma_s$  ( $OabcD$ ) paths of equilibrium and subequilibrium order→disorder transitions, where  $\Delta \sigma_h$  denotes hysteresis order degree

range from onset temperature ( $T_{\text{onset}}$ ) to jumping  $T_j$ -temperature, that is only about 100 K interval; 3) Upon increasing heating rate, the  $T_{\text{onset}}$ -temperature increases, and the  $T_j$ -temperature decreases, i.e., so called retro-effect; 4) The  $\Delta G_s^m - T$  path at any temperature is higher than the equilibrium  $\Delta G_{\min}^m - T$  path, even after the  $T_j$ -temperature (Fig. 1(c)). Their difference ( $\Delta G_{\min}^m(T) - \Delta G_s^m(T)$ ) is the superheated driving Gibbs energy of the subequilibrium alloy, i.e., thermal hysteresis Gibbs energy; 5) There exists a thermal hysteresis Gibbs energy loop between the order→disorder and disorder→order transitions, that is not concerned in this work. These behaviors demonstrate that all experimental order→disorder paths by any heating rate belong to subequilibrium ones.

#### 4 EHNP and SHNP charts of AG-concentrations

“Properties are determined by structures”. The description of alloy phase structures has been translated

from a probability of the constituent atom concentrations to a probability of the alloy gene concentrations, due to discovery of the alloy genes. The EHNP and SHNP charts of thermodynamic properties on disordering  $\text{AuCuI}(A_8^{\text{Au}}A_4^{\text{Cu}})$  are respectively determined by the EHNP and SHNP charts of the AG-concentrations. The AG-concentration  $x_i^{\text{Au}}$  and  $x_i^{\text{Cu}}$  paths on disordering  $\text{AuCuI}(A_8^{\text{Au}}A_4^{\text{Cu}})$  may be described by two modes: 1) three-dimensional  $x_i^{\text{Au}} - T - i$  and  $x_i^{\text{Cu}} - T - i$  SHNP charts, from which two-dimensional iso-order degree  $x_{i,\sigma}^{\text{Au}} - i$  and  $x_{i,\sigma}^{\text{Cu}} - i$  paths can be obtained, where  $x_i^{\text{Au}}$  and  $x_i^{\text{Cu}}$  are the probabilities occupied at the  $G_i^{\text{Au}}(T)$  and  $G_i^{\text{Cu}}(T)$  energy levels in the AG-arranging band structure (Figs. 2(a), (b), (c), (d)); 2) three-dimension  $x_i^{\text{Au}} - T - \sigma$  and  $x_i^{\text{Cu}} - T - \sigma$  SHNP charts, from which two-dimensional  $x_i^{\text{Au}} - \sigma$  and  $x_i^{\text{Cu}} - \sigma$  paths can be obtained, where the  $x_i^{\text{Au}}$  and  $x_i^{\text{Cu}}$  are the probabilities occupied at the lattice sites in the AG-arranging crystal structure (Figs. 2(e), (f), (g), (h)). The AG-concentration EHNP charts are shown in Fig. B.1 in Appendix B. Their systematic correlativity

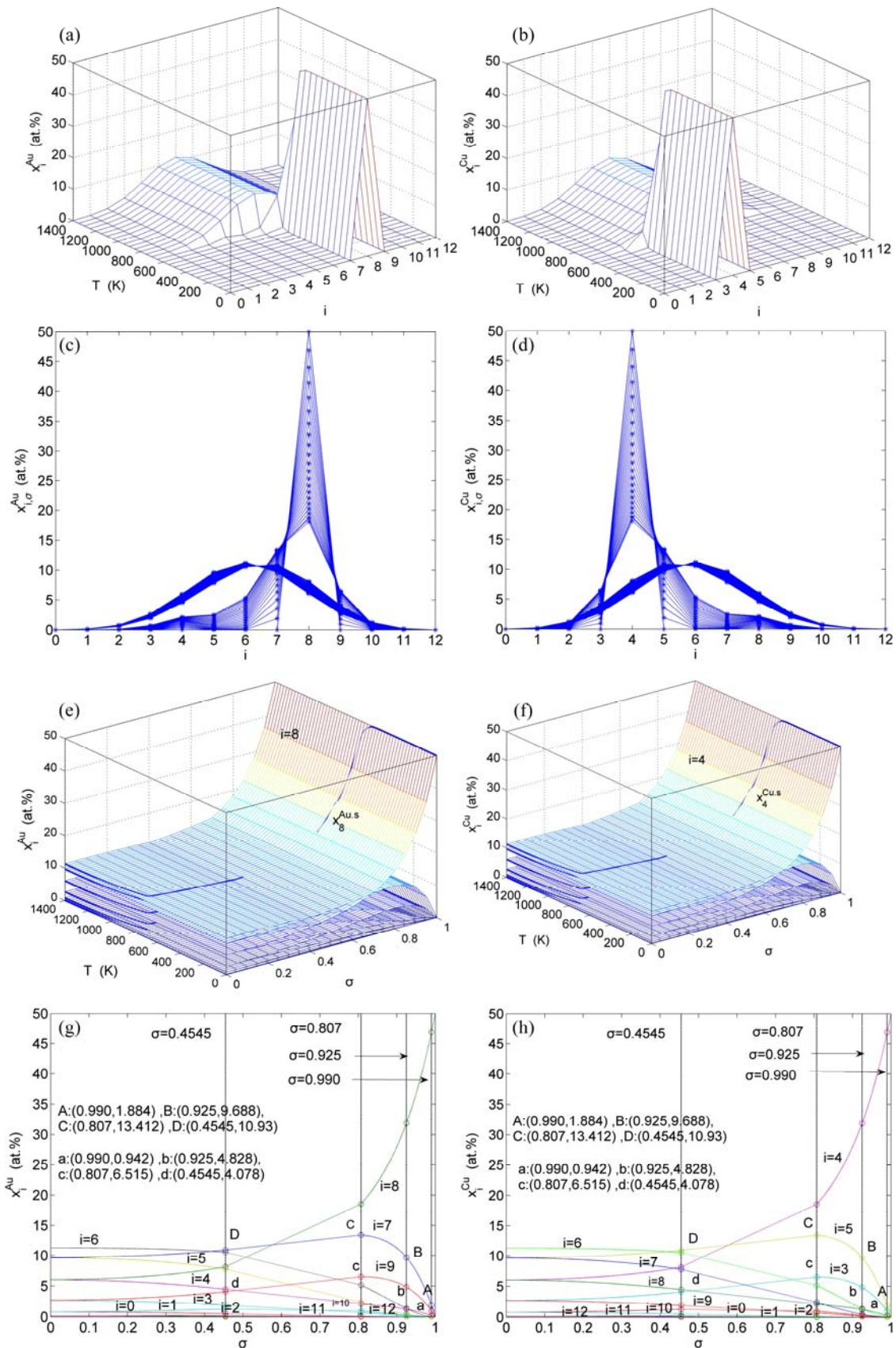


**Fig. 2** AG-concentration SHNP charts on disordering  $\text{AuCuI}(A_8^{\text{Au}}A_4^{\text{Cu}})$ : (a), (b) Three-dimensional  $x_i^{\text{Au}} - T - i$  and  $x_i^{\text{Cu}} - T - i$  SHNP charts; (c), (d) Two-dimensional iso-order degree  $x_{i,\sigma}^{\text{Au}} - i$  and  $x_{i,\sigma}^{\text{Cu}} - i$  SHNP charts; (e), (f) Three-dimensional  $x_i^{\text{Au}} - T - \sigma$  and  $x_i^{\text{Cu}} - T - \sigma$  SHNP charts with  $x_i^{\text{Au},s} - T$  and  $x_i^{\text{Cu},s} - T$  paths; (g), (h) Two-dimensional iso-Gibbs energy level  $x_i^{\text{Au}} - \sigma$  and  $x_i^{\text{Cu}} - \sigma$  SHNP charts

is listed in Tables B.1 and B.2 in Appendix B. From the EHNP and SHNP charts of the AG-concentrations, we have obtained the following common knowledge: 1) The essence of order→disorder transition of the AuCuI ( $A_8^{Au} A_4^{Cu}$ ) is that the  $A_8^{Au}$  and  $A_4^{Cu}$  stem alloy genes are split into the  $A_i^{Au}$ - and  $A_i^{Cu}$ -sequences; 2) The equilibrium order→disorder transition is a continuous one. The subequilibrium order→disorder transition is a discontinuous one.

## 5 Ability of structure stabilization

Any system has ability to keep structure stabilization against a changing environment. We have discovered that the ability of AuCuI ( $A_8^{Au} A_4^{Cu}$ ) to keep structure stabilization against changing temperature is attributed to the fact that the AG-potential well depths greatly surpass superheated driving Gibbs energy and AG-vibration energies. When  $0 \text{ K} \leq T < T_{\text{onset}}$ , it is the unchanged period of the AuCuI ( $A_8^{Au} A_4^{Cu}$ ). Its behaviors are as follows: 1) There exists no variation in order degree until  $T_{\text{onset}}$  (593 K)-temperature (Figs. 1(c) and (d)). Namely, there exists no positional exchange between  $A_8^{Au}$  and  $A_4^{Cu}$  alloy genes, which are still occupied at the  $G_8^{Au}$  and  $G_4^{Cu}$  energy levels, respectively; 2) The superheated driving Gibbs energy ( $\Delta G_{\min}^m(T) - \Delta G_s^m(T)$ ) between the equilibrium ( $OABC$ ) and subequilibrium ( $Oabc$ ) paths increases with rising temperature. Their difference is  $-373 \text{ J/mol}$  at 593 K (Fig. 1(c)), which is too small to exchange AG-positions; 3) The generalized vibration energies of  $A_8^{Au}$  and  $A_4^{Cu}$  alloy genes increase with rising temperature, but their values are much smaller than their potential well depths (Tables C.1 to C.6 in Appendix C). At 593 K, the  $|U_8^{Au,v}/E_8^{Au}|$  and  $|U_4^{Cu,v}/E_4^{Cu}|$  ratios are about 1/27. It means that only depending on superheated driving Gibbs energy and vibration energy, the  $A_8^{Au}$  and  $A_4^{Cu}$  alloy genes can not surmount potential barriers to alternate positions.

## 6 Resonance activating (RA)-synchro alternating (SA) mechanism

Any system has a mechanism to change structure for suiting variation in environments. According to the peculiar orders of the AG- $x_i^{Au}$  and  $x_i^{Cu}$  concentrations at the beginning period on disordering AuCuI ( $A_8^{Au} A_4^{Cu}$ ), we have discovered the 3(RA-SA) mechanism, which is that three AG-pairs in a cell-scale region occur resonance to accumulate vibration energies and synchronistically alternate their lattice positions to change their energetic states (see Appendix D). The RA-SA mechanism together with superheated driving Gibbs energy ( $\Delta G_{\min}^m(T) - \Delta G_s^m(T)$ ) and jumping order degree, as well

as atom-vacancy alternating (AVA) mechanism, control kinetic behaviors of the heterogeneous subequilibrium successive transition periods on disordering AuCuI ( $A_8^{Au} A_4^{Cu}$ ).

1) When  $T_{\text{onset}}(593 \text{ K}) < T \leq 620 \text{ K}$  and  $1.000 > \sigma_s \geq 0.990$ , it is the growing period of the high order degree AuCu(H) alloy. Its behaviors are as follows: (1) Some  $A_8^{Au}$ - and  $A_4^{Cu}$ -stem alloy genes are split respectively into the  $A_7^{Au}$ ,  $A_9^{Au}$ ,  $A_4^{Au}$ ,  $A_6^{Au}$  and  $A_5^{Au}$ ;  $A_5^{Cu}$ ,  $A_3^{Cu}$ ,  $A_8^{Cu}$ ,  $A_6^{Cu}$  and  $A_7^{Cu}$ , through the 3(RA-SA) mechanism with two manners (Figs. 3(a) and (b), Figs. 4(a) and (b), Fig. D.5 in Appendix D); (2) Their peculiar orders in concentrations obtained by the 3(RA-SA) mechanism are respectively:  $x_4^{Au} > x_6^{Au} > x_5^{Au}$  and  $x_8^{Cu} > x_6^{Cu} > x_7^{Cu}$ , although the  $A_4^{Au}$  signal alloy gene of 3(RA-SA) mechanism is further away from  $A_8^{Au}$  than  $A_6^{Au}$  and  $A_5^{Au}$ , and the  $A_8^{Cu}$  signal alloy gene of 3(RA-SA) mechanism is further away from  $A_4^{Au}$  than  $A_6^{Au}$  and  $A_7^{Cu}$  (Figs. 3(a) and (b), Tables B.1 and B.2 in Appendix B); (3) There exists cell-scale (nucleation) heterogeneity in the growing period of the AuCu(H) alloy. Namely, the early-3(RA-SA) cell region with more 3(RA-SA) cells, middle-3(RA-SA) cells region with less 3(RA-SA) cells and late-AuCuI ( $A_8^{Au} A_4^{Cu}$ ) cell region without 3(RA-SA) cell co-exist in the AuCu(H) alloy (Fig. 4(c)).

2) When  $620 \text{ K} < T \leq 650 \text{ K}$  and  $0.990 > \sigma_s \geq 0.925$ , it is the growing period of the SPAP-AuCuII region. Its behaviors are as follows: (1) As  $T_s=637 \text{ K}$  and  $\sigma_s=0.967$ , the concentrations  $x_9^{Au}$  and  $x_3^{Cu}$  of the  $A_9^{Au}$ - and  $A_3^{Cu}$ -jumping alloy genes begin to display the emergent phenomenon, which is defined as that their concentrations are larger than the ones of the corresponding alloy genes in the disorder state:  $x_9^{Au} > x_{9,\text{dis}}^{Au}$ ,  $x_3^{Cu} > x_{3,\text{dis}}^{Cu}$ ; (2) As  $T_s=650 \text{ K}$  and  $\sigma_s=0.925$ , the concentrations  $x_7^{Au}$  and  $x_5^{Cu}$  of the  $A_7^{Au}$ - and  $A_5^{Cu}$ -jumping alloy genes begin to display the emergent phenomenon:  $x_7^{Au} > x_{7,\text{dis}}^{Au}$ ,  $x_5^{Cu} > x_{5,\text{dis}}^{Cu}$  (Figs. 3(c) and (d), Tables B.1 and B.2 in Appendix B). (3) During this period, there exists region-scale (nucleus growing) heterogeneity: the original early-3 (RA-SA) cell regions with more 3(RA-SA) cells grow into the early-(SPAP-AuCuII) regions, the original middle-3(RA-SA) cell regions with less 3(RA-SA) cells grow into the middle-(RA-SA) cell regions with more 3(RA-SA) cells and the original late-AuCuI ( $A_8^{Au} A_4^{Cu}$ ) cell regions grow into the late-(RA-SA) cell regions with less 3(RA-SA) cells (Fig. 4(d)). Namely, the AuCu(H) region and SPAP-AuCuII region co-exist, and two distinct X-ray diffraction patterns may be observed at the  $\sigma_s=0.925$  [3]. This subequilibrium alloy with region-scale heterogeneity is called the “pseudo-two-phases (PTP)” AuCu alloy with the AuCu(H) regions and the SPAP-AuCuII regions. The use of the phrase “PTP” is

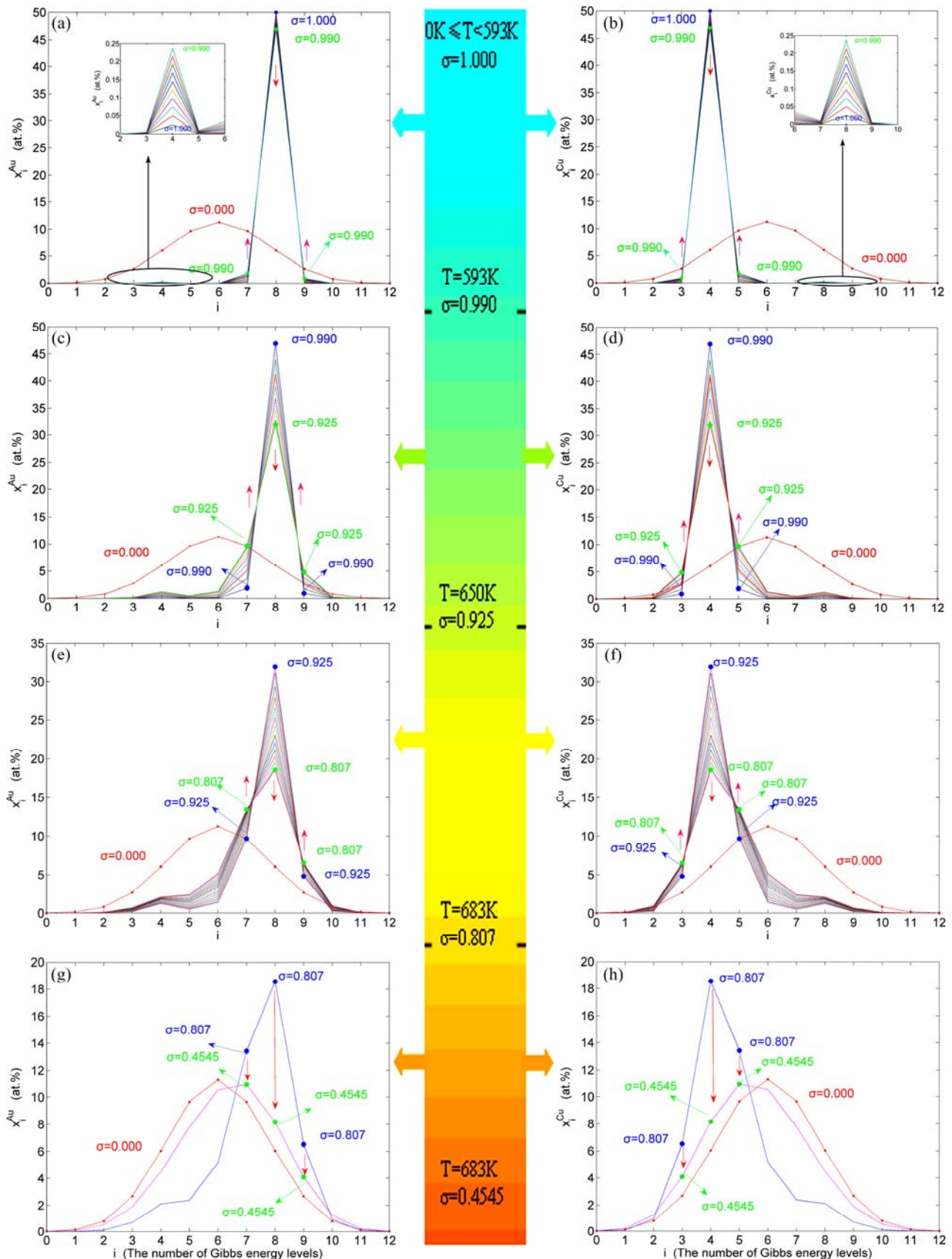


**Fig. 3**  $x_i^{\text{Au}}$  and  $x_i^{\text{Cu}}$  concentrations for tracking path on disordering  $\text{AuCuI} (A_8^{\text{Au}}A_4^{\text{Cu}})$ : (a), (b)  $0.990 \leq \sigma_s \leq 1$ ; (c), (d)  $0.925 \leq \sigma_s \leq 0.990$ ; (e), (f)  $0.807 \leq \sigma_s \leq 0.925$ ; (g), (h)  $\sigma_j = 0.807 \rightarrow \sigma_L = 0.445$

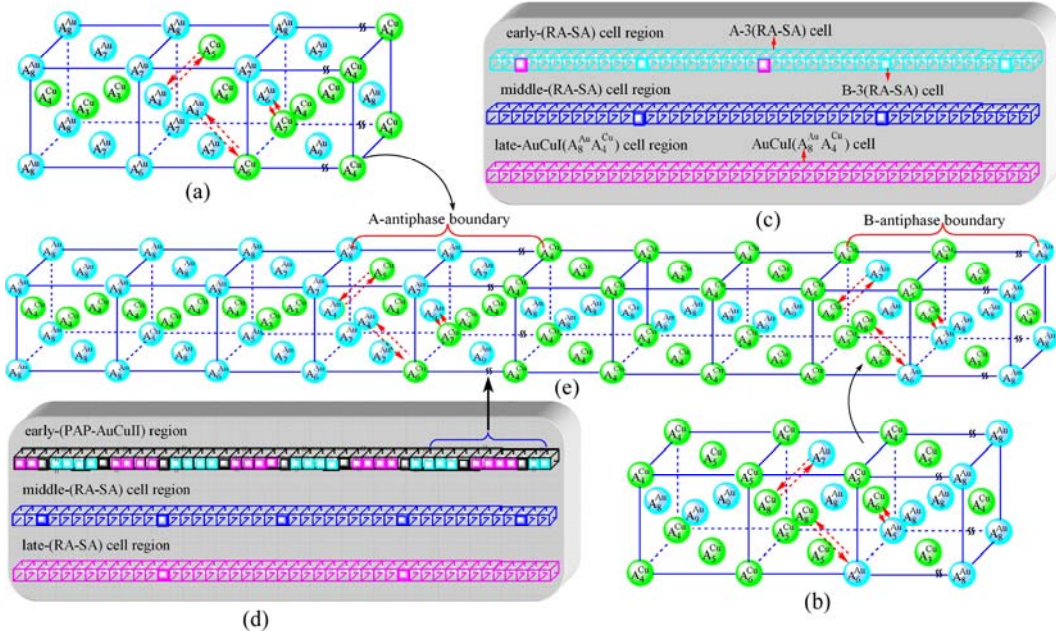


**Fig. 4** 3(RA-SA) mechanism and schemes of cell-scale and region-scale heterogeneities on disordering  $\text{AuCuI}(A_8^{\text{Au}} A_4^{\text{Cu}})$ : (a) AG arranging structure after A-manner alternating in 3(RA-SA) mechanism of three  $A_8^{\text{Au}} - A_4^{\text{Cu}}$  pairs in a single cell; (b) AG arranging structure after B-manner alternating in 3(RA-SA) mechanism of three  $A_4^{\text{Cu}} - A_8^{\text{Au}}$  pairs in a single cell; (c)  $\text{AuCu}(\text{H})$  alloy containing three regions with cell-scale heterogeneity; (d) PTP-[ $\text{AuCu}(\text{H}) + \text{PAP-AuCuII}$ ] alloy containing three regions with region-scale heterogeneity; (e) AG arranging structure of a early SPAP-AuCuII cell

intended to convey the impression that they are two heterogeneous subequilibrium regions with the same composition, different order degrees, and belong to the ordered  $\text{AuCu}$ -type sublattice phase, and that their mean properties may be calculated by the AG-Gibbs partition function of the ordered  $\text{AuCu}$ -type sublattice phase. However, their relationship cannot be described by different equilibrium thermodynamic functions of two phases.

When  $650 \text{ K} < T < 683 \text{ K}$  and  $0.925 > \sigma > 0.807$ , it is the mature period of the SPAP-AuCuII alloy. During this period, the  $\text{AuCu}(\text{H})$  regions are transferred into the SPAP-AuCuII regions (Figs. 3(e) and (f)). Therefore, the SPAP-AuCuII alloy containing early-, middle- and late-SPAP-AuCuII regions periods is a statistic periodic antiphase structure stacking of incommensurate tetragonal cells containing more  $A_8^{\text{Au}}$  and  $A_4^{\text{Cu}}$  alloy genes and antiphase boundary  $n(\text{RA-SA})$  cells containing less  $A_8^{\text{Au}}$  and  $A_4^{\text{Cu}}$  alloy genes along  $b$  axis. It has no strict long periodic cell. The number  $M$  of cells between two successive antiphase boundaries is only an average, which is about 5.

4) When  $0.807 \geq \sigma_s \geq 0.786$ , it is the jumping period of the SPAP-AuCuII alloy. In this period, there are the maximum concentration emergent phenomena of jumping alloy genes associated with jumping order degrees of the alloy. The jumping  $T_j$ -temperature is determined by the jumping order degree together with

superheated driving Gibbs energy. As  $\sigma_j=0.807$ ,  $x_9^{\text{Au}}$  and  $x_3^{\text{Cu}}$  display the maximum emergent phenomenon:  $x_9^{\text{Au}}=x_3^{\text{Cu}}=6.515\%$ . As  $\sigma=0.786$ ,  $x_7^{\text{Au}}$  and  $x_5^{\text{Cu}}$  display the “maximum emergent phenomenon”,  $x_7^{\text{Au}}=x_5^{\text{Cu}}=13.458\%$  (Figs. 3(g) and (h)). Therefore, there exists an experimental jumping  $\sigma_j$ -order degree. The  $A_7^{\text{Au}}$  and  $A_9^{\text{Au}}$  are in close vicinity to  $A_8^{\text{Au}}$ , the  $A_3^{\text{Cu}}$  and  $A_5^{\text{Cu}}$  are in close vicinity to  $A_4^{\text{Cu}}$ . They may be called the jumping alloy genes. As the  $\sigma_s$ -order degree is less than the  $\sigma_j$ -order degree, the disordering begins to translate from a single splitting of the  $A_8^{\text{Au}}$  and  $A_4^{\text{Cu}}$  stem alloy genes to a universal splitting of the stem and jumping alloy genes, which is an essential condition to happen a discontinuous jump change from the high order degree SPAP-AuCuII to the low order degree  $\text{AuCu}(\text{L})$  via complex  $n(\text{RA-SA})$  mechanism and induced fission mechanism, as well as AVA mechanism.

Therefore, the jumping  $T_j$ -temperature is arisen from jumping order degree at the beginning split of the jumping alloy genes. At the jumping temperature  $T_j=683 \text{ K}$ , the SPAP-AuCuII alloy with high order degree ( $\sigma_j=0.807$ ) jumps into the  $\text{AuCu}(\text{L})$  alloy with low order degree ( $\sigma=0.4545$ ) (Fig. 1(d), Figs. 3(g) and (h), Tables B.1 and B.2 in Appendix B). After the  $T_j$ -temperature, the  $\text{AuCu}(\text{L})$  alloy continuously transforms into the disordered  $\text{AuCu}(\text{D})$  alloy by various  $n(\text{RA-SA})$

mechanisms and AVA mechanism. The  $T_j$ -temperature measured under dynamic heat treatment shows an unexpected retrograde shift to lower temperatures upon increasing the heating rate. This retro-effect has been explained by jumping order degree (see next section). Therefore, the heterogeneous subequilibrium successive transitions on disordering stoichiometric AuCuI ( $A_8^{Au} A_4^{Cu}$ ) by slow heating rate are as follows: AuCuI ( $A_8^{Au} A_4^{Cu}$ ) → AuCu(H) → PTP-AuCu → SPAP-AuCuII → AuCu (L) → AuCu(D), of which the kinetic behaviors are closely related to heating rates.

## 7 Essence of retro-effect

Figure 5 shows that the temperature dependent  $\alpha(T)$  curves of the derivatives of the resistance  $R(T)$  functions obtained by dynamic in situ resistometry can describe dynamic behaviors on disordering AuCuI ( $A_8^{Au} A_4^{Cu}$ ) with increasing heating rates.

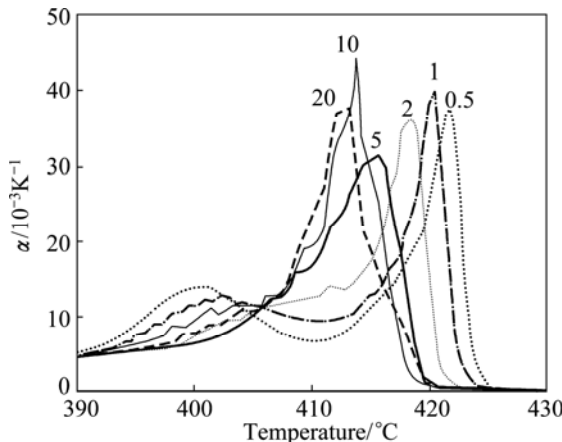


**Fig. 5** Temperature dependence of  $\alpha(T)$  curves for heating rates  $v_H=20, 10, 5, 2, 1$  and  $0.5 \text{ K}/\text{min}$  [5]

- 1) The beginning temperature  $T_{onset}$  on disordering AuCuI ( $A_8^{Au} A_4^{Cu}$ ) increases, and it is a normal effect.
- 2) The top temperature  $T_H$  of the first  $\alpha_H(T)$  peak associated with the AuCu(H) → SPTP-AuCu transition (at about  $\sigma_s=0.925$ ) increases.
- 3) The top jumping  $T_j$ -temperature of the second  $\alpha_j(T)$  peak associated with the SPAP-AuCuII(H) → AuCu(L) transition (occurred at about  $\sigma_j=0.807$ ) decreases, the temperature interval between the  $T_H$  and  $T_j$  temperatures reduces, and the width (integrated area) of  $\alpha_j(T)$  peak increases. It is a so-called retro-effect.

The retro-effect of the jumping  $T_j$ -temperature is arisen from the jumping  $\sigma_j$ -order degree. Its kinetic behaviors may be explained by the jumping order degree  $\sigma_j=0.807$  together with superheated driving Gibbs energy, based on the isothermal mixed Gibbs energy  $\Delta G_T^m - \sigma$  equilibrium network path chart (Figs. 6 and 7):

- 1) The position  $D(0.668, 683, -9435.46)$  on the

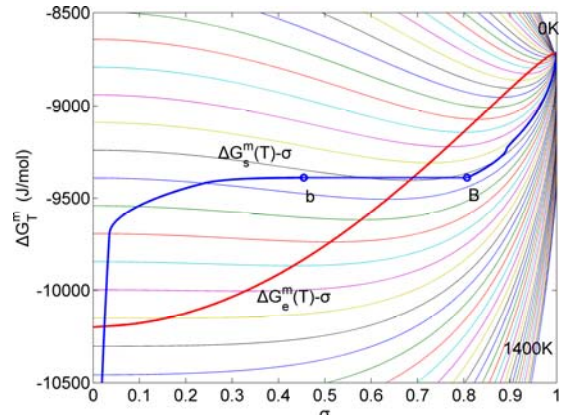


**Fig. 6** Partly isothermal  $\Delta G_T^m - \sigma$  network path charts with equilibrium  $\Delta G_e^m(T) - \sigma$  path and subequilibrium  $\Delta G_s^m(T) - \sigma$  path on disordering AuCuI ( $A_8^{Au} A_4^{Cu}$ ) drawn by steps  $\Delta T=25 \text{ K}$ ,  $\Delta \sigma=0.001$

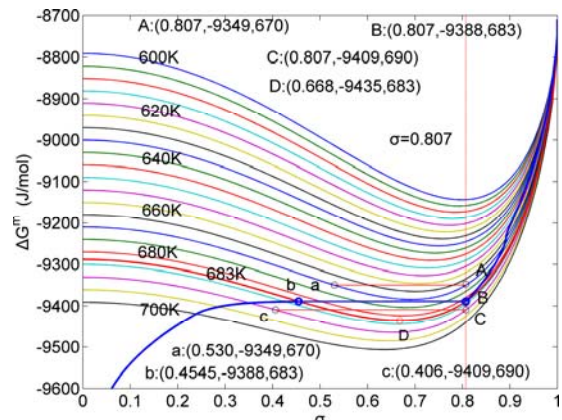


**Fig. 7** Influence of heating rate on jumping  $T_j$ -temperature and form of jumping peak

isothermal  $\Delta G_{683}^m - \sigma$  equilibrium path indicates  $\sigma_D=0.668$ ,  $T_D=683 \text{ K}$ ,  $\Delta G_D^m = -9435.46 \text{ J/mol}$ , which is the stable state standard of the AuCu alloy with the minimal mixed Gibbs energy at 683 K.

2) The jumping position  $B(0.807, 683, -9388)$  on the  $\Delta G_s^m - \sigma$  subequilibrium path with heating  $v_B$ -rate indicates  $\sigma_B=0.807$ ,  $T_{j,B}=683 \text{ K}$ ,  $\Delta G_{j,B}^m = -9388 \text{ J/mol}$ . It is the metastable state of the AuCu alloy at the 683 K, because  $\Delta G_D^m (-9435.46 \text{ J/mol}) < \Delta G_{j,B}^m (-9388 \text{ J/mol})$ .

3) As the heating rate  $v_A > v_B$ , the jumping position  $A(0.807, 670, -9349)$  on the  $\Delta G_s^m - \sigma$  subequilibrium path with heating  $v_A$ -rate should be higher than the jumping position  $B(0.807, 683, -9388)$ , i.e.,  $T_{j,A}(670 \text{ K}) < T_{j,B}(683 \text{ K})$ , because it has less stability (i.e., larger superheated driving Gibbs energy) than the  $B$ -position:  $\Delta G_{j,A}^m (-9349 \text{ J/mol}) > \Delta G_{j,B}^m (-9388 \text{ J/mol})$ . Its part width (or integrated area) before the  $T_{j,A}$ -temperature of the second jumping peak increases, because the more order degree partly checked during the AuCuI(H) → PTP-[AuCuI(H)+PAP-AuCuII] period occurs transition, in order to meet the essential jumping condition  $\sigma_j=0.807$ .

As the heating rate  $v=20$  K/min, the first jumping peak cannot be observed.

4) As the heating rate  $v_C < v_B$ , the jumping position  $C(0.807, 690, -9409)$  should be lower than the jumping position  $B(0.807, 683, -9388)$ , i.e.,  $T_{j,C}(690 \text{ K}) > T_{j,B}(683 \text{ K})$ , because it has higher stability (i.e., smaller superheated driving Gibbs energy) than  $B$ -position:  $\Delta G_{j,C}^m(-9409 \text{ J/mol}) < \Delta G_{j,B}^m(-9388 \text{ J/mol})$ . Its part width before the  $T_{j,C}$ -temperature of the second jumping peak should decrease, because the less order degree partly checked during the  $\text{AuCuI(H)} \rightarrow \text{PTP}[\text{AuCuI(H)} + \text{PAP-AuCuII}]$  period occurs transition, in order to meet the necessary jumping condition  $\sigma_j = 0.807$ .

5) Due to balances between  $A$  and  $a$ ,  $B$  and  $b$ ,  $C$  and  $c$  positions, their order degrees in the low ordered  $\text{AuCu(L)}$  alloys are respectively  $\sigma_a$  (0.530),  $\sigma_b$  (0.4545) and  $\sigma_c$  (0.4060). Therefore, the part width after the  $T_j$ -temperature of the second jumping peak increases with increasing heating rate.

## 8 Discussion

### 8.1 Discussion on alloy gene

While forming alloy by pure elements, it is a fact without dispute that the component atomic states are split into the atomic state sequence due to influence of the nearest coordinative configurations. Therefore, in the FCC-based lattice  $\text{Au-Cu}$  system, the central characteristic atom  $A_i^{\text{Au}}$ - and  $A_i^{\text{Cu}}$ - sequences respectively in the basic coordination cluster  $B_i^{\text{Au}} = A_i^{\text{Au}} \cdot [(I-i)\text{Au} + i\text{Cu}]$  and  $B_i^{\text{Cu}} = A_i^{\text{Cu}} \cdot [(I-i)\text{Au} + i\text{Cu}]$  sequences should be taken as basic structure unit sequences. Here,  $I$  is the coordinative number and is equal to 12,  $i$  is the number of Cu-atoms and can change from 0 to 12. A characteristic atom is the smallest structure unit of alloy phase level. A biological gene is defined as a basic structure unit to carry and transmit genetic information. Analogously, with the biological gene, an alloy gene is defined as a characteristic atom to carry and transmit structure and properties information: the coordinative configuration of its coordinative cluster, the potential energy ( $E(0)$ ) and volume ( $V(0)$ ) separated out from the potential energies and volumes of pure elements and intermetallics, as well as disordered alloys obtained by experimental methods [1,10,11] or by quantum mechanical ab initio calculation (QMAC) method [12], and then the valence electron structure ( $\psi(0)$ ), cohesive energy ( $E_{c,i}$ ), potential energy curve ( $W(r)$ ), Debye temperature ( $\theta_i$ ) and bulk modulus ( $B_i$ ), as well as a set of temperature-dependent thermodynamic properties: the generalized vibration heat capacity ( $c_{p,i}^v(T)$ ), which includes Debye vibration heat capacity ( $c_{p,i}^D(T)$ ) and attaching vibration heat capacity ( $c_{p,i}^E(T)$ );

the generalized vibration energy ( $U_i^v(T)$ ), which includes Debye vibration energy ( $U_i^D(T)$ ) and attaching vibration energy ( $U_i^E(T)$ ); the generalized vibration entropy ( $S_i^v(T)$ ), which includes Debye vibration entropy ( $S_i^D(T)$ ) and attaching vibration entropy ( $S_i^E(T)$ ); the enthalpy ( $H_i(T)$ ), which includes a temperature-independent potential energy ( $E(0)$ ) and generalized vibration energy ( $U_i^v(T)$ ); the generalized vibration free energy ( $X_i^v(T)$ ), which includes the generalized vibration energy ( $U_i^v(T)$ ) and generalized vibration entropy energy ( $TS_i^v(T)$ ); and the Gibbs energy ( $G_i(T)$ ), which may be described by potential energy ( $E_i(0)$ ) and generalized vibration free energy ( $X_i^v(T)$ ) or by enthalpy ( $H_i(T)$ ) and generalized vibration entropy energy ( $TS_i^v(T)$ ). The attaching vibration energy includes contributions of electron excitation energy, energy of formation of holes and variations of potential energy  $E(0)$  and thermal expansion work ( $PV(T)$ ) of volume with temperature, which are obtained by the AG-valence bond theory and thermodynamics of characteristic crystals [1,13], which includes valence bond theory of pure metals [14–16]. Therefore, the alloy gene, characteristic atom and characteristic crystal are synonym.

Up to now, scientists of QMAC-community have still adopted “quantum state electrons” as structure units to carry energies and space distribution information; and scientists of calculation of phase diagrams (CALPHAD) community have got used to taking “component atoms”, “component atom pairs” and “component atom clusters” as structure units to carry interaction energies. The limitations of the currently used solution models in QMAC and CALPHAD communities are attributed to the fact that these structure units carry very few information.

The “materials genome” was given a rather vague definition in US president Obama’s announcement about the “Materials Genome Initiative” to accelerate advanced materials discovery and deployment in the United States [17]. Recently, the CALPHAD-founder and his cooperator argued that “the materials genome should be defined as a set of information (database) allowing prediction of a materials structure, as well as its response to processing and usage conditions” [18]. Obviously, this “material genome” to represent a set of information (databases) has nothing in common with the biological genome to represent basic structure units to carry and transmit genetic information.

### 8.2 Discussion on Gibbs free energy function

In the alloy gene arranging (AGA)-statistic thermodynamics of the SMMS framework, the AGA-Gibbs free energy function  $G(x, T, \sigma)$  is derived from the AGA-Gibbs free energy partition function,

which describes the relation of AG-characteristic Gibbs free energy  $G_i(T)$ -levels and AG-concentrations  $x_i^{\text{Au}}(x, T, \sigma)$  and  $x_i^{\text{Cu}}(x, T, \sigma)$  occupied at the  $G_i(T)$ -levels. The  $G_i(T)$  is a complex function, i.e.,  $G_i(T, E_i, \theta_i, c_{p,i}^D, c_{p,i}^E, U_i^D, U_i^E, X_i^D, X_i^E, H_i, X_i^y)$ . If the vibration energy is neglected, the AGA-Gibbs free energy partition function becomes the AGA-potential free energy partition function, from which only the AGA-potential free energy function  $E(x, T, \sigma)$  can be derived [12]. The equilibrium minimal mixed Gibbs free energy  $\Delta G_{\min}^m - T$  path on disordering AuCuI ( $A_8^{\text{Au}}A_4^{\text{Cu}}$ ) compound, which is the standard path for studying subequilibrium  $\Delta G_s^m - T$  path, can be obtained only by  $G(x, T, \sigma)$  function, not by  $E(x, T, \sigma)$  function.

In the QMAC-thermodynamics, the QMAC-Gibbs free energy function is obtained by combining the QMAC-potential energies of some pure metals and intermetallics with the cluster variation method [19]. Because the vibration energy is neglected and the basic structure units are the “component atom clusters” for calculating effective cluster interaction parameter and configurational entropy, which are questionable, the QMAC-Gibbs free energy function is the potential free energy function and can not give the equilibrium mixed Gibbs free energy  $\Delta G_{\min}^m - T$  path.

In the CALPHAD-thermodynamics, the CALPHAD-Gibbs free energy function contains a number of unknown parameters. These parameters may be adjusted until the G-function is capable of representing the chosen information well. For the Au-Cu system, the chosen information about that the assessed experiment  $\Delta H^m - T$  path on disordering AuCu compound is erroneously considered the equilibrium path, the experimental jumping  $T_j$ -temperature is erroneously considered the assessed  $T_c$ -critical temperature of the order-disorder equilibrium transition, and that the composition-dependent  $T_j(x)$ -experimental temperatures are erroneously considered as the composition-dependent  $T_c(x)$ - critical temperatures. Therefore, the CALPHAD-Gibbs free energy function for Au-Cu system, the calculated  $\Delta G_{\min}^m - T$  and  $\Delta H^m - T$  paths on disordering AuCu compound and the assessed Au-Cu phase diagram obtained by fitting to these erroneous knowledge information are crude [20,21]. Therefore, the CALPHAD-field was criticized by both experimentalists and theoreticians. “The former thought that it was based on questionable data and the latter that the theoretical analysis was too crude [19].” We think that the QMAC and CALPHAD communities have still adopted erroneous knowledge to experimental data and have not found the materials genome having analogy to biological genome for establishing materials gene arranging Gibbs free energy partition function. The QMAC- and

CALPHAD-Gibbs free energy functions were established by “component atoms”, “component atom pairs” and “component atom clusters” to carry very few information, which are incomplete structure unit sequences [12].

### 8.3 Discussion on equilibrium and subequilibrium paths

According to the AGA-Gibbs free energy function and the essential definition of equilibrium order-disorder transition, the calculated equilibrium  $\Delta G_{\min}^m - T$  path is a standard for studying subequilibrium path: 1) All subequilibrium  $\Delta G_s^m - T$  paths calculated based on experimental  $\Delta H_s^m - T$  paths obtained by various heating and cooling rates are higher than  $\Delta G_{\min}^m - T$  path. 2) The concept of thermal hysteresis effect has been spread. The thermal hysteresis driving Gibbs energy at each temperature on the  $\Delta G_s^m - T$  path may be calculated:  $\Delta G_h(T) = \Delta G_{\min}(T) - \Delta G_s(T)$ . We have discovered that all experimental order→disorder paths by any heating rates belong to subequilibrium ones, even by extremely heating rates, because the AG-potential well depths greatly surpass superheated driving Gibbs energy and AG-vibration energies. For example,  $T_{\text{onset}}=593$  K,  $E_8^{\text{Au}}=-378357$  J/mol,  $U_8^{\text{Au,v}}=13619$  J/mol,  $|E_8^{\text{Au}}-U_8^{\text{Au,v}}|=364738$  J/mol,  $E_4^{\text{Cu}}=-343136$  J/mol,  $U_4^{\text{Cu,v}}=12655$  J/mol,  $|E_4^{\text{Cu}}-U_4^{\text{Cu,v}}|=330480$  J/mol,  $\Delta G_h^m = \Delta G_{\min}^m - \Delta G_{\sigma=1}^m = -373$  J/mol. It means that this transition needs a special atom movement mechanism together with superheated driving Gibbs energy. 3) The  $T_c$ -critical temperature of the equilibrium order-disorder transition may be defined as the cross point of the  $\Delta G_{\min}^m - T$  and  $\Delta G_{\sigma=0}^m - T$  lines. 4) We can prove that the so-called equilibrium  $\Delta G_{\min}^m - T$  paths calculated by the QMAC- and CALPHAD-Gibbs free energy functions, which are obtained through fitting to erroneous knowledge information about that the assessed experimental  $\Delta H_s^m - T$  path is erroneously considered the equilibrium path and that the assessed experimental jumping  $T_j$ -temperature is erroneously considered the  $T_c$ -critical temperature, are higher than the  $\Delta G_{\min}^m - T$  path calculated by AGA-Gibbs free energy function.

The calculated  $x_i^{\text{Au}} - T - i$  and  $x_i^{\text{Cu}} - T - i$ ,  $x_i^{\text{Au}} - T - \sigma$  and  $x_i^{\text{Cu}} - T - \sigma$  path charts of equilibrium and subequilibrium order→disorder transitions are of great significance: 1) The essential definitions of equilibrium and subequilibrium order→disorder transitions have been given. 2) The A-manner 3(RA-SA) and B-manner 3(RA-SA) mechanisms have been discovered. The 3(RA-SA) cells are the nuclei of disordering AuCuI ( $A_8^{\text{Au}}A_4^{\text{Cu}}$ ) compound. The SPAP-AuCuII may be explained by nucleation heterogeneity of the A- and B-manner 3(RA-SA)

mechanisms and their growing heterogeneity of the complex  $n$ (RA-SA) mechanism. 3) The single splitting of the  $A_8^{\text{Au}}$  and  $A_4^{\text{Cu}}$  stem alloy genes have been discovered. 4) The emergent phenomenon and jumping  $\sigma_j$ -order degree of the  $A_7^{\text{Au}}$ ,  $A_9^{\text{Au}}$ ,  $A_3^{\text{Cu}}$  and  $A_5^{\text{Cu}}$  jumping alloy genes have been discovered. The essence of the jumping  $T_j$ -temperature is that the disordering begins to translate from a single splitting of the  $A_8^{\text{Au}}$  and  $A_4^{\text{Cu}}$  stem alloy genes to the universal splitting of the jumping alloy genes together with the stem alloy genes. The retro-effect of the jumping  $T_j$ -temperature may be explained by the jumping order degree together with superheated driving Gibbs energy. These advantages are attributed to that the AGA-Gibbs free energy partition function is established based on two rules: 1) The structural units used for calculating configuration entropy should be in agreement with the structural units used for calculating corresponding energy levels. 2) The configuration entropy of each ordered alloy can change continually from the configuration entropy of the maximum order degree  $\sigma_{\max}$  state to one of the ideal disordered state, which needs not to induct any parameter. It means that we should take the ideal disordered state as the standard. However, these two rules are often neglected in the QMCA- and CALPHAD-thermodynamic models of alloy phases.

## 9 Conclusions

1) The essential definitions of equilibrium and subequilibrium order-disorder transitions are proposed, based on the AG-Gibbs energy partition function of AuCu-type ordered sublattice system. The essential on disordering  $\text{AuCuI}(A_8^{\text{Au}} A_4^{\text{Cu}})$  is that the  $A_8^{\text{Au}}$  and  $A_4^{\text{Cu}}$  stem alloy genes are split into the  $A_i^{\text{Au}}$  and  $A_i^{\text{Cu}}$  sequences in the disordered state.

2) The minimum mixed Gibbs energy  $\Delta G_{\min} - T$  path and order degree  $\sigma_e - T$  path are established by the iso-order degree (or isothermal) Gibbs energy equilibrium path method. Then, a set of the EHNP charts of thermodynamic properties are calculated by the AGA-Gibbs free energy partition function.

3) The subequilibrium order  $\sigma_s - T$  path is obtained by the experimental mixed enthalpy path method based on the iso-order degree mixed enthalpy  $\Delta H_{\sigma}^{\text{m}} - T$  equilibrium path chart. Then, a set of the SHNP charts of thermodynamic properties are calculated by the AGA-Gibbs free energy partition function.

4) The  $A_8^{\text{Au}}$  and  $A_4^{\text{Cu}}$  stem alloy genes are responsible for consisting AuCu compound, the  $A_4^{\text{Au}}$  and  $A_8^{\text{Cu}}$  signal alloy genes are responsible for finding atom movement mechanism, and the  $A_7^{\text{Au}}$ ,  $A_9^{\text{Au}}$ ,  $A_3^{\text{Cu}}$  and  $A_5^{\text{Cu}}$  jumping alloy genes are responsible for arising jumping  $T_j$ -temperature, according to the

AG-concentrations for tracking path on disordering  $\text{AuCuI}(A_8^{\text{Au}} A_4^{\text{Cu}})$ .

5) The heterogeneous subequilibrium successive transitions on disordering  $\text{AuCuI}(A_8^{\text{Au}} A_4^{\text{Cu}})$  are determined as:  $\text{AuCuI}(A_8^{\text{Au}} A_4^{\text{Cu}}) \rightarrow \text{AuCu(H)} \rightarrow \text{PTP-AuCu} \rightarrow \text{SPAP-AuCuII} \rightarrow \text{AuCu(L)} \rightarrow \text{AuCu(D)}$ , of which the kinetic behaviors related to heating rates are controlled by the RA-SA mechanism, superheated driving Gibbs energy and jumping ordering degree, as well as atom-vacancy mechanism in the high temperature.

6) We have discovered the RA-SA mechanism leading to cell-scale and region-scale heterogeneities of subequilibrium alloy phases, and the jumping order degree leading to the jumping  $T_j$ -temperature and its retro-effect.

## Appendices

### A Equilibrium and subequilibrium holographic network path (EHNP and SHNP) charts on disordering $\text{AuCuI}(A_8^{\text{Au}} A_4^{\text{Cu}})$

#### A.1 Method and results of EHNP charts

The  $\Delta G^{\text{m}} - T - \sigma$  EHNP chart with the minimal mixed Gibbs energy  $\Delta G_{\min}^{\text{m}} - T$  and corresponding equilibrium order degree  $\sigma_e - T$  paths on disordering stoichiometric  $\text{AuCuI}(A_8^{\text{Au}} A_4^{\text{Cu}})$  have been obtained (Fig. A.1). Then, a set of EHNP charts of thermodynamic properties have been calculated (Figs. A.3–A.13). These charts are calculated by the temperature step  $\Delta T = 1$  K and order degree precision in  $\Delta\sigma = \pm 0.0001$ . This method is called the equilibrium mixed Gibbs energy path method, which includes the equilibrium iso-order degree  $\Delta G_{\sigma}^{\text{m}} - T$  paths method (Fig. A.1) and the equilibrium isothermal  $\Delta G_T^{\text{m}} - \sigma$  paths method (Figs. 6 and 7).

#### A.2 Experimental mixed enthalpy $\Delta H_s^{\text{m}} - T$ path method and results of SHNP charts

Because the AG-generalized vibration energies are much smaller than their potential well depths (Appendix C), the AG-Gibbs energies ( $G_i^{\text{Au}}(T)$ ,  $G_i^{\text{Cu}}(T)$ ) can respond immediately and change synchronously with each small variation in temperature, but the AG-concentrations ( $x_i^{\text{Au}}(T)$ ,  $x_i^{\text{Cu}}(T)$ ) occupied at  $G_i^{\text{Au}}(T)$ - and  $G_i^{\text{Cu}}(T)$ -energy levels can not change synchronously. Therefore, all of measured paths on disordering  $\text{AuCuI}(A_8^{\text{Au}} A_4^{\text{Cu}})$  belong to subequilibrium, even extremely slow heating rate. Now, we have obtained the subequilibrium order degree  $\sigma_s - T$  path by “the experimental mixed enthalpy  $\Delta H_s^{\text{m}} - T$  path method”. In this method, the experimental  $\Delta H_s^{\text{m}} - T$  curve is drawn up on the equilibrium iso-order degree mixed enthalpy  $\Delta H_{\sigma}^{\text{m}} - T$  EHNP charts (Fig. A.2), and then the  $\sigma_s - T$  path can be obtained. According to the

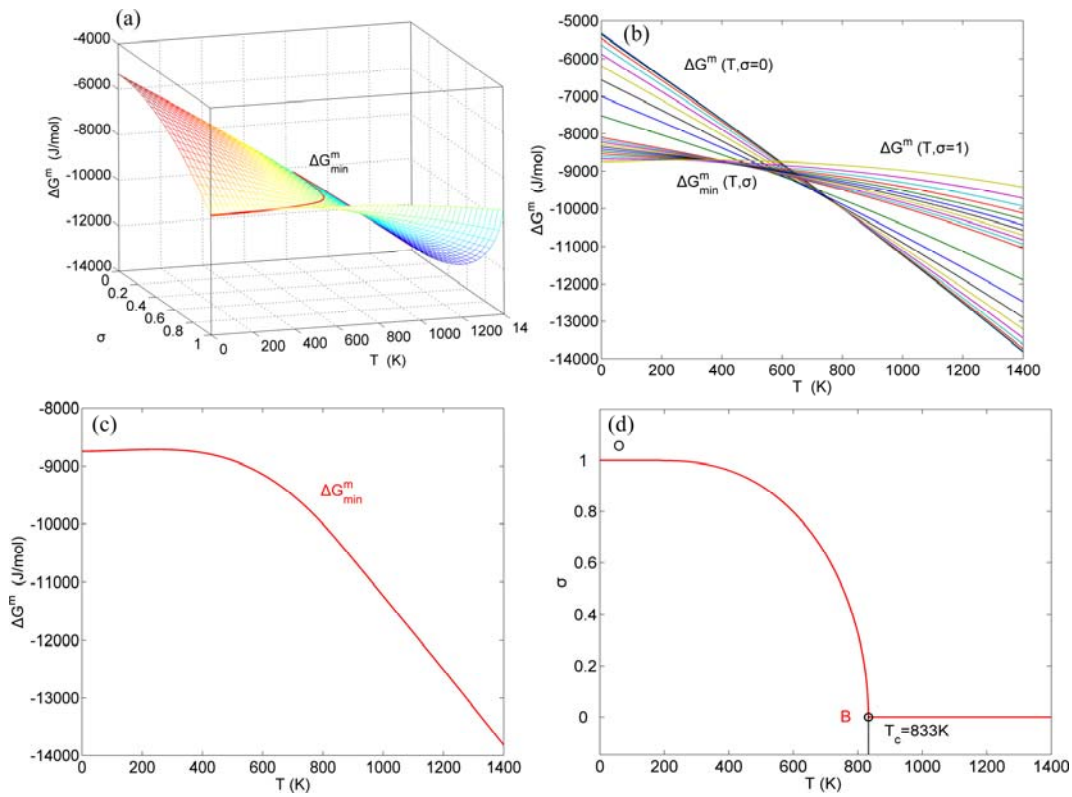


**Fig. A.1** Minimal mixed Gibbs energy equilibrium path method: (a) Three-dimensional  $\Delta G^m$  –  $T$  –  $\sigma$  EHNP chart; (b) Minimal mixed Gibbs energy  $\Delta G_{\min}^m$  –  $T$  equilibrium path obtained by iso-order degree  $\Delta G_{\sigma}^m$  –  $T$  paths method; (c) Equilibrium  $\Delta G_{\min}^m$  –  $T$  path; (d) Equilibrium  $\sigma_e$  –  $T$  path on disordering AuCuI( $A_8^{Au} A_4^{Cu}$ )

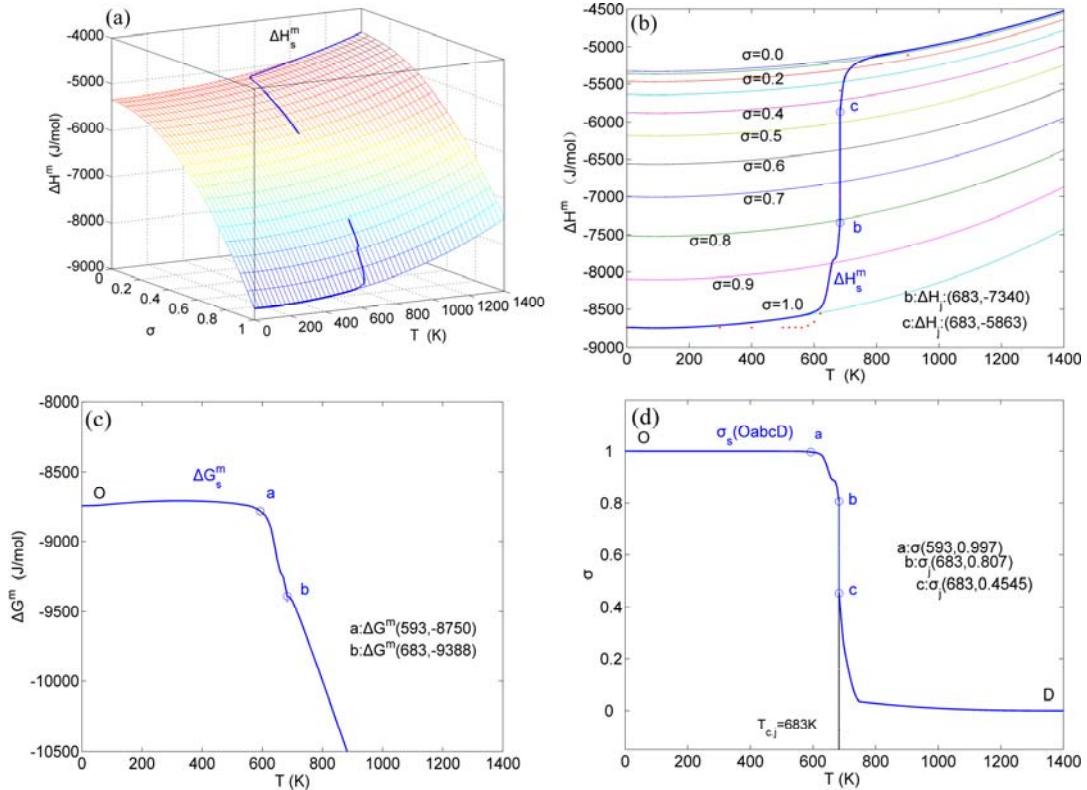


**Fig. A.2** Experimental mixed enthalpy  $\Delta H^m$  –  $T$  path method: (a) Three-dimensional  $\Delta H^m$  –  $T$  –  $\sigma$  EHNP chart with  $\Delta H_s^m$  –  $T$  path; (b) Mixed enthalpy  $\Delta H_s^m$  –  $T$  subequilibrium path drawn on equilibrium iso-order mixed enthalpy  $\Delta H_{\sigma}^m$  –  $T$  EHNP chart; (c)  $\Delta G_s^m$  –  $T$  subequilibrium path; (d)  $\sigma_s$  –  $T$  subequilibrium path on disordering AuCuI( $A_8^{Au} A_4^{Cu}$ )

$\sigma-T$  path, a set of SHNP charts of thermodynamic properties have been calculated by the AG-Gibbs energy partition function of the AuCu-type sublattice system (Figs. A.3 to A.18). These SHNP charts may be also obtained by other experimental thermodynamic

properties path methods, such as the experimental mixed volume  $\Delta V_s^m-T$  path method, based on the equilibrium iso-order degree mixed volume  $\Delta V_\sigma^m-T$  EHNP chart. These methods may be called the AG-tracking method.

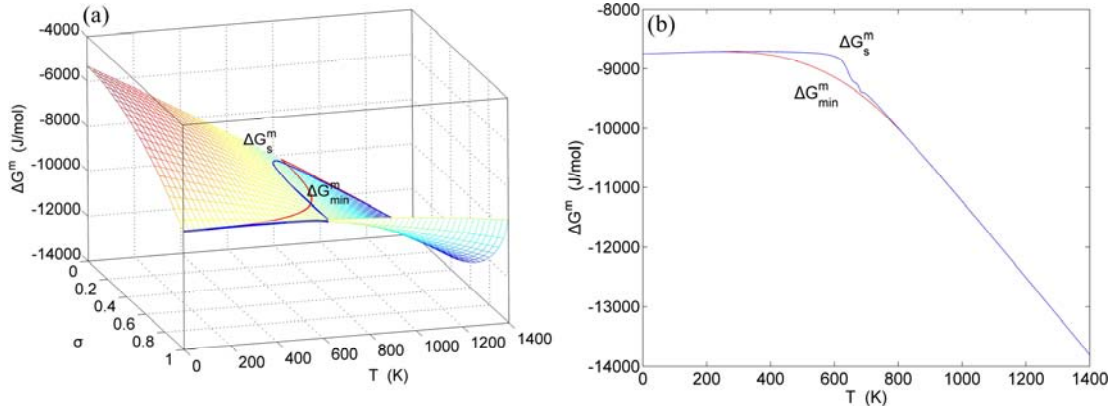


**Fig. A.3** EHNP charts with EHNP and SHNP curves of first order thermodynamic properties on disordering  $\text{AuCuI}(A_8^{\text{Au}}A_4^{\text{Cu}})$ : (a) Three-dimensional mixed Gibbs energy  $\Delta G^m-T-\sigma$  EHNP chart with  $\Delta G_e^m-T$  and  $\Delta G_s^m-T$  paths; (b)  $\Delta G_e^m-T$  and  $\Delta G_s^m-T$  paths

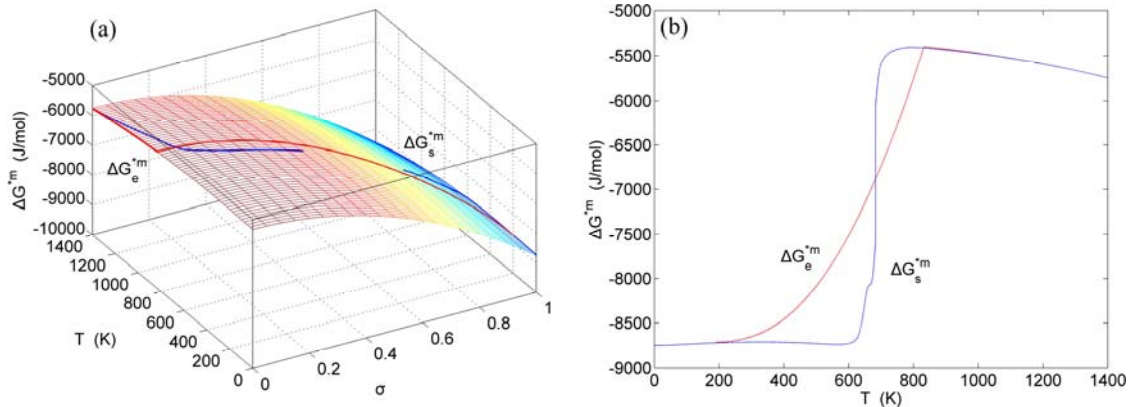


**Fig. A.4** EHNP charts with EHNP and SHNP curves of first order thermodynamic properties on disordering  $\text{AuCuI}(A_8^{\text{Au}}A_4^{\text{Cu}})$ : (a) Three-dimensional mixed characteristic Gibbs energy  $\Delta G^{*m}-T-\sigma$  EHNP chart with  $\Delta G_e^{*m}-T$  and  $\Delta G_s^{*m}-T$  paths; (b)  $\Delta G_e^{*m}-T$  and  $\Delta G_s^{*m}-T$  paths

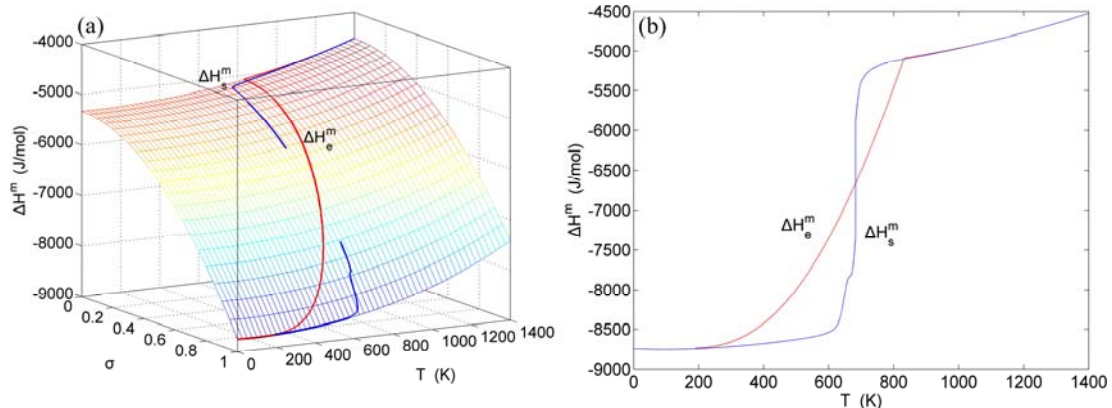


**Fig. A.5** EHNP charts with EHNP and SHNP curves of first order thermodynamic properties on disordering  $\text{AuCuI}(A_8^{\text{Au}}A_4^{\text{Cu}})$ : (a) Three-dimensional mixed enthalpy  $\Delta H^m-T-\sigma$  EHNP chart with  $\Delta H_e^m-T$  and  $\Delta H_s^m-T$  paths; (b)  $\Delta H_e^m-T$  and  $\Delta H_s^m-T$  paths

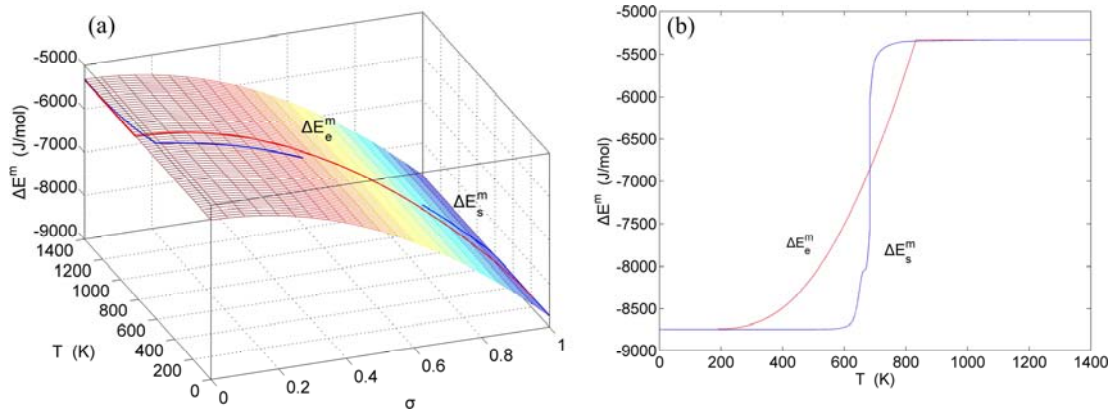


**Fig. A.6** EHNP charts with EHNP and SHNP curves of first order thermodynamic properties on disordering  $\text{AuCuI}(A_8^{\text{Au}}A_4^{\text{Cu}})$ : (a) Three-dimensional mixed potential energy  $\Delta E^m - T - \sigma$  EHNP chart with  $\Delta E_e^m - T$  and  $\Delta E_s^m - T$  paths; (b)  $\Delta E_e^m - T$  and  $\Delta E_s^m - T$  paths

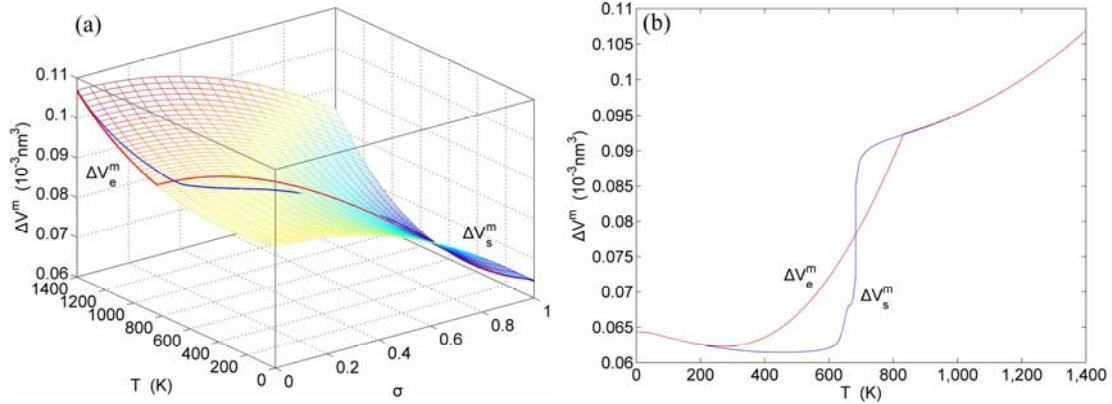


**Fig. A.7** EHNP charts with EHNP and SHNP curves of first order thermodynamic properties on disordering  $\text{AuCuI}(A_8^{\text{Au}}A_4^{\text{Cu}})$ : (a) Three-dimensional mixed volume  $\Delta V^m - T - \sigma$  EHNP chart with  $\Delta V_e^m - T$  and  $\Delta V_s^m - T$  paths; (b)  $\Delta V_e^m - T$  and  $\Delta V_s^m - T$  paths

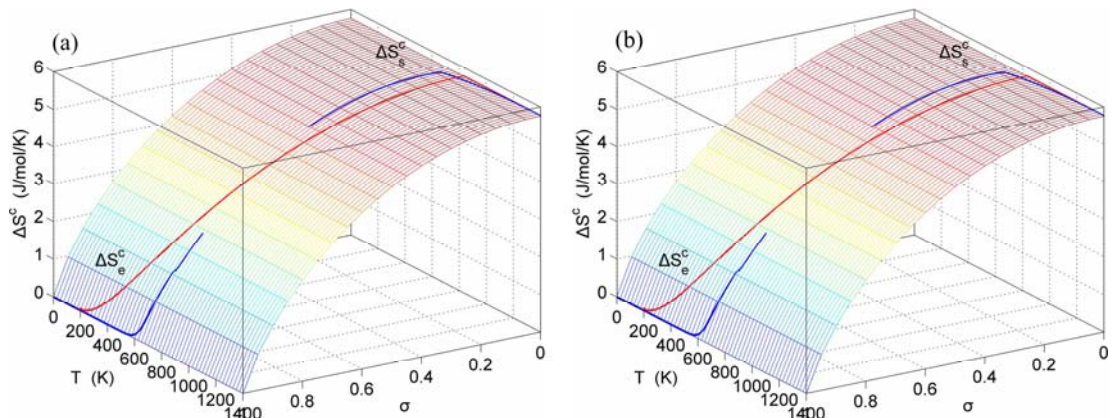


**Fig. A.8** EHNP charts with EHNP and SHNP curves of first order thermodynamic properties on disordering  $\text{AuCuI}(A_8^{\text{Au}}A_4^{\text{Cu}})$ : (a) Three-dimensional configurational entropy  $S^c - T - \sigma$  EHNP chart with  $S_e^c - T$  and  $S_s^c - T$  paths; (b)  $S_e^c - T$  and  $S_s^c - T$  paths

## B EHNP charts of AG-concentration $x_i^{\text{Au}}$ and $x_i^{\text{Cu}}$ on disordering $\text{AuCuI}(A_8^{\text{Au}}A_4^{\text{Cu}})$

The AG-concentration  $x_i^{\text{Au}}$  and  $x_i^{\text{Cu}}$  on disordering  $\text{AuCuI}(A_8^{\text{Au}}A_4^{\text{Cu}})$  may be described by two modes: 1) Three-dimensional  $x_i^{\text{Au}} - T - i$  and

$x_i^{\text{Cu}} - T - i$  EHNP charts, from which two-dimensional iso-order degree  $x_{i,\sigma}^{\text{Au}} - i$  and  $x_{i,\sigma}^{\text{Cu}} - i$  paths can be obtained, where the  $x_i^{\text{Au}}$  and  $x_i^{\text{Cu}}$  are the probabilities occupied at the  $G_i^{\text{Au}}(T)$  and  $G_i^{\text{Cu}}(T)$  energy levels in the AG-arranging band structure (Figs. B.1(a), (b), (c))

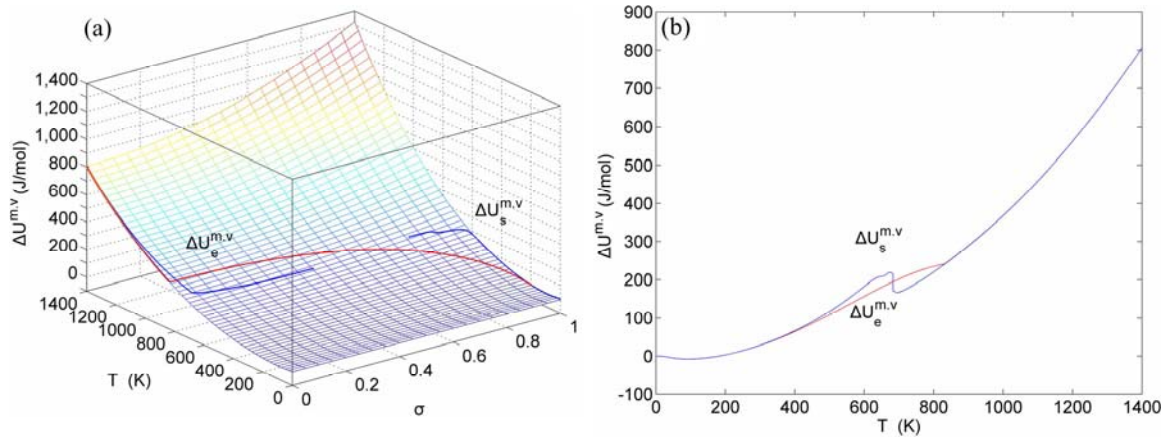


**Fig. A.9** EHNP charts with EHNP and SHNP curves of first order thermodynamic properties on disordering  $\text{AuCuI}(A_8^{\text{Au}}A_4^{\text{Cu}})$ :  
(a) Three-dimensional generalized vibration energy  $\Delta U^{\text{m.v.}} - T - \sigma$  EHNP chart with  $\Delta U_e^{\text{m.v.}} - T$  and  $\Delta U_s^{\text{m.v.}} - T$  paths;  
(b)  $\Delta U_e^{\text{m.v.}} - T$  and  $\Delta U_s^{\text{m.v.}} - T$  paths

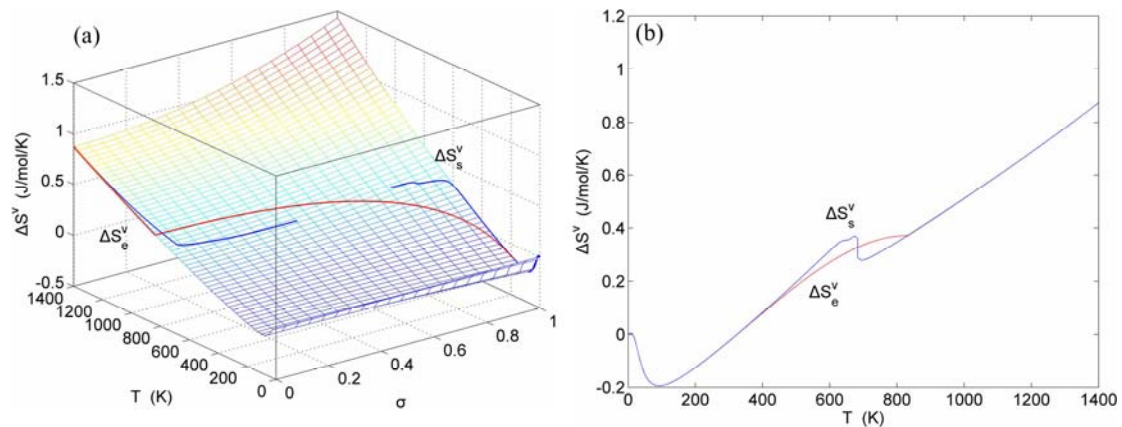


**Fig. A.10** EHNP charts with EHNP and SHNP curves of first order thermodynamic properties on disordering  $\text{AuCuI}(A_8^{\text{Au}}A_4^{\text{Cu}})$ :  
(a) Three-dimensional generalized vibration entropy  $\Delta S^{\text{v}} - T - \sigma$  EHNP chart with  $\Delta S_e^{\text{v}} - T$  and  $\Delta S_s^{\text{v}} - T$  paths; (b)  $\Delta S_e^{\text{v}} - T$  and  $\Delta S_s^{\text{v}} - T$  paths

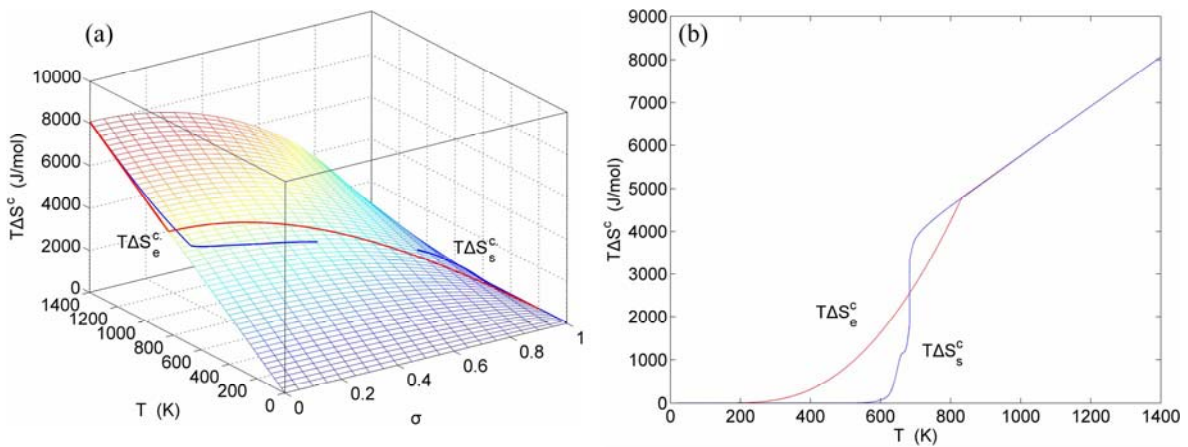


**Fig. A.11** EHNP charts with EHNP and SHNP curves of first order thermodynamic properties on disordering  $\text{AuCuI}(A_8^{\text{Au}}A_4^{\text{Cu}})$ :  
(a) Three-dimensional configurational entropy energy  $T\Delta S^c - T - \sigma$  EHNP chart with  $T\Delta S^c - T$  and  $T\Delta S^c - T$  paths; (B)  $T\Delta S^c - T$  and  $T\Delta S^c - T$  paths

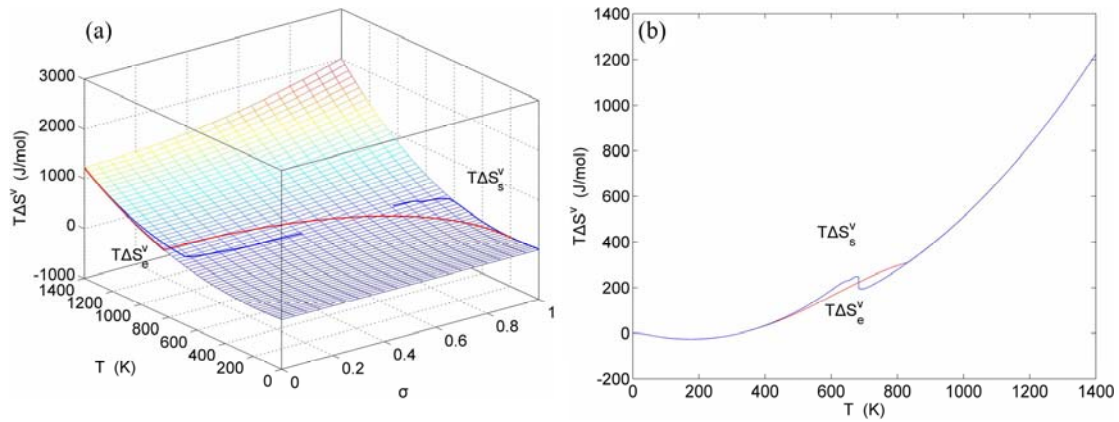


**Fig. A.12** EHNP charts with EHNP and SHNP curves of first order thermodynamic properties on disordering  $\text{AuCuI}(A_8^{\text{Au}}A_4^{\text{Cu}})$ :  
(a) Three-dimensional generalized vibration entropy energy  $T\Delta S^V - T - \sigma$  EHNP chart with  $T\Delta S_e^V - T$  and  $T\Delta S_s^V - T$  paths;  
(b)  $T\Delta S_e^V - T$  and  $T\Delta S_s^V - T$  paths

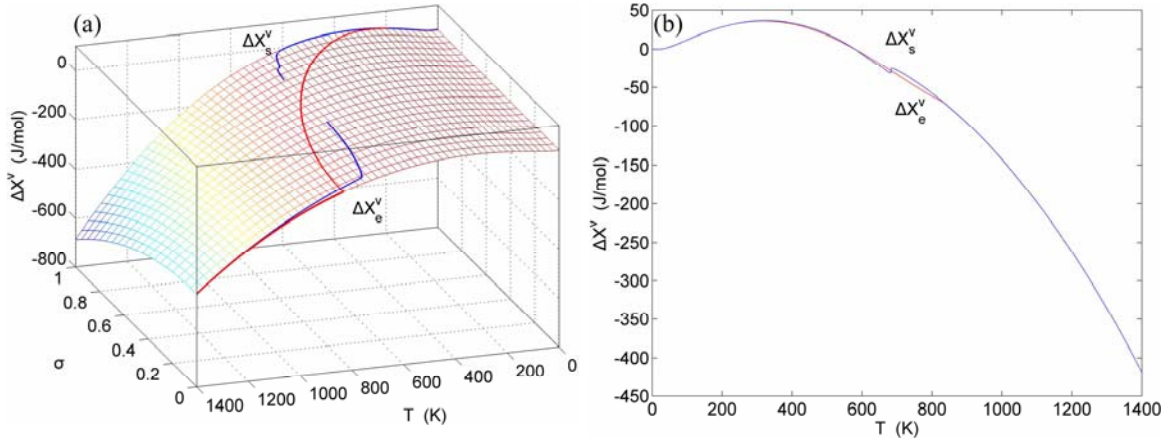


**Fig. A.13** EHNP charts with EHNP and SHNP curves of first order thermodynamic properties on disordering  $\text{AuCuI}(A_8^{\text{Au}}A_4^{\text{Cu}})$ :  
(a) Three-dimensional generalized vibration free energy  $\Delta X^V - T - \sigma$  EHNP chart with  $\Delta X_e^V - T$  and  $\Delta X_s^V - T$  paths;  
(b)  $\Delta X_e^V - T$  and  $\Delta X_s^V - T$  paths

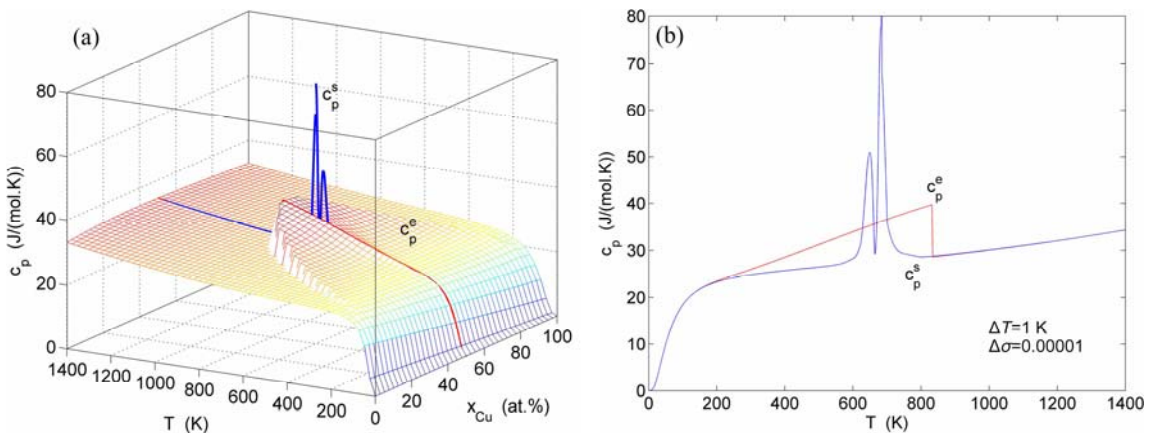


**Fig. A.14** Second order thermodynamic properties (specific heat capacity and thermal expansion coefficient) on disordering  $\text{AuCuI}(A_8^{\text{Au}}A_4^{\text{Cu}})$ : (a)  $c_p^e - T$  and  $c_p^s - T$  paths on  $c_p - x - T$  EHNP diagram; (b)  $c_p^e - T$  and  $c_p^s - T$  paths

and (d)); 2) Three-dimensional  $x_i^{\text{Au}} - T - \sigma$  and  $x_i^{\text{Cu}} - T - \sigma$  EHNP charts, from which two-dimensional  $x_i^{\text{Au}} - \sigma$  and  $x_i^{\text{Cu}} - \sigma$  paths can be obtained, where the  $x_i^{\text{Au}}$  and  $x_i^{\text{Cu}}$  are the probabilities occupied at the lattice

sites in the AG-arranging crystal structure (Figs. B.1(e), (f), (g) and (h)). The AG-concentration SHNP charts are shown in Fig. 2. Their systematic correlativities are listed in supplementary Tables B.1 and B.2.

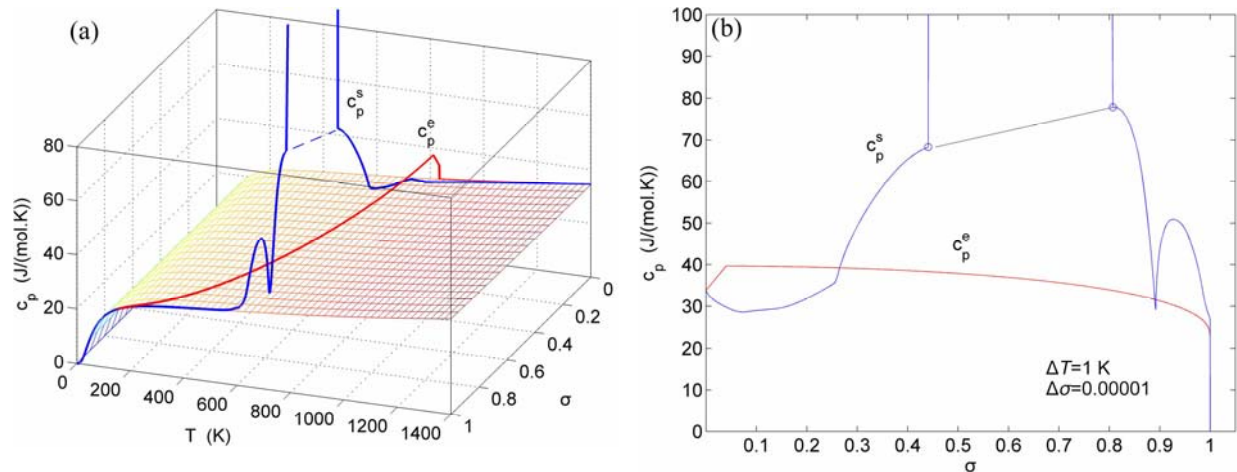


**Fig. A.15** Second order thermodynamic properties (specific heat capacity and thermal expansion coefficient) on disordering  $AuCuI(A_8^{Au}A_4^{Cu})$ : (a)  $c_p^e-T$  and  $c_p^s-T$  paths on  $c_p-T-\sigma$  EHNP chart; (b)  $c_p^e-\sigma$  and  $c_p^s-\sigma$  paths

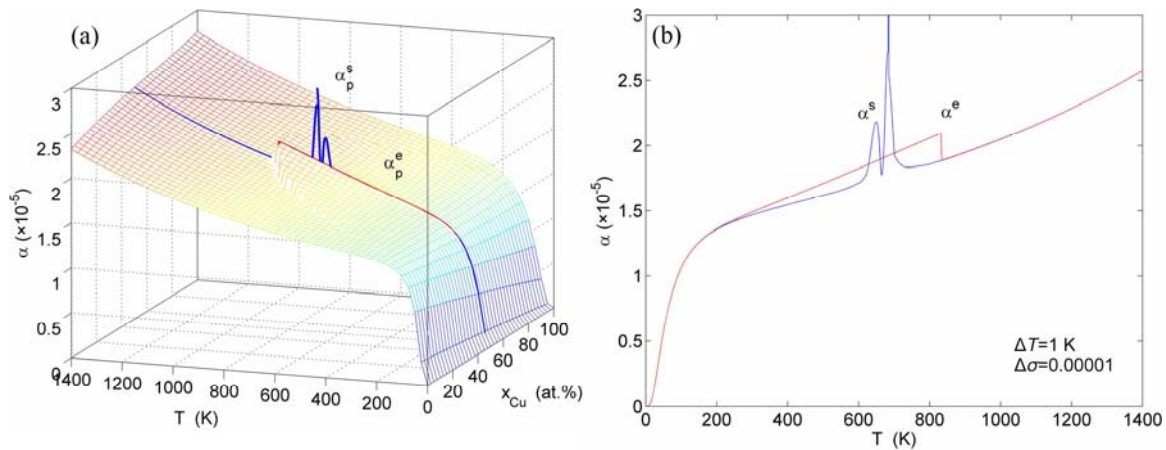


**Fig. A.16** Second order thermodynamic properties (specific heat capacity and thermal expansion coefficient) on disordering  $AuCuI(A_8^{Au}A_4^{Cu})$ : (a)  $\alpha^e-T$  and  $\alpha^s-T$  paths on the  $\alpha-x-T$  EHNP chart; (b)  $\alpha^e-T$  and  $\alpha^s-T$  paths

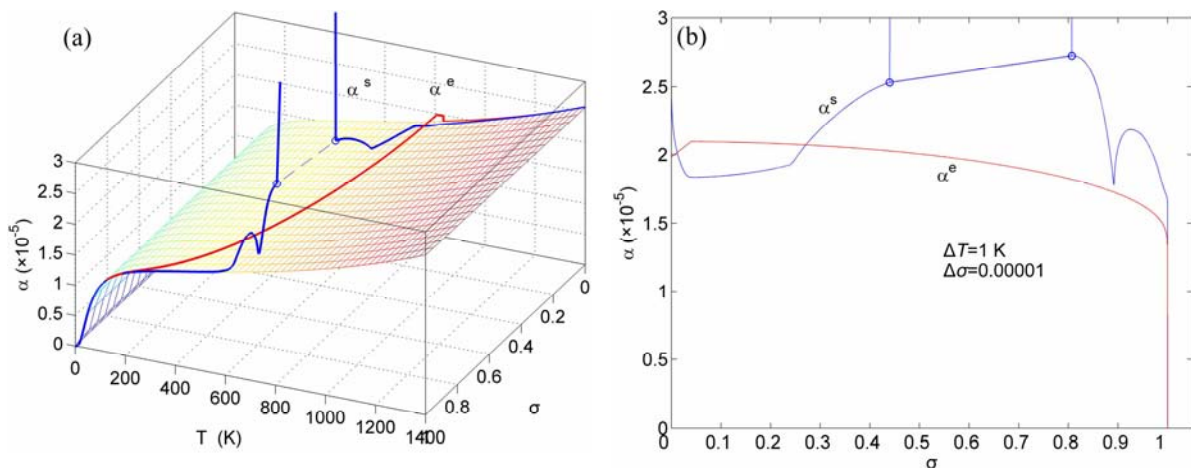


**Fig. A.17** Second order thermodynamic properties (specific heat capacity and thermal expansion coefficient) on disordering  $AuCuI(A_8^{Au}A_4^{Cu})$ : (a)  $\alpha^e-T$  and  $\alpha^s-T$  paths on  $\alpha-T-\sigma$  EHNP diagram; (b)  $\alpha^e-\sigma$  and  $\alpha^s-\sigma$  paths (These charts are calculated by temperature step  $\Delta T = 1$  K and order degree step  $\Delta \sigma = 0.00001$ )

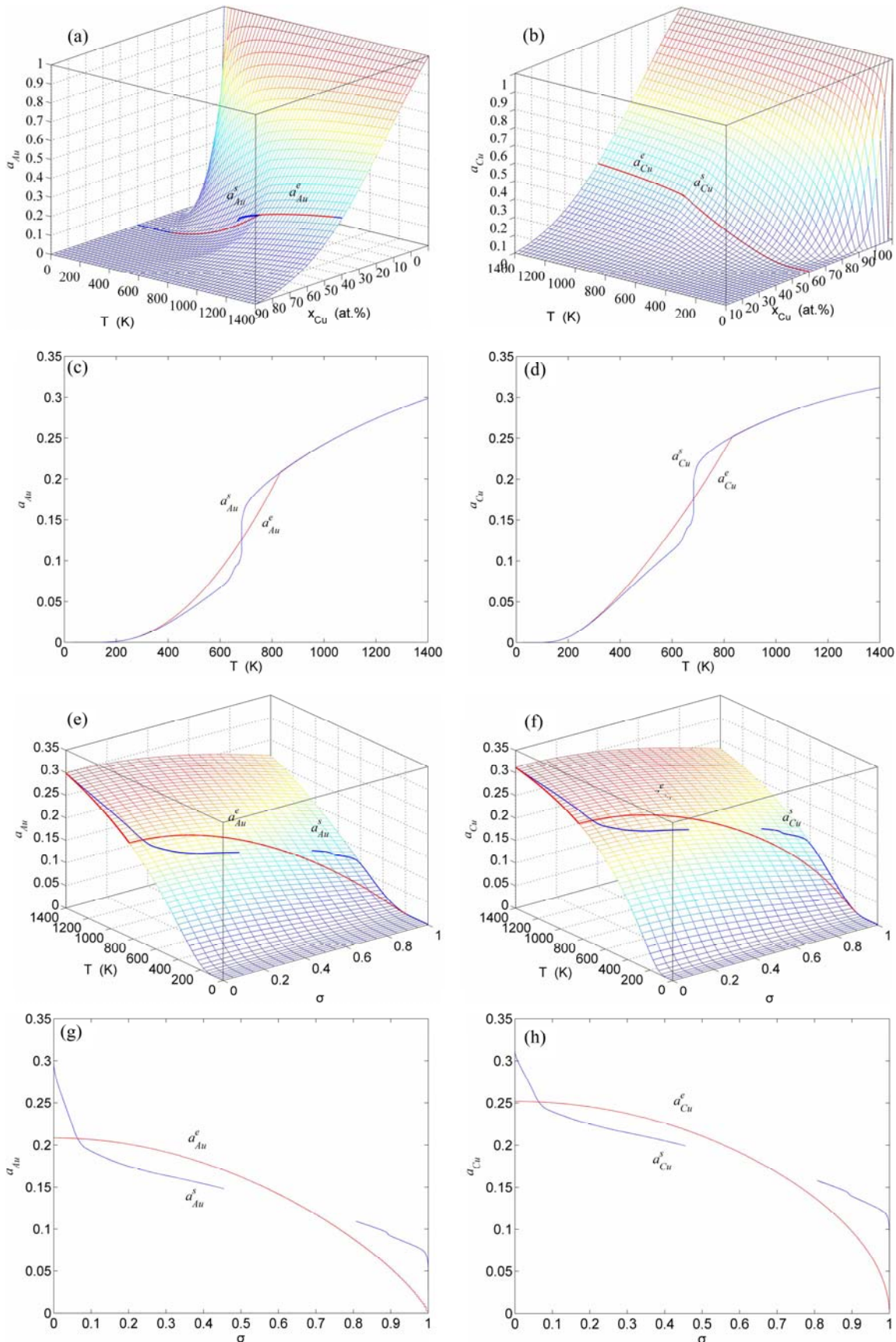


**Fig. A.18** Activities on disordering  $\text{AuCuI}(A_8\text{Au}_4\text{Cu})$ : (a), (b)  $a_{\text{Au}}^e - T$ ,  $a_{\text{Au}}^s - T$  and  $a_{\text{Cu}}^e - T$ ,  $a_{\text{Cu}}^s - T$  paths on  $a_{\text{Au}} - x - T$  and  $a_{\text{Cu}} - x - T$  EHNP diagrams; (c), (d)  $a_{\text{Au}}^e - T$ ,  $a_{\text{Au}}^s - T$  and  $a_{\text{Cu}}^e - T$ ,  $a_{\text{Cu}}^s - T$  paths on  $a_{\text{Au}} - T - \sigma$  and  $a_{\text{Cu}} - T - \sigma$  EHNP charts; (e), (f)  $a_{\text{Au}}^e - T$ ,  $a_{\text{Au}}^s - T$  and  $a_{\text{Cu}}^e - T$ ,  $a_{\text{Cu}}^s - T$  paths on  $a_{\text{Au}} - T - \sigma$  and  $a_{\text{Cu}} - T - \sigma$  EHNP charts; (g), (h)  $a_{\text{Au}}^e - \sigma$ ,  $a_{\text{Au}}^s - \sigma$  and  $a_{\text{Cu}}^e - \sigma$ ,  $a_{\text{Cu}}^s - \sigma$  paths

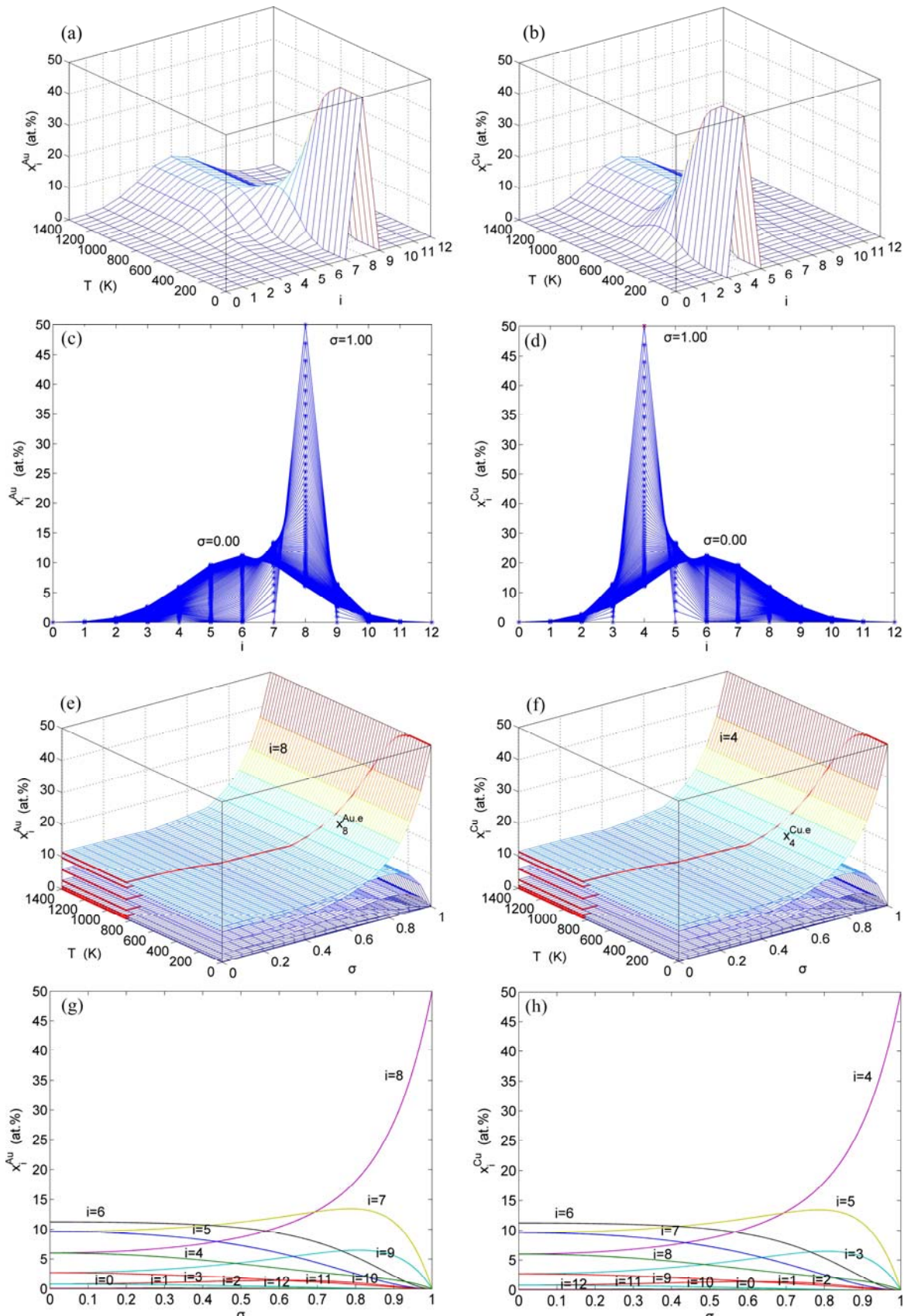


**Fig. B.1** AG-concentration EHNP charts on disordering  $\text{AuCuI}(A_8^{\text{Au}}A_4^{\text{Cu}})$ : (a), (b) Three-dimensional  $x_i^{\text{Au}} - T - i$  and  $x_i^{\text{Cu}} - T - i$  EHNP charts; (c), (d) Two-dimensional iso-order degree  $x_{i,\sigma}^{\text{Au}} - i$  and  $x_{i,\sigma}^{\text{Cu}} - i$  EHNP charts; (e), (f) Three-dimensional  $x_i^{\text{Au}} - T - \sigma$  and  $x_i^{\text{Cu}} - T - \sigma$  EHNP charts with  $x_i^{\text{Au},e} - T$  and  $x_i^{\text{Cu},e} - T$  paths; (g), (h) Two-dimensional iso-Gibbs energy level  $x_i^{\text{Au}} - \sigma$  and  $x_i^{\text{Cu}} - \sigma$  EHNP charts

**Table B.1** Systematic correlativity of equilibrium transition temperature  $T_e$ , subequilibrium transition temperature  $T_s$ , order degree  $\sigma$  and  $A_i^{\text{Au}}$  – alloy gene concentrations ( $x_i^{\text{Au}}$ ) on disordering  $\text{AuCuI}(A_8^{\text{Au}} A_4^{\text{Cu}})$  compound

$T_e/\text{K}$	$T_s/\text{K}$	$\sigma^1$	$x_0^{\text{Au}}$	$x_1^{\text{Au}}$	$x_2^{\text{Au}}$	$x_3^{\text{Au}}$	$x_4^{\text{Au}}$	$x_5^{\text{Au}}$	$x_6^{\text{Au}}$	$x_7^{\text{Au}}$	$x_8^{\text{Au}}$	$x_9^{\text{Au}}$	$x_{10}^{\text{Au}}$	$x_{11}^{\text{Au}}$	$x_{12}^{\text{Au}}$
0	0	1.000	0.000	0.000	0.000	0.000	0.000	0.000	0.000	50.000	0.000	0.000	0.000	0.000	
191	571	0.999	0.000	0.000	0.000	0.000	0.025	0.000	0.000	0.199	49.676	0.099	0.000	0.000	
227	585	0.998	0.000	0.000	0.000	0.000	0.049	0.000	0.001	0.395	49.355	0.198	0.000	0.000	
245	593	0.997	0.000	0.000	0.000	0.000	0.074	0.001	0.003	0.589	49.037	0.295	0.001	0.000	
257	600	0.996	0.000	0.000	0.000	0.001	0.098	0.002	0.005	0.781	48.722	0.391	0.001	0.000	
268	605	0.995	0.000	0.000	0.000	0.001	0.121	0.002	0.009	0.970	48.409	0.485	0.002	0.000	
277	610	0.994	0.000	0.000	0.000	0.002	0.145	0.004	0.012	1.158	48.099	0.579	0.003	0.000	
613	613	0.993	0.000	0.000	0.000	0.002	0.168	0.005	0.017	1.343	47.791	0.671	0.004	0.000	
616	616	0.992	0.000	0.000	0.000	0.003	0.191	0.006	0.022	1.525	47.486	0.763	0.005	0.000	
618	618	0.991	0.000	0.000	0.000	0.004	0.213	0.008	0.027	1.706	47.184	0.853	0.006	0.000	
304	620	0.990	0.000	0.000	0.000	0.005	0.236	0.010	0.033	1.884	46.884	0.942	0.007	0.000	
348	631	0.980	0.000	0.000	0.000	0.018	0.445	0.038	0.127	3.551	44.019	1.775	0.027	0.000	
379	636	0.970	0.000	0.000	0.001	0.038	0.630	0.085	0.271	5.021	41.386	2.509	0.057	0.001	
387	637	0.967	0.000	0.000	0.001	0.045	0.682	0.102	0.323	5.427	40.638	2.712	0.068	0.001	
403	640	0.960	0.000	0.000	0.002	0.064	0.796	0.147	0.459	6.315	38.965	3.155	0.096	0.001	
424	643	0.950	0.000	0.000	0.004	0.095	0.943	0.225	0.683	7.449	36.737	3.719	0.142	0.002	
443	646	0.940	0.000	0.000	0.006	0.130	1.075	0.317	0.936	8.440	34.687	4.211	0.194	0.004	
444	646	0.939	0.000	0.000	0.006	0.134	1.087	0.327	0.963	8.531	34.491	4.256	0.200	0.004	
459	648	0.930	0.000	0.000	0.009	0.168	1.193	0.422	1.214	9.302	32.799	4.637	0.250	0.006	
467	650	0.925	0.000	0.000	0.011	0.188	1.248	0.479	1.360	9.688	31.911	4.828	0.279	0.007	
474	651	0.920	0.000	0.000	0.013	0.209	1.300	0.539	1.510	10.048	31.059	5.004	0.309	0.009	
488	654	0.910	0.000	0.001	0.017	0.251	1.397	0.666	1.821	10.691	29.456	5.318	0.370	0.012	
501	657	0.900	0.000	0.001	0.023	0.294	1.486	0.804	2.142	11.241	27.976	5.584	0.433	0.015	
513	668	0.890	0.000	0.001	0.029	0.339	1.568	0.950	2.471	11.709	26.611	5.808	0.496	0.019	
525	673	0.880	0.000	0.001	0.036	0.384	1.644	1.104	2.804	12.103	25.349	5.993	0.559	0.023	
536	676	0.870	0.000	0.002	0.043	0.429	1.716	1.264	3.138	12.432	24.182	6.144	0.621	0.028	
546	677	0.860	0.000	0.003	0.051	0.474	1.783	1.431	3.472	12.702	23.103	6.264	0.682	0.034	
556	678	0.850	0.000	0.003	0.060	0.519	1.848	1.604	3.804	12.921	22.102	6.357	0.741	0.039	
565	679	0.840	0.000	0.004	0.070	0.564	1.910	1.780	4.131	13.095	21.175	6.426	0.798	0.045	
574	680	0.830	0.000	0.005	0.080	0.608	1.971	1.961	4.453	13.229	20.314	6.474	0.854	0.051	
583	681	0.820	0.000	0.006	0.090	0.651	2.030	2.144	4.768	13.328	19.514	6.502	0.906	0.058	
591	682	0.810	0.000	0.007	0.101	0.694	2.089	2.330	5.076	13.397	18.770	6.514	0.957	0.065	
593	683	0.807	0.000	0.007	0.104	0.706	2.107	2.386	5.166	13.412	18.557	6.515	0.971	0.067	
599	–	0.800	0.000	0.008	0.112	0.736	2.148	2.518	5.375	13.438	18.077	6.511	1.004	0.071	
606	–	0.790	0.000	0.009	0.124	0.777	2.206	2.707	5.665	13.456	17.430	6.495	1.049	0.078	
610	–	0.786	0.000	0.010	0.129	0.793	2.230	2.782	5.779	13.458	17.184	6.486	1.066	0.081	
635	–	0.750	0.001	0.015	0.173	0.935	2.445	3.464	6.731	13.354	15.239	6.332	1.199	0.107	
665	–	0.700	0.001	0.025	0.239	1.117	2.763	4.387	7.838	12.994	13.176	5.990	1.323	0.141	
692	–	0.650	0.002	0.037	0.304	1.287	3.104	5.248	8.711	12.532	11.627	5.583	1.386	0.171	
715	–	0.600	0.003	0.050	0.368	1.450	3.460	6.029	9.384	12.061	10.431	5.163	1.398	0.194	
736	–	0.550	0.004	0.063	0.430	1.608	3.820	6.719	9.893	11.623	9.486	4.759	1.374	0.209	
754	–	0.500	0.005	0.076	0.487	1.762	4.174	7.319	10.275	11.234	8.727	4.386	1.324	0.217	
771	683	0.4545	0.006	0.088	0.536	1.897	4.477	7.785	10.534	10.929	8.167	4.082	1.265	0.218	
783	687	0.400	0.008	0.101	0.591	2.055	4.822	8.267	10.771	10.611	7.608	3.752	1.185	0.213	
795	690	0.350	0.009	0.111	0.637	2.190	5.103	8.628	10.927	10.372	7.198	3.494	1.109	0.205	
805	694	0.300	0.010	0.120	0.679	2.313	5.350	8.925	11.042	10.173	6.866	3.274	1.037	0.194	
814	699	0.250	0.010	0.128	0.716	2.422	5.561	9.164	11.127	10.012	6.600	3.091	0.971	0.183	
821	706	0.200	0.011	0.135	0.747	2.514	5.734	9.352	11.188	9.885	6.392	2.943	0.913	0.171	
826	715	0.150	0.012	0.140	0.772	2.588	5.869	9.493	11.230	9.788	6.236	2.829	0.867	0.161	
829	724	0.100	0.012	0.144	0.791	2.642	5.966	9.591	11.258	9.721	6.127	2.749	0.833	0.153	
832	738	0.050	0.012	0.146	0.802	2.675	6.023	9.649	11.274	9.681	6.064	2.701	0.813	0.148	
833	1357	0.000	0.012	0.146	0.806	2.686	6.042	9.668	11.279	9.668	6.042	2.686	0.806	0.146	

1): The  $\sigma$  denotes  $\sigma_e$  corresponding to  $T_e$  or  $\sigma_s$  corresponding to  $T_s$

**Table B.2** Systematic correlativity of equilibrium transition temperature  $T_e$ , subequilibrium transition temperature  $T_s$ , order degree  $\sigma$  and  $A_i^{\text{Cu}}$  – alloy gene concentrations ( $x_i^{\text{Cu}}$ ) on disordering  $\text{AuCuI}(A_8^{\text{Au}} A_4^{\text{Cu}})$  compound

$T_e/\text{K}$	$T_s/\text{K}$	$\sigma^{1)}$	$x_0^{\text{Cu}}$	$x_1^{\text{Cu}}$	$x_2^{\text{Cu}}$	$x_3^{\text{Cu}}$	$x_4^{\text{Cu}}$	$x_5^{\text{Cu}}$	$x_6^{\text{Cu}}$	$x_7^{\text{Cu}}$	$x_8^{\text{Cu}}$	$x_9^{\text{Cu}}$	$x_{10}^{\text{Cu}}$	$x_{11}^{\text{Cu}}$	$x_{12}^{\text{Cu}}$
0	0	1.000	0.000	0.000	0.000	0.000	50.000	0.000	0.000	0.000	0.000	0.000	0.000	0.000	0.000
191	571	0.999	0.000	0.000	0.000	0.099	49.676	0.199	0.000	0.000	0.025	0.000	0.000	0.000	0.000
227	585	0.998	0.000	0.000	0.000	0.198	49.355	0.395	0.001	0.000	0.049	0.000	0.000	0.000	0.000
245	593	0.997	0.000	0.000	0.001	0.295	49.037	0.589	0.003	0.001	0.074	0.000	0.000	0.000	0.000
257	600	0.996	0.000	0.000	0.001	0.391	48.722	0.781	0.005	0.002	0.098	0.001	0.000	0.000	0.000
268	605	0.995	0.000	0.000	0.002	0.485	48.409	0.970	0.009	0.002	0.121	0.001	0.000	0.000	0.000
277	610	0.994	0.000	0.000	0.003	0.579	48.099	1.158	0.012	0.004	0.145	0.002	0.000	0.000	0.000
613	613	0.993	0.000	0.000	0.004	0.671	47.791	1.343	0.017	0.005	0.168	0.002	0.000	0.000	0.000
616	616	0.992	0.000	0.000	0.005	0.763	47.486	1.525	0.022	0.006	0.191	0.003	0.000	0.000	0.000
618	618	0.991	0.000	0.000	0.006	0.853	47.184	1.706	0.027	0.008	0.213	0.004	0.000	0.000	0.000
304	620	0.990	0.000	0.000	0.007	0.942	46.884	1.884	0.033	0.010	0.236	0.005	0.000	0.000	0.000
348	631	0.980	0.000	0.000	0.027	1.775	44.019	3.551	0.127	0.038	0.445	0.018	0.000	0.000	0.000
379	636	0.970	0.000	0.001	0.057	2.509	41.386	5.021	0.271	0.085	0.630	0.038	0.001	0.000	0.000
387	637	0.967	0.000	0.001	0.068	2.712	40.638	5.427	0.323	0.102	0.682	0.045	0.001	0.000	0.000
403	640	0.960	0.000	0.001	0.096	3.155	38.965	6.315	0.459	0.147	0.796	0.064	0.002	0.000	0.000
424	643	0.950	0.000	0.002	0.142	3.719	36.737	7.449	0.683	0.225	0.943	0.095	0.004	0.000	0.000
443	646	0.940	0.000	0.004	0.194	4.211	34.687	8.440	0.936	0.317	1.075	0.130	0.006	0.000	0.000
444	646	0.939	0.000	0.004	0.200	4.256	34.491	8.531	0.963	0.327	1.087	0.134	0.006	0.000	0.000
459	648	0.930	0.000	0.006	0.250	4.637	32.799	9.302	1.214	0.422	1.193	0.168	0.009	0.000	0.000
467	650	0.925	0.000	0.007	0.279	4.828	31.911	9.688	1.360	0.479	1.248	0.188	0.011	0.000	0.000
474	651	0.920	0.000	0.009	0.309	5.004	31.059	10.048	1.510	0.539	1.300	0.209	0.013	0.000	0.000
488	654	0.910	0.000	0.012	0.370	5.318	29.456	10.691	1.821	0.666	1.397	0.251	0.017	0.001	0.000
501	657	0.900	0.000	0.015	0.433	5.584	27.976	11.241	2.142	0.804	1.486	0.294	0.023	0.001	0.000
513	668	0.890	0.000	0.019	0.496	5.808	26.611	11.709	2.471	0.950	1.568	0.339	0.029	0.001	0.000
525	673	0.880	0.000	0.023	0.559	5.993	25.349	12.103	2.804	1.104	1.644	0.384	0.036	0.001	0.000
536	676	0.870	0.000	0.028	0.621	6.144	24.182	12.432	3.138	1.264	1.716	0.429	0.043	0.002	0.000
546	677	0.860	0.001	0.034	0.682	6.264	23.103	12.702	3.472	1.431	1.783	0.474	0.051	0.003	0.000
556	678	0.850	0.001	0.039	0.741	6.357	22.102	12.921	3.804	1.604	1.848	0.519	0.060	0.003	0.000
565	679	0.840	0.001	0.045	0.798	6.426	21.175	13.095	4.131	1.780	1.910	0.564	0.070	0.004	0.000
574	680	0.830	0.001	0.051	0.854	6.474	20.314	13.229	4.453	1.961	1.971	0.608	0.080	0.005	0.000
583	681	0.820	0.001	0.058	0.906	6.502	19.514	13.328	4.768	2.144	2.030	0.651	0.090	0.006	0.000
591	682	0.810	0.002	0.065	0.957	6.514	18.770	13.397	5.076	2.330	2.089	0.694	0.101	0.007	0.000
593	683	0.807	0.002	0.067	0.971	6.515	18.557	13.412	5.166	2.386	2.107	0.706	0.104	0.007	0.000
599	683	0.800	0.002	0.071	1.004	6.511	18.077	13.438	5.375	2.518	2.148	0.736	0.112	0.008	0.000
606	683	0.790	0.002	0.078	1.049	6.495	17.430	13.456	5.665	2.707	2.206	0.777	0.124	0.009	0.000
610	683	0.786	0.002	0.081	1.066	6.486	17.184	13.458	5.779	2.782	2.230	0.793	0.129	0.010	0.000
635	—	0.750	0.004	0.107	1.199	6.332	15.239	13.354	6.731	3.464	2.445	0.935	0.173	0.015	0.001
665	—	0.700	0.006	0.141	1.323	5.990	13.176	12.994	7.838	4.387	2.763	1.117	0.239	0.025	0.001
692	—	0.650	0.008	0.171	1.386	5.583	11.627	12.532	8.711	5.248	3.104	1.287	0.304	0.037	0.002
715	—	0.600	0.011	0.194	1.398	5.163	10.431	12.061	9.384	6.029	3.460	1.450	0.368	0.050	0.003
736	—	0.550	0.013	0.209	1.374	4.759	9.486	11.623	9.893	6.719	3.820	1.608	0.430	0.063	0.004
754	—	0.500	0.015	0.217	1.324	4.386	8.727	11.234	10.275	7.319	4.174	1.762	0.487	0.076	0.005
771	683	0.4545	0.016	0.218	1.265	4.082	8.167	10.929	10.534	7.785	4.477	1.897	0.536	0.088	0.006
783	687	0.400	0.017	0.213	1.185	3.752	7.608	10.611	10.771	8.267	4.822	2.055	0.591	0.101	0.008
795	690	0.350	0.017	0.205	1.109	3.494	7.198	10.372	10.927	8.628	5.103	2.190	0.637	0.111	0.009
805	694	0.300	0.016	0.194	1.037	3.274	6.866	10.173	11.042	8.925	5.350	2.313	0.679	0.120	0.010
814	699	0.250	0.016	0.183	0.971	3.091	6.600	10.012	11.127	9.164	5.561	2.422	0.716	0.128	0.010
821	706	0.200	0.015	0.171	0.913	2.943	6.392	9.885	11.188	9.352	5.734	2.514	0.747	0.135	0.011
826	715	0.150	0.014	0.161	0.867	2.829	6.236	9.788	11.230	9.493	5.869	2.588	0.772	0.140	0.012
829	724	0.100	0.013	0.153	0.833	2.749	6.127	9.721	11.258	9.591	5.966	2.642	0.791	0.144	0.012
832	738	0.050	0.012	0.148	0.813	2.701	6.064	9.681	11.274	9.649	6.023	2.675	0.802	0.146	0.012
833	1357	0.000	0.012	0.146	0.806	2.686	6.042	9.668	11.279	9.668	6.042	2.686	0.806	0.146	0.012

1): The  $\sigma$  denotes  $\sigma_e$  corresponding to  $T_e$  or  $\sigma_s$  corresponding to  $T_s$

### C Ability to keep stable structure against changing temperature for Au–Cu system

The ability to keep stable structure against the changing temperature for Au–Cu system is attributed to the fact that the generalized vibration energies of the  $A_i^{\text{Au}}$ - and  $A_i^{\text{Cu}}$ -alloy genes are much smaller than their potential well depths, which may be described by the ratio of potential energy to generalized vibration energy of alloy genes.

The potential energy  $E_i^{\text{Au}}$  and  $E_i^{\text{Cu}}$ , generalized vibration energy  $U_i^{\text{Au.v}}$  and  $U_i^{\text{Cu.v}}$ , specific heat capacity  $c_{p_i}^{\text{Au}}$  and  $c_{p_i}^{\text{Cu}}$ , enthalpy  $H_i^{\text{Au}} = (E_i^{\text{Au}} + U_i^{\text{Au.v}})$  and  $H_i^{\text{Cu}} = (E_i^{\text{Cu}} + U_i^{\text{Cu.v}})$ , vibration entropy energy ( $T \times S_i^{\text{Au.v}}$ ) and ( $T \times S_i^{\text{Cu.v}}$ ), characteristic Gibbs energy  $G_i^{\text{Au}}$ ,  $G_i^{\text{Cu}}$  and the ratio  $|E_i^{\text{Au}}/U_i^{\text{Au.v}}|$ ,  $|E_i^{\text{Cu}}/U_i^{\text{Cu.v}}|$  of the  $A_i^{\text{Au}}$  and  $A_i^{\text{Cu}}$  alloy genes have been obtained from the AG-database of Au–Cu system. The results show that the generalized vibration energies of  $A_i^{\text{Au}}$ - and  $A_i^{\text{Cu}}$ -alloy genes are much smaller than their potential well depths (Tables C.1 to C.6, Fig. C.1). It means that only depending on vibration energies, the alloy genes cannot surmount potential barriers to alternate positions, if without a specific mechanism. It should be pointed out that the generalized vibration energies of alloy genes include

Debye vibration energies and attaching vibration energies, which contain contributions of the existing energies of electrons, forming energies of holes, expansion works of volumes and variations in potential energies with temperature, because the thermodynamic properties of  $A_i^{\text{Au}}$ - and  $A_i^{\text{Cu}}$ -alloy genes are separated out from the experimental mixed enthalpy  $\Delta H_{\text{exp}}^m - T$  and mixed volume  $\Delta V_{\text{exp}}^m - T$  paths.

### D. Resonance activating (RA)-synchro alternating (SA) mechanism

#### D.1 Stem alloy genes

In the  $A_i^{\text{Au}}$ - and  $A_i^{\text{Cu}}$ -sequences of the Au–Cu system, there are stem alloy genes, which are the  $A_0^{\text{Au}}$ ,  $A_4^{\text{Au}}$ ,  $A_8^{\text{Au}}$ ,  $A_{12}^{\text{Au}}$  and  $A_0^{\text{Cu}}$ ,  $A_4^{\text{Cu}}$ ,  $A_8^{\text{Cu}}$ ,  $A_{12}^{\text{Cu}}$ . Their characters are as follows.

1) The pure  $A_0^{\text{Au}}$ -metal and  $A_{12}^{\text{Cu}}$ -metal consist of the  $A_0^{\text{Au}}$  and  $A_{12}^{\text{Cu}}$  stem alloy genes, respectively. The  $\text{Au}_3\text{Cu}$  compound consists of the  $A_4^{\text{Au}}$  and  $A_0^{\text{Cu}}$  stem alloy genes. Its formula is  $(A_4^{\text{Au}})_3 A_0^{\text{Cu}}$ . The  $\text{AuCu}$  compound consists of the  $A_8^{\text{Au}}$  and  $A_4^{\text{Cu}}$  stem alloy genes. Its formula is  $A_8^{\text{Au}} A_4^{\text{Cu}}$ . The  $\text{AuCu}_3$  compound consists of the  $A_{12}^{\text{Au}}$  and  $A_8^{\text{Cu}}$  stem alloy genes. Its formula is  $A_{12}^{\text{Au}} (A_8^{\text{Cu}})_3$ .

2) The essence of the order→disorder transition of

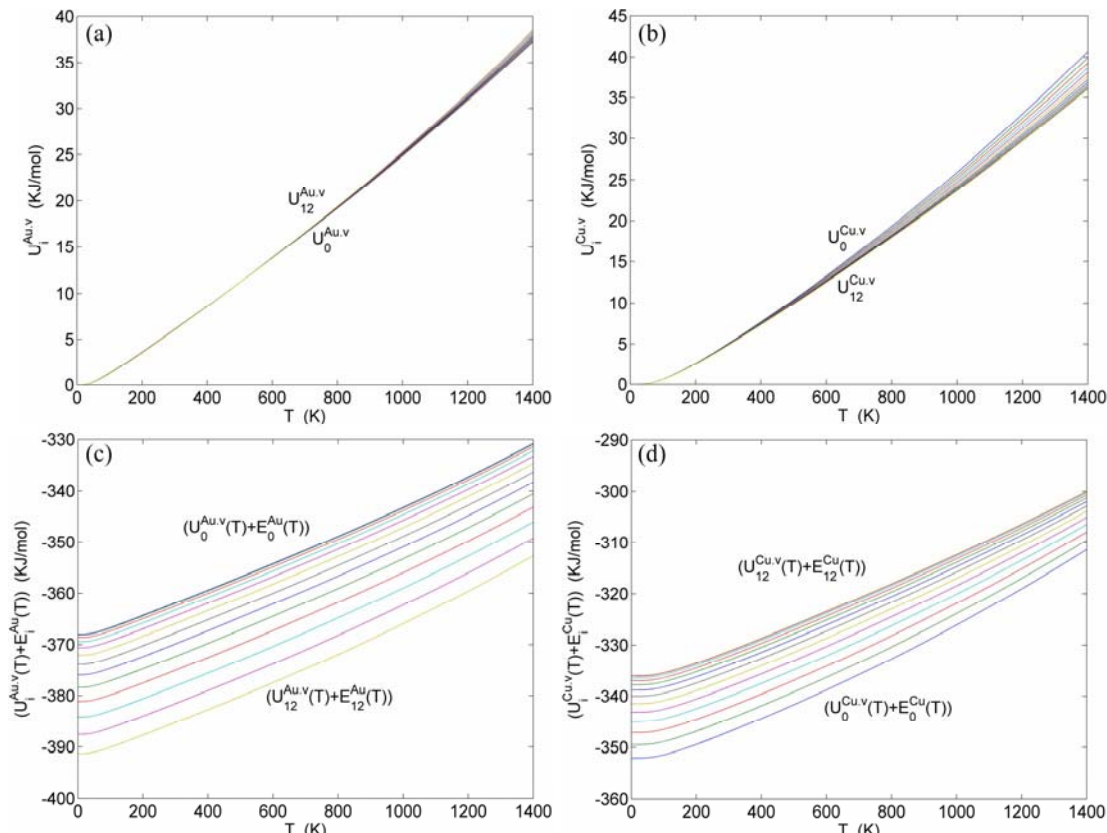


**Fig. C.1** Potential energy and general vibration energies of alloy  $A_i^{\text{Au}}$ - and  $A_i^{\text{Cu}}$ -alloy gene sequences: (a) Generalized vibration energies:  $U_0^{\text{Au.v}}(T)\dots U_i^{\text{Au.v}}(T)\dots U_{12}^{\text{Au.v}}(T)$ ; (b) Generalized vibration energies:  $U_0^{\text{Cu.v}}(T)\dots U_i^{\text{Cu.v}}(T)\dots U_{12}^{\text{Cu.v}}(T)$ ; (c) Different values between generalized vibration energies and potential energies of  $A_i^{\text{Au}}$ -alloy genes; (d) Different values between generalized vibration energies and potential energies of  $A_i^{\text{Cu}}$ -alloy genes

**Table C.1**  $E_0^{\text{Au}}$ ,  $U_0^{\text{Au.v}}$ ,  $c_{p_0}^{\text{Au}}$  ( $E_0^{\text{Au}}+U_0^{\text{Au.v}}$ ),  $(T \times S_0^{\text{Au.v}})$ ,  $G_0^{\text{Au}}$ ,  $|E_0^{\text{Au}}/U_0^{\text{Au.v}}|$  of  $A_0^{\text{Au}}$ -alloy gene

T/K	$E_0^{\text{Au}} / (\text{J}\cdot\text{mol}^{-1})$	$U_0^{\text{Au.v} \text{ 1)} / (\text{J}\cdot\text{mol}^{-1})$	$c_{p_0}^{\text{Au}} / (\text{J}\cdot\text{mol}^{-1}\cdot\text{K}^{-1})$	$(E_0^{\text{Au}}+U_0^{\text{Au.v}}) / (\text{J}\cdot\text{mol}^{-1})$	$(T \times S_0^{\text{Au.v}}) / (\text{J}\cdot\text{mol}^{-1})$	$G_0^{\text{Au}} / (\text{J}\cdot\text{mol}^{-1})$	$ E_0^{\text{Au}}/U_0^{\text{Au.v}} $
0	-368000	0	0.00	-368000	0	-368000	—
50	-368000	310	15.30	-367690	460	-368150	1188.84
100	-368000	1281	21.89	-366719	2241	-368959	287.19
150	-368000	2426	23.59	-365574	4750	-370324	151.69
200	-368000	3625	24.28	-364375	7712	-372087	101.52
250	-368000	4849	24.67	-363151	11005	-374156	75.89
300	-368000	6090	24.95	-361910	14563	-376473	60.43
350	-368000	7344	25.18	-360656	18343	-379000	50.11
400	-368000	8608	25.41	-359392	22314	-381706	42.75
450	-368000	9884	25.63	-358116	26456	-384572	37.23
500	-368000	11171	25.86	-356829	30752	-387580	32.94
550	-368000	12471	26.11	-355529	35189	-390718	29.51
593	-368000	13598	26.33	-354402	39111	-393512	27.06
600	-368000	13782	26.37	-354218	39758	-393975	26.70
620	-368000	14311	26.48	-353689	41620	-395309	25.71
637	-368000	14762	26.57	-353238	43218	-396457	24.93
650	-368000	15108	26.65	-352892	44450	-397342	24.36
683	-368000	15990	26.84	-352010	47611	-399621	23.01
700	-368000	16447	26.94	-351553	49259	-400811	22.37
750	-368000	17802	27.26	-350198	54179	-404377	20.67
769	-368000	18321	27.38	-349679	56077	-405756	20.09
800	-368000	19173	27.59	-348827	59207	-408034	19.19
850	-368000	20562	27.95	-347438	64338	-411777	17.90
900	-368000	21968	28.32	-346032	69570	-415602	16.75
950	-368000	23394	28.72	-344606	74900	-419505	15.73
1000	-368000	24840	29.13	-343160	80325	-423485	14.81
1050	-368000	26308	29.57	-341692	85845	-427537	13.99
1100	-368000	27797	30.02	-340203	91457	-431660	13.24
1150	-368000	29310	30.50	-338690	97161	-435851	12.56
1200	-368000	30848	31.00	-337152	102955	-440108	11.93
1250	-368000	32410	31.52	-335590	108840	-444430	11.35
1300	-368000	34000	32.06	-334000	114814	-448815	10.82
1336 <sup>2)</sup>	-368000	35161	32.46	-332839	119171	-452010	10.47
1350	-368000	35617	32.62	-332383	120878	-453261	10.33
1356 <sup>3)</sup>	-368000	35813	32.69	-332187	121611	-453799	10.28
1400	-368000	37262	33.20	-330738	127030	-457768	9.88

1) The generalized vibration energy includes contributions of Debye vibration energy, existing energy of electrons, forming energy of holes, expansion work of volume and variation in potential energy with temperature. 2) The melting of pure Au metal. 3) The melting of pure Cu metal.

**Table C.2**  $E_8^{\text{Au}}$ ,  $U_8^{\text{Au.v}}$ ,  $c_{p_8}^{\text{Au}}$  ( $E_8^{\text{Au}} + U_8^{\text{Au.v}}$ ),  $(T \times S_8^{\text{Au.v}})$ ,  $G_8^{\text{Au}}$ ,  $|E_8^{\text{Au}} / U_8^{\text{Au.v}}|$  of  $A_8^{\text{Au}}$ -alloy gene

T/K	$E_8^{\text{Au}} / (\text{J}\cdot\text{mol}^{-1})$	$U_8^{\text{Au.v}}{}^1 / (\text{J}\cdot\text{mol}^{-1})$	$c_{p_8}^{\text{Au}} / (\text{J}\cdot\text{mol}^{-1}\cdot\text{K}^{-1})$	$(E_8^{\text{Au}} + U_8^{\text{Au.v}}) / (\text{J}\cdot\text{mol}^{-1})$	$(T \times S_8^{\text{Au.v}}) / (\text{J}\cdot\text{mol}^{-1})$	$G_8^{\text{Au}} / (\text{J}\cdot\text{mol}^{-1})$	$ E_8^{\text{Au}} / U_8^{\text{Au.v}} $
0	-378357	0	0.00	-378357	0	-378357	—
50	-378357	298	14.94	-378059	440	-378499	1270.68
100	-378357	1258	21.75	-377099	2184	-379283	300.82
150	-378357	2398	23.54	-375959	4660	-380619	157.78
200	-378357	3596	24.28	-374761	7590	-382351	105.22
250	-378357	4821	24.71	-373536	10855	-384390	78.48
300	-378357	6065	25.02	-372292	14386	-386678	62.39
350	-378357	7322	25.28	-371035	18140	-389175	51.67
400	-378357	8592	25.53	-369764	22088	-391853	44.03
450	-378357	9875	25.79	-368481	26209	-394690	38.31
500	-378357	11172	26.06	-367185	30487	-397672	33.87
550	-378357	12481	26.34	-365875	34908	-400784	30.31
593	-378357	13619	26.59	-364737	38819	-403556	27.78
600	-378357	13806	26.64	-364551	39465	-404016	27.41
620	-378357	14340	26.76	-364017	41323	-405340	26.39
637	-378357	14796	26.87	-363561	42918	-406479	25.57
650	-378357	15145	26.96	-363211	44147	-407359	24.98
683	-378357	16039	27.18	-362318	47304	-409622	23.59
700	-378357	16502	27.30	-361855	48950	-410805	22.93
750	-378357	17876	27.66	-360481	53869	-414350	21.17
769	-378357	18403	27.80	-359954	55767	-415721	20.56
800	-378357	19268	28.04	-359089	58898	-417986	19.64
850	-378357	20680	28.45	-357676	64034	-421710	18.30
900	-378357	22114	28.88	-356243	69275	-425518	17.11
950	-378357	23569	29.33	-354788	74619	-429407	16.05
1000	-378357	25048	29.81	-353309	80063	-433372	15.11
1050	-378357	26551	30.31	-351806	85606	-437412	14.25
1100	-378357	28079	30.83	-350278	91247	-441524	13.47
1150	-378357	29634	31.38	-348722	96984	-445707	12.77
1200	-378357	31217	31.95	-347139	102818	-449957	12.12
1250	-378357	32830	32.54	-345527	108747	-454274	11.52
1300	-378357	34472	33.16	-343884	114772	-458656	10.98
1336 <sup>2)</sup>	-378357	35674	33.62	-342682	119169	-461851	10.61
1350	-378357	36146	33.80	-342210	120892	-463102	10.47
1356 <sup>3)</sup>	-378357	36349	33.88	-342007	121633	-463640	10.41
1400	-378357	37853	34.47	-340504	127107	-467611	10.00

1) The generalized vibration energy includes contributions of Debye vibration energy, existing energy of electrons, forming energy of holes, expansion work of volume and variation in potential energy with temperature. 2) The melting of pure Au metal. 3) The melting of pure Cu metal.

**Table C.3**  $E_{12}^{\text{Au}}$ ,  $U_{12}^{\text{Au.v}}$ ,  $c_{p12}^{\text{Au}}$ , ( $E_{12}^{\text{Au}} + U_{12}^{\text{Au.v}}$ ), ( $T \times S_{12}^{\text{Au.v}}$ ),  $G_{12}^{\text{Au}}$ ,  $|E_{12}^{\text{Au}} / U_{12}^{\text{Au.v}}|$  of  $A_{12}^{\text{Au}}$ -alloy gene

$T/K$	$E_{12}^{\text{Au}} / (\text{J}\cdot\text{mol}^{-1})$	$U_{12}^{\text{Au.v} \text{ 1)}} / (\text{J}\cdot\text{mol}^{-1})$	$c_{p12}^{\text{Au}} / (\text{J}\cdot\text{mol}^{-1}\cdot\text{K}^{-1})$	$(E_{12}^{\text{Au}} + U_{12}^{\text{Au.v}}) / (\text{J}\cdot\text{mol}^{-1})$	$(T \times S_{12}^{\text{Au.v}}) / (\text{J}\cdot\text{mol}^{-1})$	$G_{12}^{\text{Au}} / (\text{J}\cdot\text{mol}^{-1})$	$ E_{12}^{\text{Au}} / U_{12}^{\text{Au.v}} $
0	-391303	0	0.00	-391303	0	-391303	—
50	-391303	283	14.49	-391020	416	-391435	1382.57
100	-391303	1228	21.58	-390074	2114	-392188	318.59
150	-391303	2363	23.48	-388940	4547	-393487	165.60
200	-391303	3559	24.29	-387743	7439	-395182	109.93
250	-391303	4786	24.75	-386517	10667	-397183	81.76
300	-391303	6033	25.10	-385270	14163	-399433	64.86
350	-391303	7295	25.40	-384007	17886	-401893	53.64
400	-391303	8573	25.69	-382730	21805	-404535	45.65
450	-391303	9865	25.99	-381438	25900	-407339	39.67
500	-391303	11172	26.30	-380131	30155	-410286	35.03
550	-391303	12495	26.63	-378808	34558	-413366	31.32
593	-391303	13646	26.92	-377657	38455	-416111	28.68
600	-391303	13835	26.98	-377468	39098	-416566	28.28
620	-391303	14376	27.12	-376927	40951	-417879	27.22
637	-391303	14838	27.25	-376465	42543	-419008	26.37
650	-391303	15193	27.35	-376110	43769	-419879	25.76
683	-391303	16099	27.61	-375203	46921	-422124	24.31
700	-391303	16570	27.74	-374733	48565	-423298	23.62
750	-391303	17967	28.16	-373335	53480	-426815	21.78
769	-391303	18504	28.33	-372799	55378	-428177	21.15
800	-391303	19387	28.61	-371916	58511	-430427	20.18
850	-391303	20829	29.08	-370474	63654	-434128	18.79
900	-391303	22295	29.58	-369007	68907	-437914	17.55
950	-391303	23788	30.11	-367515	74268	-441783	16.45
1000	-391303	25307	30.66	-365996	79735	-445731	15.46
1050	-391303	26854	31.24	-364448	85307	-449756	14.57
1100	-391303	28431	31.85	-362871	90984	-453855	13.76
1150	-391303	30039	32.48	-361263	96763	-458027	13.03
1200	-391303	31680	33.14	-359623	102646	-462269	12.35
1250	-391303	33354	33.83	-357949	108631	-466580	11.73
1300	-391303	35063	34.54	-356240	114719	-470959	11.16
1336 <sup>2)</sup>	-391303	36316	35.07	-354987	119166	-474153	10.77
1350	-391303	36809	35.28	-354494	120910	-475404	10.63
1356 <sup>3)</sup>	-391303	37021	35.37	-354282	121660	-475942	10.57
1400	-391303	38592	36.05	-352711	127204	-479915	10.14

1) The generalized vibration energy includes contributions of Debye vibration energy, existing energy of electrons, forming energy of holes, expansion work of volume and variation in potential energy with temperature. 2) The melting of pure Au metal. 3) The melting of pure Cu metal.

**Table C.4**  $E_0^{\text{Cu}}$ ,  $U_0^{\text{Cu.v}}$ ,  $c_{p_0}^{\text{Cu}}$ ,  $(E_0^{\text{Cu}} + U_0^{\text{Cu.v}})$ ,  $(T \times S_0^{\text{Cu.v}})$ ,  $G_0^{\text{Cu}}$ ,  $|E_0^{\text{Cu}} / U_0^{\text{Cu.v}}|$  of  $A_0^{\text{Cu}}$ -alloy gene

T/K	$E_0^{\text{Cu}} / (\text{J}\cdot\text{mol}^{-1})$	$U_0^{\text{Cu.v}}{}^1 / (\text{J}\cdot\text{mol}^{-1})$	$c_{p_0}^{\text{Cu}} / (\text{J}\cdot\text{mol}^{-1}\cdot\text{K}^{-1})$	$(E_0^{\text{Cu}} + U_0^{\text{Cu.v}}) / (\text{J}\cdot\text{mol}^{-1})$	$(T \times S_0^{\text{Cu.v}}) / (\text{J}\cdot\text{mol}^{-1})$	$G_0^{\text{Cu}} / (\text{J}\cdot\text{mol}^{-1})$	$ E_0^{\text{Cu}} / U_0^{\text{Cu.v}} $
0	-352055	0	0.00	-352055	0	-352055	—
50	-352055	76	5.27	-351979	108	-352087	4619.24
100	-352055	613	15.36	-351442	918	-352361	574.17
150	-352055	1523	20.39	-350532	2474	-353006	231.16
200	-352055	2612	22.90	-349444	4548	-353992	134.80
250	-352055	3796	24.38	-348259	7005	-355264	92.73
300	-352055	5042	25.41	-347013	9769	-356782	69.82
350	-352055	6333	26.20	-345722	12789	-358511	55.59
400	-352055	7661	26.89	-344394	16034	-360428	45.95
450	-352055	9021	27.51	-343034	19480	-362514	39.03
500	-352055	10411	28.10	-341644	23109	-364753	33.81
550	-352055	11830	28.67	-340225	26907	-367132	29.76
593	-352055	13074	29.16	-338982	30301	-369283	26.93
600	-352055	13278	29.23	-338777	30864	-369642	26.51
620	-352055	13865	29.46	-338190	32490	-370680	25.39
637	-352055	14367	29.65	-337688	33890	-371578	24.50
650	-352055	14754	29.80	-337302	34972	-372274	23.86
683	-352055	15744	30.18	-336312	37762	-374074	22.36
700	-352055	16258	30.38	-335797	39223	-375020	21.65
750	-352055	17792	30.96	-334264	43611	-377875	19.79
769	-352055	18382	31.19	-333673	45314	-378987	19.15
800	-352055	19355	31.56	-332701	48132	-380833	18.19
850	-352055	20947	32.16	-331108	52782	-383890	16.81
900	-352055	22571	32.79	-329484	57557	-387042	15.60
950	-352055	24226	33.42	-327829	62455	-390284	14.53
1000	-352055	25914	34.07	-326142	67473	-393615	13.59
1050	-352055	27634	34.74	-324421	72609	-397031	12.74
1100	-352055	29388	35.43	-322667	77862	-400529	11.98
1150	-352055	31177	36.13	-320878	83230	-404108	11.29
1200	-352055	33001	36.85	-319054	88712	-407766	10.67
1250	-352055	34862	37.58	-317193	94307	-411500	10.10
1300	-352055	36760	38.33	-315296	100014	-415310	9.58
1336 <sup>2)</sup>	-352055	38150	38.89	-313906	104193	-418099	9.23
1350	-352055	38696	39.10	-313360	105834	-419193	9.10
1356 <sup>3)</sup>	-352055	38930	39.20	-313125	106539	-419664	9.04
1400	-352055	40670	39.89	-311385	111764	-423149	8.66

1) The generalized vibration energy includes contributions of Debye vibration energy, existing energy of electrons, forming energy of holes, expansion work of volume and variation in potential energy with temperature. 2) The melting of pure Au metal. 3) The melting of pure Cu metal.

**Table C.5**  $E_4^{\text{Cu}}$ ,  $U_4^{\text{Cu.v}}$ ,  $c_{p4}^{\text{Cu}}$ ,  $(E_4^{\text{Cu}} + U_4^{\text{Cu.v}})$ ,  $(T \times S_4^{\text{Cu.v}})$ ,  $G_4^{\text{Cu}}$ ,  $|E_4^{\text{Cu}} / U_4^{\text{Cu.v}}|$  of  $A_4^{\text{Cu}}$ -alloy gene

T/K	$E_4^{\text{Cu}} / (\text{J}\cdot\text{mol}^{-1})$	$U_4^{\text{Cu.v}}{}^1 / (\text{J}\cdot\text{mol}^{-1})$	$c_{p4}^{\text{Cu}} / (\text{J}\cdot\text{mol}^{-1}\cdot\text{K}^{-1})$	$(E_4^{\text{Cu}} + U_4^{\text{Cu.v}}) / (\text{J}\cdot\text{mol}^{-1})$	$(T \times S_4^{\text{Cu.v}}) / (\text{J}\cdot\text{mol}^{-1})$	$G_4^{\text{Cu}} / (\text{J}\cdot\text{mol}^{-1})$	$ E_4^{\text{Cu}} / U_4^{\text{Cu.v}} $
0	-343136	0	0.00	-343136	0	-343136	-
50	-343136	73	5.16	-343062	102	-343164	4670.88
100	-343136	602	15.14	-342534	896	-343430	569.91
150	-343136	1498	20.06	-341638	2424	-344062	229.08
200	-343136	2567	22.44	-340569	4459	-345028	133.69
250	-343136	3725	23.80	-339410	6865	-346275	92.10
300	-343136	4939	24.70	-338196	9565	-347762	69.47
350	-343136	6192	25.38	-336943	12511	-349454	55.41
400	-343136	7475	25.94	-335660	15669	-351329	45.90
450	-343136	8785	26.43	-334351	19015	-353366	39.06
500	-343136	10117	26.88	-333018	22532	-355550	33.92
550	-343136	11473	27.32	-331663	26205	-357868	29.91
593	-343136	12655	27.69	-330480	29482	-359962	27.11
600	-343136	12849	27.75	-330286	30025	-360311	26.70
620	-343136	13406	27.92	-329730	31592	-361321	25.60
637	-343136	13882	28.07	-329254	32940	-362194	24.72
650	-343136	14248	28.18	-328888	33982	-362870	24.08
683	-343136	15182	28.47	-327953	36665	-364619	22.60
700	-343136	15668	28.62	-327468	38069	-365537	21.90
750	-343136	17109	29.06	-326026	42280	-368307	20.06
769	-343136	17663	29.23	-325473	43912	-369385	19.43
800	-343136	18573	29.51	-324562	46611	-371173	18.47
850	-343136	20060	29.97	-323075	51056	-374131	17.11
900	-343136	21570	30.44	-321565	55613	-377178	15.91
950	-343136	23105	30.93	-320031	60278	-380309	14.85
1000	-343136	24663	31.42	-318473	65050	-383522	13.91
1050	-343136	26247	31.94	-316889	69925	-386814	13.07
1100	-343136	27857	32.46	-315279	74902	-390181	12.32
1150	-343136	29494	33.00	-313642	79980	-393622	11.63
1200	-343136	31158	33.56	-311978	85157	-397135	11.01
1250	-343136	32850	34.13	-310286	90432	-400718	10.45
1300	-343136	34571	34.71	-308565	95804	-404369	9.93
1336 <sup>2)</sup>	-343136	35828	35.14	-307308	99732	-407039	9.58
1350	-343136	36321	35.31	-306814	101273	-408087	9.45
1356 <sup>3)</sup>	-343136	36533	35.39	-306602	101935	-408538	9.39
1400	-343136	38102	35.93	-305033	106837	-411870	9.01

<sup>1)</sup> The generalized vibration energy includes contributions of Debye vibration energy, existing energy of electrons, forming energy of holes, expansion work of volume and variation in potential energy with temperature. <sup>2)</sup> The melting of pure Au metal. <sup>3)</sup> The melting of pure Cu metal.

**Table C.6**  $E_{12}^{\text{Cu}}$ ,  $U_{12}^{\text{Cu.v}}$ ,  $c_{p12}^{\text{Cu}}$ , ( $E_{12}^{\text{Cu}} + U_{12}^{\text{Cu.v}}$ ), ( $T \times S_{12}^{\text{Cu.v}}$ ),  $G_{12}^{\text{Cu}}$ ,  $|E_{12}^{\text{Cu}} / U_{12}^{\text{Cu.v}}$  of  $A_{12}^{\text{Cu}}$ -alloy gene

$T/K$	$E_{12}^{\text{Cu}} / (\text{J}\cdot\text{mol}^{-1})$	$U_{12}^{\text{Cu.v}}{}^1 / (\text{J}\cdot\text{mol}^{-1})$	$c_{p12}^{\text{Cu}} / (\text{J}\cdot\text{mol}^{-1}\cdot\text{K}^{-1})$	$(E_{12}^{\text{Cu}} + U_{12}^{\text{Cu.v}}) / (\text{J}\cdot\text{mol}^{-1})$	$(T \times S_{12}^{\text{Cu.v}}) / (\text{J}\cdot\text{mol}^{-1})$	$G_{12}^{\text{Cu}} / (\text{J}\cdot\text{mol}^{-1})$	$ E_{12}^{\text{Cu}} / U_{12}^{\text{Cu.v}} $
0	-336000	0	0.00	-336000	0	-336000	—
50	-336000	71	5.08	-335929	98	-336026	4715.07
100	-336000	593	14.96	-335407	879	-336286	566.38
150	-336000	1478	19.78	-334522	2384	-336907	227.37
200	-336000	2531	22.08	-333469	4387	-337857	132.77
250	-336000	3669	23.34	-332331	6753	-339084	91.58
300	-336000	4857	24.14	-331143	9403	-340546	69.18
350	-336000	6079	24.72	-329921	12288	-342209	55.27
400	-336000	7327	25.17	-328673	15376	-344049	45.86
450	-336000	8596	25.56	-327404	18643	-346047	39.09
500	-336000	9882	25.91	-326118	22070	-348188	34.00
550	-336000	11186	26.24	-324814	25644	-350458	30.04
593	-336000	12321	26.52	-323679	28826	-352506	27.27
600	-336000	12507	26.57	-323493	29354	-352847	26.87
620	-336000	13039	26.69	-322961	30873	-353834	25.77
637	-336000	13494	26.80	-322506	32181	-354687	24.90
650	-336000	13843	26.88	-322157	33190	-355347	24.27
683	-336000	14734	27.10	-321266	35788	-357054	22.81
700	-336000	15195	27.21	-320805	37146	-357951	22.11
750	-336000	16564	27.53	-319436	41215	-360652	20.29
769	-336000	17088	27.66	-318912	42790	-361703	19.66
800	-336000	17949	27.87	-318051	45393	-363445	18.72
850	-336000	19351	28.21	-316649	49675	-366324	17.36
900	-336000	20770	28.56	-315230	54057	-369287	16.18
950	-336000	22207	28.93	-313793	58537	-372330	15.13
1000	-336000	23663	29.30	-312337	63111	-375448	14.20
1050	-336000	25138	29.69	-310862	67778	-378640	13.37
1100	-336000	26632	30.09	-309368	72534	-381902	12.62
1150	-336000	28147	30.50	-307853	77380	-385233	11.94
1200	-336000	29683	30.93	-306317	82313	-388630	11.32
1250	-336000	31240	31.37	-304760	87332	-392092	10.76
1300	-336000	32819	31.82	-303181	92436	-395616	10.24
1336 <sup>2)</sup>	-336000	33971	32.15	-302029	96163	-398192	9.89
1350	-336000	34422	32.28	-301578	97624	-399202	9.76
1356 <sup>3)</sup>	-336000	34616	32.34	-301384	98252	-399636	9.71
1400	-336000	36048	32.76	-299952	102895	-402847	9.32

1) The generalized vibration energy includes contributions of Debye vibration energy, existing energy of electrons, forming energy of holes, expansion work of volume and variation in potential energy with temperature. 2) The melting of pure Au metal. 3) The melting of pure Cu metal.

the  $A_8^{Au}A_4^{Cu}$  compound is that the  $A_8^{Au}$  and  $A_4^{Cu}$  stem alloy genes are split into the  $A_i^{Au}$ - and  $A_i^{Cu}$ -sequences, otherwise, the essence of the disorder→order transition of the stoichiometric disordered AuCu alloy is that the  $A_i^{Au}$ - and  $A_i^{Cu}$ -sequences are degenerated into the  $A_8^{Au}$  and  $A_4^{Cu}$  stem alloy genes. The  $(A_4^{Au})_3A_0^{Cu}$  and  $A_{12}^{Au}(A_8^{Cu})_3$  compounds possess oneself of analogous essence to  $A_8^{Au}A_4^{Cu}$  compound.

3) The  $A_4^{Au}$  and  $A_8^{Cu}$  stem alloy genes are the signal alloy genes of the  $n$ (RA-SA) mechanism in the beginning period on disordering  $A_8^{Au}A_4^{Cu}$  compound. In this period, there are very peculiar orders of the splitting off alloy genes:  $x_4^{Au} > x_6^{Au} > x_5^{Au}$ ,  $x_8^{Cu} > x_6^{Cu} > x_7^{Cu}$ , the  $A_4^{Au}$  is farther away from the  $A_8^{Au}$  than  $A_4^{Cu}$  and  $A_5^{Au}$ , and the  $A_8^{Cu}$  is farther away from the  $A_4^{Cu}$  than  $A_6^{Cu}$  and  $A_7^{Cu}$  (Tables B.1 and B.2). Namely, the Gibbs energy level difference ( $\Delta G_4^{Au} - \Delta G_8^{Au}$ ) is larger than ( $\Delta G_6^{Au} - \Delta G_8^{Au}$ ) and ( $\Delta G_5^{Au} - \Delta G_8^{Au}$ ), and ( $\Delta G_8^{Cu} - \Delta G_4^{Cu}$ ) is larger than ( $\Delta G_6^{Cu} - \Delta G_4^{Cu}$ ) and ( $\Delta G_7^{Cu} - \Delta G_4^{Cu}$ ). The  $A_0^{Au}$  and  $A_4^{Cu}$  stem alloy genes are signal alloy genes of the  $n$ (RA-SA) mechanism in the

beginning period on disordering  $(A_4^{Au})_3A_0^{Cu}$  compound (Fig. D.1), and the  $A_8^{Au}$  and  $A_{12}^{Cu}$  stem alloy genes are signal alloy genes of the  $n$ (RA-SA) mechanism of the beginning period on disordering  $A_{12}^{Au}(A_8^{Cu})_3$  compound (Fig. D.2).

## D.2 Choice among $n$ (RA-SA) mechanisms

It is generally accepted that the atom movement, which is necessary for any atom-arranging structural changes of alloys, occurs by atom jumps to vacant neighboring lattice sites, that may be called atom-vacancy alternating (AVA) mechanism. The  $n$ (RA-SA) mechanism has more functions than the AVA mechanism at low temperature.

We have studied the  $n$ (RA-SA) mechanisms in the beginning period on disordering AuCuI ( $A_8^{Au}A_4^{Cu}$ ) compound, where  $n$  equals one, two, three and four AG-pairs of the  $A_8^{Au} - A_4^{Cu}$  type in a single cell of AuCuI ( $A_8^{Au}A_4^{Cu}$ ). The results demonstrate that the 3(RA-SA) mechanism of three  $A_8^{Au} - A_4^{Cu}$  pairs is the most suitable to simulate AG-concentration order in the beginning period on disordering the AuCuI ( $A_8^{Au}A_4^{Cu}$ ).

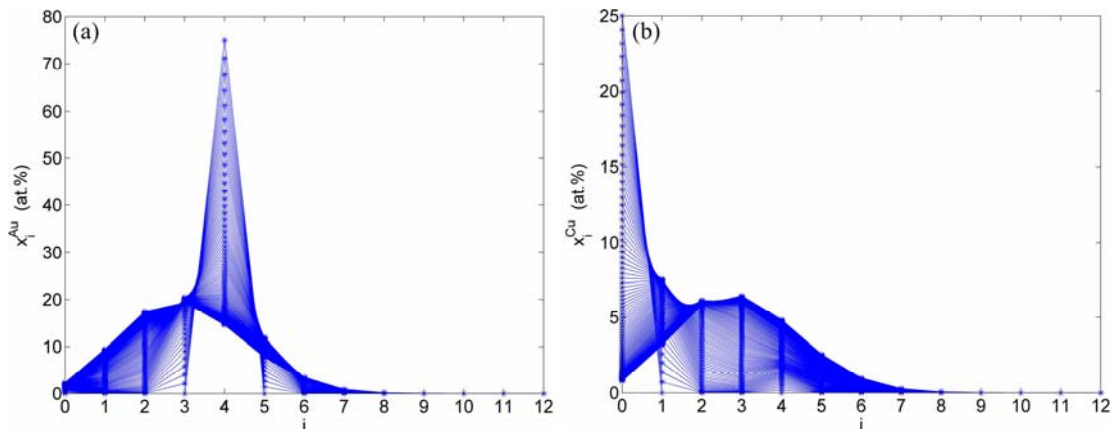


**Fig. D.1** AG-concentration EHNP charts on disordering  $(A_4^{Au})_3A_0^{Cu}$  compound: Two-dimensional iso-order degree  $x_{i,\sigma}^{Au} - i$  (a) and  $x_{i,\sigma}^{Cu} - i$  (b) EHNP charts

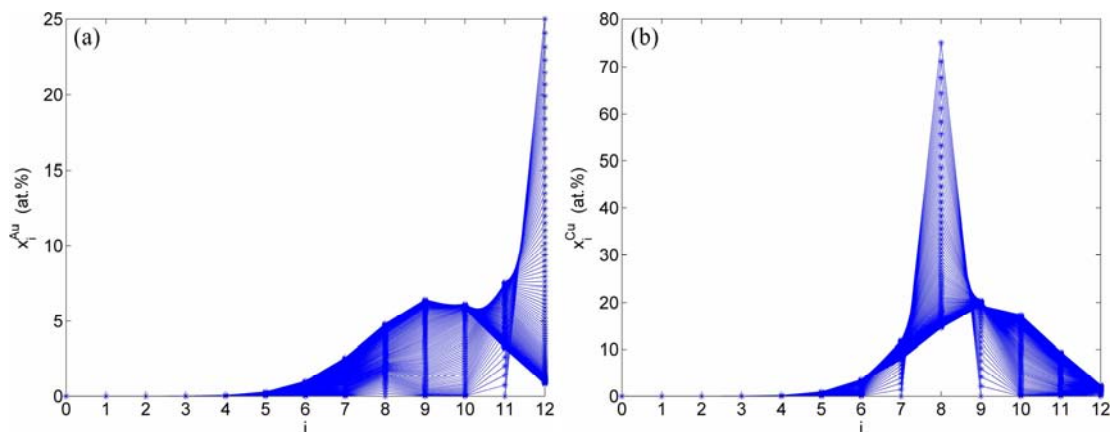


**Fig. D.2** AG-concentration EHNP charts on disordering  $A_{12}^{Au}(A_8^{Cu})_3$  compound: Two-dimensional iso-order degree  $x_{i,\sigma}^{Au} - i$  (a) and  $x_{i,\sigma}^{Cu} - i$  (b) EHNP charts

At the order degree  $\sigma=0.990$  (Tables B.1 and B.2), the order in AG-concentrations is (atomic fraction, %):

$$\begin{cases} x_8^{\text{Au}}(46.884) > x_7^{\text{Au}}(1.884) > x_9^{\text{Au}}(0.942) > \\ x_4^{\text{Au}}(0.236) > x_6^{\text{Au}}(0.033) > x_5^{\text{Au}}(0.010) \\ x_4^{\text{Cu}}(46.884) > x_5^{\text{Cu}}(1.884) > x_3^{\text{Cu}}(0.942) > \\ x_8^{\text{Cu}}(0.236) > x_6^{\text{Cu}}(0.033) > x_7^{\text{Cu}}(0.010) \end{cases} \quad (\text{D.1})$$

According to 1(RA-SA) mechanism of one pair of the  $A_8^{\text{Au}} - A_4^{\text{Cu}}$  type in a single cell of the AuCuI( $A_8^{\text{Au}} A_4^{\text{Cu}}$ ) (Fig. D.3, Tables D.1 and D.2), the order of AG-concentrations in the 1(RA-SA)-cell cluster consisting of a central 1(RA-SA)-cell and its 26 neighbouring cells is as follows (atomic fraction, %):

After A-manner alternating 1(RA-SA) mechanism (Fig. D.3(a)),

$$\begin{cases} x_8^{\text{Au}}(44.444) > x_7^{\text{Au}}(4.630) > x_5^{\text{Au}}(0.926) \\ x_4^{\text{Cu}}(42.593) > x_5^{\text{Cu}}(4.630) > x_3^{\text{Cu}}(1.852) > x_7^{\text{Cu}}(0.926) \end{cases} \quad (\text{D.2})$$

After B-manner alternating 1(RA-SA) mechanism (Fig. D.3(b)),

$$\begin{cases} x_8^{\text{Au}}(42.593) > x_7^{\text{Au}}(4.630) > x_9^{\text{Au}}(1.852) > x_5^{\text{Au}}(0.926) \\ x_4^{\text{Cu}}(44.444) > x_5^{\text{Cu}}(4.630) > x_7^{\text{Cu}}(0.926) \end{cases} \quad (\text{D.3})$$

Because they have the same probability, their mean results are

$$\begin{cases} x_8^{\text{Au}}(43.519) > x_7^{\text{Au}}(4.630) > x_5^{\text{Au}}(0.926) = x_9^{\text{Au}}(0.926) \\ x_4^{\text{Cu}}(43.519) > x_5^{\text{Cu}}(4.630) > x_3^{\text{Cu}}(0.926) = x_7^{\text{Cu}}(0.926) \end{cases} \quad (\text{D.4})$$

These results demonstrate that the 1(RA-SA) mechanism cannot be suitable to simulate AG-concentration order in the beginning period on disordering AuCuI( $A_8^{\text{Au}} A_4^{\text{Cu}}$ ).

2) According to 2(RA-SA) mechanism of two pairs of the  $A_8^{\text{Au}} - A_4^{\text{Cu}}$  type in a single cell of the AuCuI( $A_8^{\text{Au}} A_4^{\text{Cu}}$ ) (Fig. D.4, Tables D.1 and D.2), the order in AG-concentrations in the 2(RA-SA)-cell cluster consisting of a central 2(RA-SA)-cell and its 26 neighbouring cells is as follows (atomic fraction, %):

After A-manner alternating 2(RA-SA) mechanism (Fig. D.4(a)),

$$\begin{cases} x_8^{\text{Au}}(38.889) > x_7^{\text{Au}}(5.556) > x_9^{\text{Au}}(2.778) > \\ x_4^{\text{Au}}(0.926) = x_6^{\text{Au}}(0.926) = x_5^{\text{Au}}(0.926) \\ x_4^{\text{Cu}}(36.111) > x_5^{\text{Cu}}(9.259) > x_3^{\text{Cu}}(2.778) > \\ x_6^{\text{Cu}}(0.926) = x_7^{\text{Cu}}(0.926) \end{cases} \quad (\text{D.5})$$

After B-manner alternating 2(RA-SA) mechanism (Fig. D.4(b)),

$$\begin{cases} x_8^{\text{Au}}(36.111) > x_7^{\text{Au}}(9.259) > x_9^{\text{Au}}(2.778) > \\ x_6^{\text{Au}}(0.926) = x_5^{\text{Au}}(0.926) \\ x_4^{\text{Cu}}(38.889) > x_5^{\text{Cu}}(5.556) > x_3^{\text{Cu}}(2.778) > \\ x_6^{\text{Cu}}(0.926) = x_7^{\text{Cu}}(0.926) = x_8^{\text{Cu}}(0.926) \end{cases} \quad (\text{D.6})$$

**Table D.1** Number of AG  $A_i^{\text{Au}}$  in  $n(\text{RA-SA})$  region consisting of a central  $n(\text{RA-SA})$  cell and its 26 neighbouring cells

Manner	$n$	$A_0^{\text{Au}}$	$A_1^{\text{Au}}$	$A_2^{\text{Au}}$	$A_3^{\text{Au}}$	$A_4^{\text{Au}}$	$A_5^{\text{Au}}$	$A_6^{\text{Au}}$	$A_7^{\text{Au}}$	$A_8^{\text{Au}}$	$A_9^{\text{Au}}$	$A_{10}^{\text{Au}}$	$A_{11}^{\text{Au}}$	$A_{12}^{\text{Au}}$
1(RA-SA)-A	1	0	0	0	0	0	1	0	5	48	0	0	0	0
1(RA-SA)-B	1	0	0	0	0	0	1	0	5	46	2	0	0	0
2(RA-SA)-A	2	0	0	0	0	1	1	1	6	42	3	0	0	0
2(RA-SA)-B	2	0	0	0	0	0	1	1	10	39	3	0	0	0
3(RA-SA)-A	3	0	0	0	0	2	0	2	8	38	4	0	0	0
3(RA-SA)-B	3	0	0	0	0	0	1	2	12	36	3	0	0	0
4(RA-SA)-A	4	0	0	0	1	1	1	4	6	37	4	0	0	0
4(RA-SA)-B	4	0	0	0	0	0	1	5	13	31	4	0	0	0

**Table D.2** Number of AG  $A_i^{\text{Cu}}$  in  $n(\text{RA-SA})$  region consisting of a central  $n(\text{RA-SA})$  cell and its 26 neighbouring cells

Manner	$n$	$A_0^{\text{Cu}}$	$A_1^{\text{Cu}}$	$A_2^{\text{Cu}}$	$A_3^{\text{Cu}}$	$A_4^{\text{Cu}}$	$A_5^{\text{Cu}}$	$A_6^{\text{Cu}}$	$A_7^{\text{Cu}}$	$A_8^{\text{Cu}}$	$A_9^{\text{Cu}}$	$A_{10}^{\text{Cu}}$	$A_{11}^{\text{Cu}}$	$A_{12}^{\text{Cu}}$
1(RA-SA)-A	1	0	0	0	2	46	5	0	1	0	0	0	0	0
1(RA-SA)-B	1	0	0	0	0	48	5	0	1	0	0	0	0	0
2(RA-SA)-A	2	0	0	0	3	39	10	1	1	0	0	0	0	0
2(RA-SA)-B	2	0	0	0	3	42	6	1	1	1	0	0	0	0
3(RA-SA)-A	3	0	0	0	3	36	12	2	1	0	0	0	0	0
3(RA-SA)-B	3	0	0	0	4	38	8	2	0	2	0	0	0	0
4(RA-SA)-A	4	0	0	0	4	31	13	5	1	0	0	0	0	0
4(RA-SA)-B	4	0	0	0	4	37	6	4	1	1	1	0	0	0

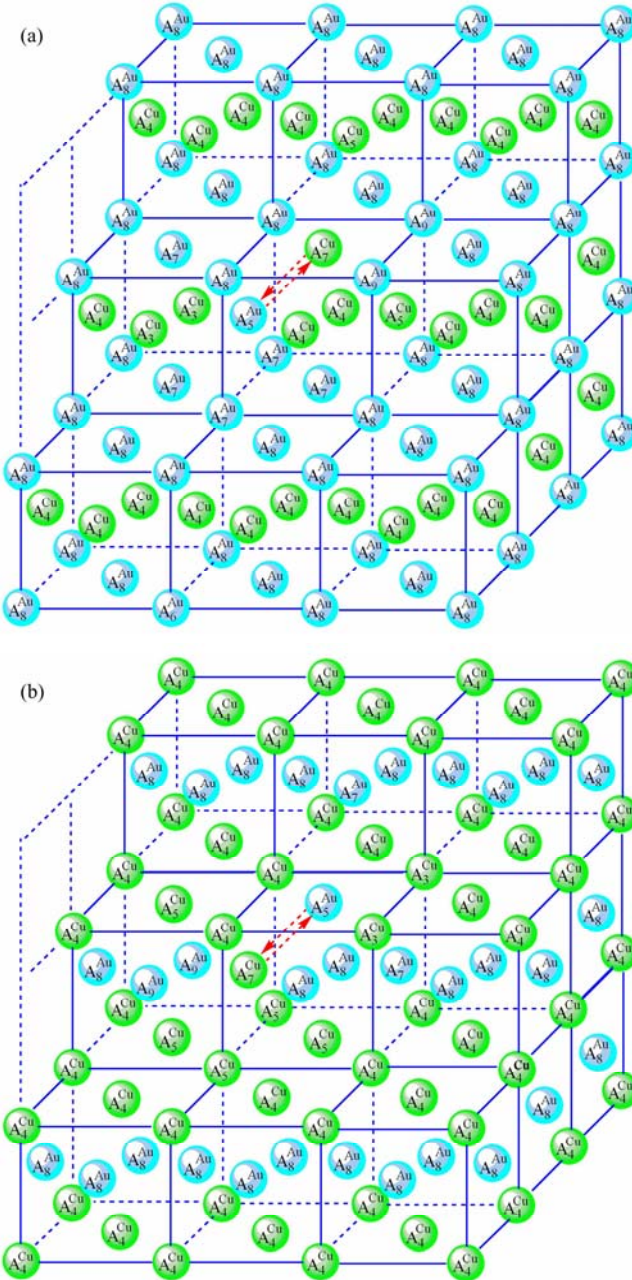


**Fig. D.3** 1(RA-SA)-cell cluster: (a) A-manner alternating in 1(RA-SA) mechanism; (b) B-manner alternating in 1(RA-SA) mechanism

Because they have the same probability, their mean results are

$$\left\{ \begin{array}{l} x_8^{\text{Au}} (37.500) > x_7^{\text{Au}} (7.407) > x_9^{\text{Au}} (2.778) > \\ x_5^{\text{Au}} (0.926) = x_6^{\text{Au}} (0.926) > x_4^{\text{Au}} (0.463) \\ x_4^{\text{Cu}} (37.500) > x_5^{\text{Cu}} (7.407) > x_3^{\text{Cu}} (2.778) > \\ x_6^{\text{Cu}} (0.926) = x_7^{\text{Cu}} (0.926) > x_8^{\text{Cu}} (0.463) \end{array} \right. \quad (\text{D.7})$$

These results demonstrate that the 2(RA-SA) mechanism cannot be suitable to simulate AG-concentration order in the beginning period on disordering  $\text{AuCuI}(A_8^{\text{Au}} A_4^{\text{Cu}})$ .

3) According to 3(RA-SA) mechanism of three pairs of the  $A_8^{\text{Au}} - A_4^{\text{Cu}}$  type in a single cell of the

$\text{AuCuI}(A_8^{\text{Au}} A_4^{\text{Cu}})$  (Fig. D.5, Tables D.1 and D.2), the order in AG-concentrations in the 3(RA-SA)-cell cluster consisting of a central 3(RA-SA)-cell and its 26 neighbouring cells is as follows (atomic fraction, %):

After A-manner alternating 3(RA-SA) mechanism (Fig. D.5(a)),

$$\left\{ \begin{array}{l} x_8^{\text{Au}} (35.185) > x_7^{\text{Au}} (7.407) > x_9^{\text{Au}} (3.704) > \\ x_4^{\text{Au}} (1.852) = x_6^{\text{Au}} (1.852) \\ x_4^{\text{Cu}} (33.333) > x_5^{\text{Cu}} (11.111) > x_3^{\text{Cu}} (2.778) > \\ x_6^{\text{Cu}} (1.852) > x_7^{\text{Cu}} (0.926) \end{array} \right. \quad (\text{D.8})$$

After B-manner alternating 3(RA-SA) mechanism (Fig. D.5(b)),

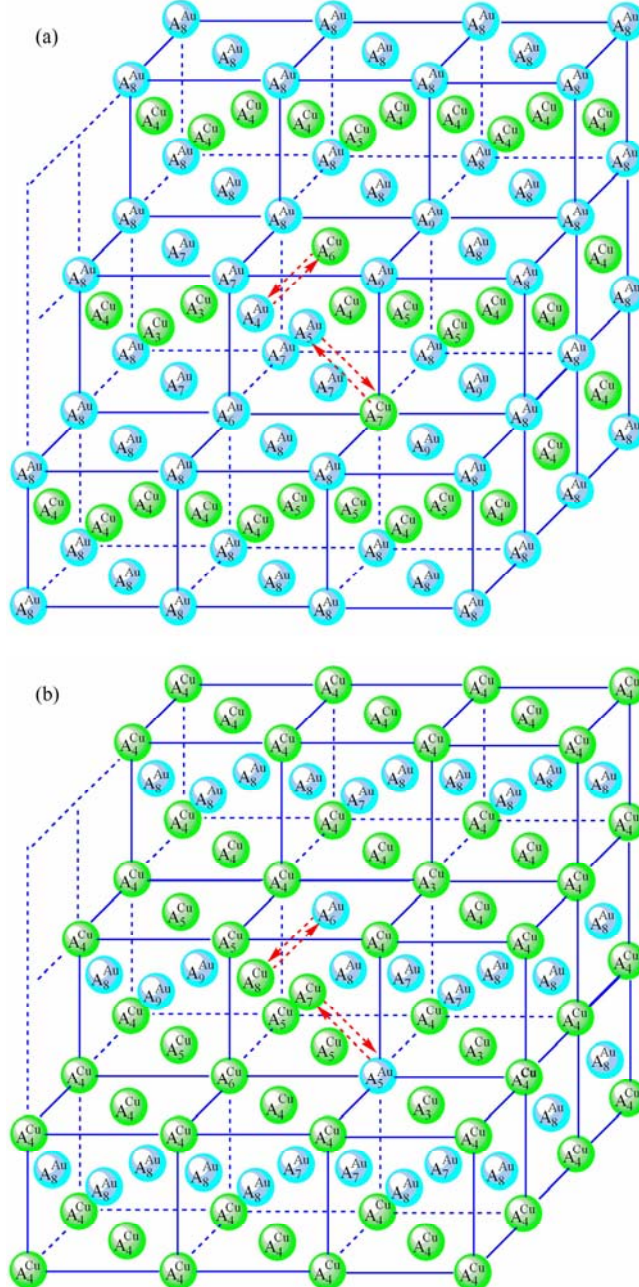


**Fig. D.4** 2(RA-SA)-cell cluster: (a) A-manner alternating in 2(RA-SA) mechanism; (b) B-manner alternating in 2(RA-SA) mechanism

$$\left\{ \begin{array}{l} x_8^{\text{Au}} (33.333) > x_7^{\text{Au}} (11.111) > x_9^{\text{Au}} (2.778) > \\ x_6^{\text{Au}} (1.852) > x_5^{\text{Au}} (0.926) \\ x_4^{\text{Cu}} (35.185) > x_5^{\text{Cu}} (7.407) > x_3^{\text{Cu}} (3.704) > \\ x_6^{\text{Cu}} (1.852) = x_8^{\text{Cu}} (1.852) \end{array} \right. \quad (\text{D.9})$$

Because they have the same probability, their mean results are

$$\left\{ \begin{array}{l} x_8^{\text{Au}} (34.259) > x_7^{\text{Au}} (9.259) > x_9^{\text{Au}} (3.241) > \\ x_6^{\text{Au}} (1.852) > x_4^{\text{Au}} (0.926) > x_5^{\text{Au}} (0.463) \\ x_4^{\text{Cu}} (34.259) > x_5^{\text{Cu}} (9.259) > x_3^{\text{Cu}} (3.241) > \\ x_6^{\text{Cu}} (1.852) > x_8^{\text{Cu}} (0.926) > x_7^{\text{Cu}} (0.463) \end{array} \right. \quad (\text{D.10})$$

These results demonstrate that the 3(RA-SA) mechanism can be suitable to simulate AG-concentration order in the beginning period on disordering AuCuI ( $A_8^{\text{Au}} A_4^{\text{Cu}}$ ). The slight difference between Eq. (D.10) and Eq. (D.1) may be caused by supposing that the neighbouring cells have no alternating of atoms. The modified results are presented in Appendix D.4.

4) According to 4(RA-SA) mechanism of four pairs of the  $A_8^{\text{Au}} - A_4^{\text{Cu}}$  type in a single cell of the AuCuI ( $A_8^{\text{Au}} A_4^{\text{Cu}}$ ) (Fig. D.6, Tables D.1 and D.2), the order in AG-concentrations in the 4(RA-SA)-cell cluster consisting of a central 4(RA-SA)-cell and its 26

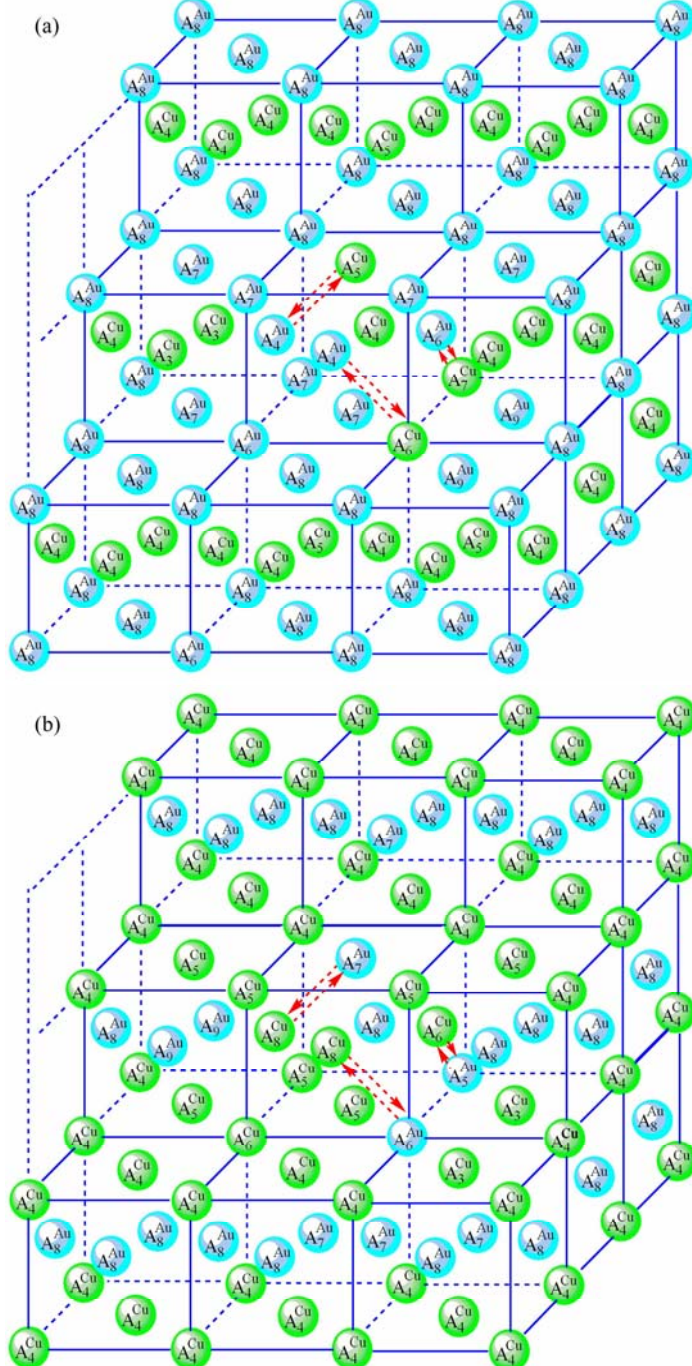


**Fig. D.5** 3(RA-SA)-cell cluster: (a) A-manner alternating in 3(RA-SA) mechanism; (b) B-manner alternating in 3(RA-SA) mechanism

neighbouring cells is as follows (atomic fraction, %):

After A-manner alternating 4(RA-SA) mechanism (Fig. D.6(a)),

$$\left\{ \begin{array}{l} x_8^{\text{Au}} (34.259) > x_7^{\text{Au}} (5.556) > x_6^{\text{Au}} (3.704) = x_9^{\text{Au}} (3.704) > \\ x_3^{\text{Au}} (0.926) = x_4^{\text{Au}} (0.926) = x_5^{\text{Au}} (0.926) \\ x_4^{\text{Cu}} (28.704) > x_5^{\text{Cu}} (12.037) > x_6^{\text{Cu}} (4.630) > x_3^{\text{Cu}} (3.704) > \\ x_7^{\text{Cu}} (0.926) \end{array} \right. \quad (\text{D.11})$$

After B-manner alternating 4(RA-SA) mechanism (Fig. D.6(b)),

$$\left\{ \begin{array}{l} x_8^{\text{Au}} (28.704) > x_7^{\text{Au}} (12.037) > x_6^{\text{Au}} (4.630) > \\ x_9^{\text{Au}} (3.704) > x_5^{\text{Au}} (0.926) \\ x_4^{\text{Cu}} (34.259) > x_5^{\text{Cu}} (5.556) > x_6^{\text{Cu}} (3.704) = x_3^{\text{Cu}} (3.704) > \\ x_7^{\text{Cu}} (0.926) = x_8^{\text{Cu}} (0.926) = x_9^{\text{Cu}} (0.926) \end{array} \right. \quad (\text{D.12})$$

Because they have the same probability, their mean

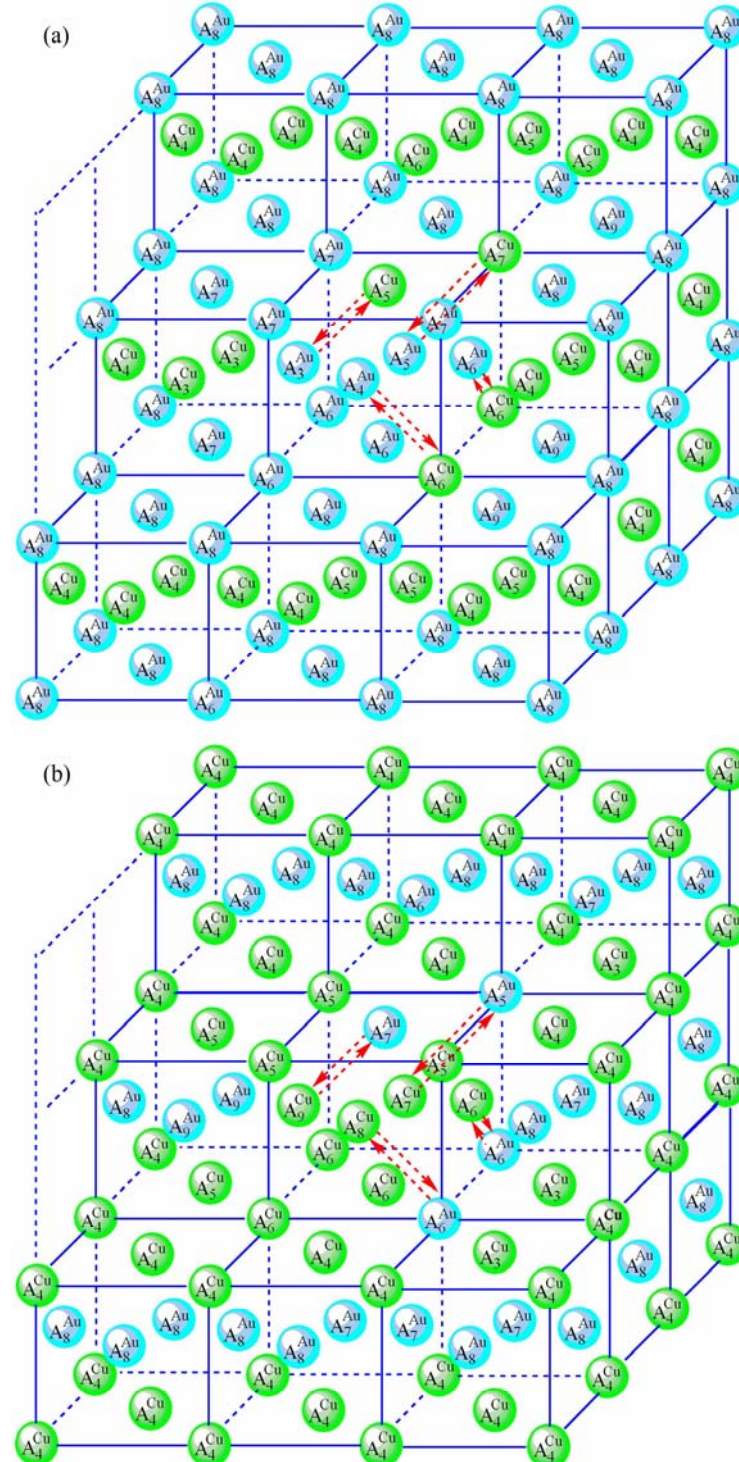


**Fig. D.6** 4(RA-SA)-cell cluster: (a) A-manner alternating in 4(RA-SA) mechanism; (b) B-manner alternating in 4(RA-SA) mechanism

results are

$$\left\{ \begin{array}{l} x_8^{\text{Au}} (31.482) > x_7^{\text{Au}} (8.796) > x_6^{\text{Au}} (4.167) > x_9^{\text{Au}} (3.704) > \\ x_5^{\text{Au}} (0.926) > x_3^{\text{Au}} (0.463) = x_4^{\text{Au}} (0.463) \\ x_4^{\text{Cu}} (31.482) > x_5^{\text{Cu}} (8.796) > x_6^{\text{Cu}} (4.167) > x_3^{\text{Cu}} (3.704) > \\ x_7^{\text{Cu}} (0.926) > x_8^{\text{Cu}} (0.463) = x_9^{\text{Cu}} (0.463) \end{array} \right. \quad (D.13)$$

These results demonstrate that the 4(RA-SA) mechanism cannot be suitable to simulate AG-concentration order in the beginning period on disordering  $\text{AuCuI}(A_8^{\text{Au}} A_4^{\text{Cu}})$ .

### D.3 Ratio ( $M_1:M_2$ ) between $\text{AuCuI}(A_8^{\text{Au}} A_4^{\text{Cu}})$ - and 3(RA-SA)-cells

During the growing period of the high order degree

AuCu(H) alloy, the decrease in order degree of the AuCu(H) alloy is reached through decreasing number of the AuCuI( $A_8^{Au}A_4^{Cu}$ )-cells and increasing number of the 3(RA-SA)-cells. According to AG-concentrations in the 3(RA-SA)-cell cluster, the ratio ( $M_1:M_2$ ) between AuCuI( $A_8^{Au}A_4^{Cu}$ )- and 3(RA-SA)-cells can be calculated by Eq. (D.10) and Eq. (D.14) and the results are listed in Table D.3. The results show that as  $\sigma_s=0.990$ ,  $M_1:M_2=79.94:20.08\approx4:1$ . The sum ( $M_1+M_2$ )=5 is equal to the experimental mean spacing between two successive boundaries of the SPAP-AuCuII.

$$\begin{aligned}
 & x_{\text{AuCuI}} \times \left( \begin{array}{l} x_4^{Au}(0) \\ x_5^{Au}(0) \\ x_6^{Au}(0) \\ x_7^{Au}(0) \\ x_8^{Au}(50) \\ x_9^{Au}(0) \end{array} \right)_{\text{AuCuI}} + x_{3(\text{RA-SA})} \times \\
 & \quad \left( \begin{array}{l} x_4^{Au}(0.926) \\ x_5^{Au}(0.430) \\ x_6^{Au}(1.852) \\ x_7^{Au}(9.259) \\ x_8^{Au}(34.259) \\ x_9^{Au}(3.241) \end{array} \right)_{3(\text{RA-SA})} = \left( \begin{array}{l} x_4^{Au} \\ x_5^{Au} \\ x_6^{Au} \\ x_7^{Au} \\ x_8^{Au} \\ x_9^{Au} \end{array} \right)_{\text{AuCu(H)}} \quad (\text{Eq.(D.14)})
 \end{aligned}$$

where  $x_{\text{AuCuI}}$  and  $x_{3(\text{RA-SA})}$  denote the percent of

**Table D.3** Systematic correlativity of temperature ( $T_s$ ), order degree ( $\sigma_s$ ), percent ( $x_{\text{AuCuI}}$  and  $x_{3(\text{RA-SA})}$ ) of AuCuI ( $A_8^{Au}A_4^{Cu}$ )-cell cluster and 3(RA-SA)-cell cluster and ratio ( $M_1:M_2$ ) of the numbers between AuCuI-cells and 3(RA-SA)-cells in AuCu(H) alloy, during beginning period on disordering AuCuI( $A_8^{Au}A_4^{Cu}$ )

$T_s/K$	$\sigma_s$	$x_{\text{AuCuI}}/\%$	$x_{3(\text{RA-SA})}/\%$	$M_1:M_2$
0	1.000	100.00	0.00	/
571	0.999	97.91	2.09	46.74:1
585	0.998	95.84	4.17	22.98:1
593	0.997	93.78	6.22	15.07:1
600	0.996	91.75	8.26	11.11:1
605	0.995	89.73	10.28	8.73:1
610	0.994	87.74	12.27	7.15:1
613	0.993	85.76	14.25	6.02:1
616	0.992	83.80	16.21	5.17:1
618	0.991	81.86	18.15	4.51:1
620	0.990	79.94	20.08	3.98:1≈4:1
622	0.989	78.04	21.98	3.55:1

AuCuI( $A_8^{Au}A_4^{Cu}$ )-cell clusters and 3(RA-SA)-cell clusters, respectively, and  $x_{\text{AuCuI}}+x_{3(\text{RA-SA})}=1$ ; the  $(x_4^{Au}, x_5^{Au}, x_6^{Au}, x_7^{Au}, x_8^{Au}, x_9^{Au})_{\text{AuCuI}}$ ,  $(x_4^{Au}, x_5^{Au}, x_6^{Au}, x_7^{Au}, x_8^{Au}, x_9^{Au})_{3(\text{RA-SA})}$  and  $(x_4^{Au}, x_5^{Au}, x_6^{Au}, x_7^{Au}, x_8^{Au}, x_9^{Au})_{\text{AuCu(H)}}$  denote respectively AG-concentrations in the AuCuI( $A_8^{Au}A_4^{Cu}$ )-cell cluster, 3(RA-SA)-cell cluster and high order degree AuCu(H) alloy with order degree  $\sigma_s$ . The latest term can be found from Table B.1.

#### D.4 Order degree of 3(RA-SA)-cell cluster

Supposing  $(M_1:M_2)=4:1$  at  $\sigma_s=0.990$ , the AG-concentrations of the 3(RA-SA)-cell cluster can be calculated by Eq. (D.14), which are respectively (atomic fraction):  $x_4^{Au}$  (1.178%),  $x_5^{Au}$  (0.049%),  $x_6^{Au}$  (0.166%),  $x_7^{Au}$  (9.420%),  $x_8^{Au}$  (34.418%) and  $x_9^{Au}$  (4.710%). Comparing these results with AG-concentrations in Table B.1, we have found that the experimental order degree of the 3(RA-SA)-cell cluster is equal approximately to 0.939, which may represent the mean order degree of 3(RA-SA)-cell clusters. Therefore, the properties of AuCu alloy with the order degree (0.939) may represent the mean properties of 3(RA-SA)-cell clusters (i.e., antiface boundary region).

#### D.5 Starting temperature of 3(RA-SA) mechanism

The mixed Gibbs  $\Delta G_{\sigma=1}^m-T$ ,  $\Delta G_{\sigma=0.939}^m-T$ ,  $\Delta G_s^m-T$  and  $\Delta G_e^m-T$  curves of the AuCuI( $A_8^{Au}A_4^{Cu}$ ) with order degree  $\sigma=1$ , AuCu alloy with order degree  $\sigma=0.939$ , AuCu alloy with experimental subequilibrium order degree  $\sigma_s$  and AuCu alloy with theoretical equilibrium order degree  $\sigma_e$  are shown in Fig. D.7. The starting temperature of the 3(RA-SA) mechanism is determined by the intersection point of the  $\Delta G_{\sigma=1}^m-T$  and  $\Delta G_{\sigma=0.939}^m-T$  curves, it is 355 K. As the temperature is higher than this temperature, the 3(RA-SA) mechanism can only take place, because the Gibbs energy  $\Delta G_{3(\text{RA-SA})}(T)$  is lower than  $\Delta G_{\sigma=1.000}^m(T)$  and  $\Delta G_s^m(T)$ . It means that the beginning temperature

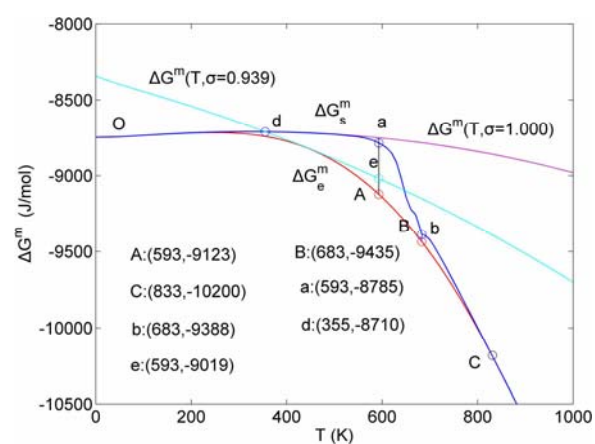


**Fig. D.7** Mixed Gibbs energy  $\Delta G_{\sigma=1}^m-T$ ,  $\Delta G_{\sigma=0.939}^m-T$ ,  $\Delta G_s^m-T$  and  $\Delta G_e^m-T$  curves

$T_{\text{onset}}$  on disordering  $\text{AuCuI}(A_8^{\text{Au}} A_4^{\text{Cu}})$  should be higher than 355 K, and that the  $\text{AuCuI}(A_8^{\text{Au}} A_4^{\text{Cu}})$  is permanently stable in the temperature range  $0 \text{ K} < T < 355 \text{ K}$ , though it is subequilibrium.

## References

- [1] XIE You-qing, LI Xiao-bo, LIU Xin-bi, NIE Yao-zhuang, PENG Hong-jian. Alloy gene Gibbs energy partition function and equilibrium holographic network phase diagrams of AuCu-type sublattice system [J]. International Journal of Communications, Network and System Sciences, 2013, 12(6): 415–442.
- [2] XIE You-qing. Systematic science of alloys [M]. Changsha: Central South University Press, 2012: 29–48. (in Chinese)
- [3] FEUTELAIS Y, LEGENDRE B, GUYMONT M. New enthalpies determination and in situ X-ray diffraction observations of order/disorder transitions in  $\text{Au}_{0.5}\text{Cu}_{0.5}$  [J]. Acta Mater, 1999, 47(8): 2539–2551.
- [4] BONNEAUX J, GUYMONT M. Study of the order-disorder transition series in AuCu by in-situ temperature electron microscopy [J]. Intermetallics, 1999, 7(7): 797–805.
- [5] SPRUŠIL B, PFEILER W. The retro-effect in stoichiometric CuAu: A resistometric study [J]. Intermetallics, 1997, 5(7): 501–505.
- [6] PFEILER W, SPRUŠIL B. Atomic ordering in alloys: Stable states and kinetics [J]. Materials Science and Engineering A, 2002, 324(1–2): 34–42.
- [7] SPRUŠIL B, CHALUPA B. Checking the model for dynamic disordering in CuAu [J]. Materials Science and Engineering A, 2002, 324(1–2): 58–61.
- [8] MIRANDA G, SILVA FS, SOARES D. Solid state transformations and equilibrium crystal structures of an Au–Cu alloy with shape memory effect [J]. Materials Science Forum, 2012, 730–732: 859–864.
- [9] HULTGREN R, DESIA P D, HAWKINS D T, GLEISER M, KELLEY K K. Selected values of thermodynamic properties of binary alloys [M]. Metal Park, OH: American Society for Metals, 1973: 158.
- [10] XIE You-qing. Atomic energies and Gibbs energy functions of Ag–Cu alloys [J]. Science in China, Series E: Technological Science, 1998, 41(2): 146–156.
- [11] XIE You-qing, ZHANG Xiao-dong. Atomic volumes and volume functions of Ag–Cu alloys [J]. Science in China, Series E: Technological Science, 1998, 41(2): 157–168.
- [12] XIE You-qing, NIE Yao-zhuang, LI Xiao-bo, LIU Xin-bi, PENG Hong-jian, LI Yan-feng. Characteristic atom potential energy partition function of  $\text{Au}_3\text{Cu}$  type ordered alloys in FP-SSA framework [J]. The Chinese Journal of Nonferrous Metals, 2011, 21(10): 2489–2501. (in Chinese)
- [13] XIE You-qing, ZHANG Xiao-dong. Electronic structures of Ag–Cu alloys [J]. Science in China, Series E: Technological Science, 1998, 41(3): 225–236.
- [14] XIE You-qing. A new potential function with many-atom interactions in solid [J]. Science in China, Series A, 1993, 36(1): 90–99.
- [15] XIE You-qing. Electronic structure and properties of pure iron [J]. Acta Metallurgica et Materialia, 1994, 42(11): 3705–3715.
- [16] XIE You-qing, ZHANG Xiao-dong, CHEN Jia-yan. Electronic structure and properties of pure cobalt [J]. Science in China, Series E: Technological Science, 1996, 39(4): 394–403.
- [17] OSTP. Materials genome initiative for global competitiveness [R]. Washington D C: Office of Science and Technology Policy, 2011.
- [18] KAUFMAN L, ÅGREN J. CALPHAD, first and second generation-birth of the materials genome [J]. Scripta Materialia, 2014, 70(1): 3–6.
- [19] MASTA M, de FORTAIN D. First-principles study of phase stability of Ti–Al intermetallic compounds [J]. J Mater Res, 1993, 8(10): 2554–2568.
- [20] SUNDMAN B, FRIES S G, OATES W A. A thermodynamic assessment of Au–Cu system [J]. CALPHAD, 1998, 22(3): 335–354.
- [21] SUNDMAN B, FRIES S G, OATES W A. A CALPHAD assessment of the Au–Cu system using the cluster variatiation method [J]. Z Metallkd, 1999, 90(5): 267–273.

## AuCuI( $A_8^{\text{Au}} A_4^{\text{Cu}}$ )化合物无序化路径跟踪的原子移动新机制

谢佑卿<sup>1,2,3</sup>, 彭红建<sup>4</sup>, 刘心笔<sup>1,2,3</sup>, 李小波<sup>5</sup>, 聂耀庄<sup>6</sup>

1. 中南大学 材料科学与工程学院, 长沙 410083;
2. 中南大学 粉末冶金研究院, 长沙 410083;
3. 中南大学 粉末冶金国家重点实验室, 长沙 410083;
4. 中南大学 化学化工学院, 长沙 410083;
5. 湘潭大学 材料科学与工程学院, 湘潭 411105;
6. 中南大学 物理与电子学院, 长沙 410083

**摘要:** 以由  $A_8^{\text{Au}}$  和  $A_4^{\text{Cu}}$  干基因组成的  $\text{AuCuI}(A_8^{\text{Au}} A_4^{\text{Cu}})$  化合物的无序化实验路径为例, 介绍了 3 个发现和 1 个方法。发现  $\text{AuCuI}(A_8^{\text{Au}} A_4^{\text{Cu}})$  化合物抗拒温度变化保持结构稳定性的能力归因于  $A_8^{\text{Au}}$  和  $A_4^{\text{Cu}}$  基因的势阱深度远超过其振动能, 这导致其无序化实验路径是亚平衡的; 发现  $\text{AuCuI}(A_8^{\text{Au}} A_4^{\text{Cu}})$  适应温度变化改变结构的原子移动新机制是合金基因的“共振激活—同步交换”机制, 这导致无序化是非均匀性和递次性的亚平衡转变; 发现无序化过程中存在跳变有序度, 导致存在跳变温度和升温速度增加跳变温度降低的“逆反效应”, 即所谓的“Retro 效应”。采用实验混合焓路径法, 建立了一整套亚平衡全息网络路径图。

**关键词:** 金属间化合物; 合金基因; 有序无序转变; 共振激活—同步交换机制; 热力学性质; 平衡和亚平衡全息网络路径图

(Edited by Yun-bin HE)